Державна наукова установа

Науково-технологічний комплекс "Інститут монокристалів"

Національна академія наук України

Кваліфікаційна наукова

праця на правах рукопису

Кобзев Дмитро Володимирович

УДК 667.287.4; 535.37; 547.7/.8; 547:544

ДИСЕРТАЦІЯ

Довгохвильові галогеновані флуоресцентні поліметинові барвники для

медико-біологічних застосувань

Спеціальність 102 «Хімія»

Галузь знань 10 «Природничі науки»

Подається на здобуття наукового ступеня доктора філософії

Дисертація містить результати власних досліджень. Використання ідей, результатів і текстів інших авторів мають посилання на відповідне джерело

_____ Д. В. Кобзев

Науковий керівник:

Татарець Анатолій Леонідович,

кандидат хімічних наук,

старший дослідник

Харків – 2023

National Academy of Sciences of Ukraine

Qualifying scientific
work on manuscript rights

Kobzev Dmytro Volodymyrovych

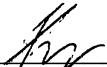UDC 667.287.4; 535.37; 547.7/.8; 547:544

THESIS

Long-wavelength halogenated fluorescent polymethine dyes for biomedical applications

Programme Subject Area 102 «Chemistry»

Field of Study 10 «Natural sciences»

Submitted for the degree of Doctor of Philosophy

The dissertation contains the results of my own research. The use of ideas, results and texts of other authors are referenced to the corresponding source.

_____ D. V. Kobzev

Scientific advisor:

Tatarets Anatoliy Leonidovych,

Cand. Sci., Senior researcher

Kharkiv – 2023

АНОТАЦІЯ

Кобзев Д.В. Довгохвильові галогеновані флуоресцентні поліметинові барвники для медико-біологічних застосувань. – Кваліфікаційна наукова праця на правах рукопису.

Дисертація на здобуття наукового ступеня доктора філософії за спеціальністю 102 Хімія. – Державна наукова установа "Науково-технологічний комплекс "Інститут монокристалів" Національної академії наук України", Харків, 2023.

На сьогоднішній день широкого розповсюдження набули флуоресцентні методи дослідження в біологічній і медичній областях, а також в клінічній діагностиці. Флуоресцентні сполуки використовуються як діагностичні засоби, оскільки вони є основними компонентами для впровадження будь-якого методу флуоресцентних досліджень. Проте, із розвитком персоналізованої медицини, що вимагає значних досліджень на живих клітинах та організмах *in vivo*, виникла ідея використання флуоресцентних барвників для отримання терапевтичного ефекту, що відкрило новий підхід у медицині – тераностику (одночасна діагностика та лікування окремих пацієнтів). Щоб отримати флуоресцентний сигнал або терапевтичний ефект від таких молекул, вони повинні поглинати світло. Слід зауважити, що лише довгохвильове світло (600–900 нм) в так званому «оптичному вікні» слабко поглинається біологічними макромолекулами, водою та іншими компонентами біооб'єктів і має незначний вплив на процеси, що відбуваються в організмі. Зрозуміло, що накладення таких обмежень на спектральну область флуоресцентних барвників істотно зменшує їх різноманітність. Крім того, будь-який флуоресцентний барвник повинен мати такі властивості:

➢ високий коефіцієнт екстинкції та квантовий вихід флуоресценції;

➢ достатня розчинність у воді та фізіологічних середовищах;

➢ прийнятна фото- і хімічна стабільність.

З кожним роком вимоги до флуоресцентних барвників стають жорсткішими. Таким чином, одержання нових яскравих довгохвильових барвників, що можна використовувати як для діагностики, так і для лікування, є актуальним завданням сьогодення. Ціаніни є найбільш перспективним класом барвників завдяки значній гнучкості їх спектральних, фотофізичних і фотохімічних властивостей. Гептаметинціанінові барвники мають дуже низьку фототоксичність і добре підходять до «оптичного вікна» у ближньому інфрачервоному (БІЧ) діапазоні, тому вони широко використовуються як діагностичні інструменти. Наприклад, Indocyanine Green використовується в *in vivo* діагностиці та хірургії. Окрім використання як флуоресцентних маркерів, гептаметинціанінові барвники можна використовувати як сенсибілізатори для фотодинамічної терапії (ФДТ). Однак, низька фототоксичність ціанінів ускладнює їх застосування для лікування. Відомий спосіб підвищення фототоксичності барвника полягає у введенні важких атомів у його структуру. Проте, у літературі вплив важких атомів галогенів, таких як бром та йод, на спектральні та фотохімічні властивості гептаметинціанінів на цей час залишається недостатньо вивченим.

Основною метою цього дослідження була розробка нових галогенованих флуоресцентних гептаметинціанінових барвників для вивчення впливу важких атомів на ці барвники з метою вдосконалення матеріалів для тераностики, фотодинамічної терапії (ФДТ) і фотоімунотерапії (ФІТ).

Для досягнення цієї мети ми синтезували ряд БІЧ ціанінових барвників з атомами йоду, брому та хлору та визначили їх спектральні властивості. Цікаво, що ми спостерігали значне підвищення квантового виходу флуоресценції (Φ_{Fl}), до 35%, і збільшення тривалості життя флуоресценції для галогенованих барвників. Загалом, атоми брому мають більший позитивний вплив на Φ_{Fl} барвників, аніж атоми йоду. Також, ми показали, що значення квантового виходу синглетного кисню (Φ_{Δ}), генерація якого збільшується завдяки наявності атомів галогенів, не такі очевидні і залежать не тільки від кількості, але й від положення атомів галогенів у гептаметинових барвниках. Так, барвник **4,6I$_4$-HITC**, що містить 4

атоми йоду в положеннях 4,6 індоленінових фрагментів, мав у 1.5 рази нижчий Φ_Δ порівняно з **5I₂-HITC** з 2 атомами йоду в положеннях 5. Ми встановили, що атоми йоду до 8.4 разів збільшують Φ_Δ гептаметинціанінів, тоді як атоми брому незначним чином впливають на Φ_Δ. Більш того, за допомогою введення атомів хлору можна отримати значення Φ_Δ гептаметинціанінів навіть нижчі ніж у незаміщеного барвника, **HITC**. Ми припускаємо, що включення важких атомів приводить до обмеження обертання індоленінових фрагментів навколо поліметинового ланцюга, таким чином збільшуючи Φ_{Fl}, час життя флуоресценції та навіть Φ_Δ для **I₆-HITC** і **4,6I₄-HITC** порівняно з **HITC**. Таким чином, ми встановили спосіб регулювання ключових властивостей (Φ_{Fl} і Φ_Δ) гептаметинціанінових барвників шляхом зміни кількості та положення атомів галогену.

Ґрунтуючись на тому, що атоми йоду приводять до більш істотного зростання Φ_Δ гептаметинціанінів, а підвищення Φ_Δ позитивно корелює зі збільшенням фототоксичності барвників, синтезовано серію БІЧ гептаметинціанінових барвників, що містять до шести атомів йоду та аліфатичну карбоксильну групу, а також досліджено їх спектральні властивості та фотоцитотоксичність до патогенів *S. aureus*, *E. coli* та *P. aeruginosa* у антимікробній фотодинамічній терапії (АФДТ). Збільшення кількості атомів йоду має несподіваний і неоднозначний фотоцитотоксичний ефект на ці бактерії, що пов'язаний з двома протидіючими факторами: (1) збільшенням інтеркомбінаційної конверсії та, відповідно, кількості генерації реактивних форм, і (2) агрегацією барвника, що викликає зниження накопичення барвника бактеріями, що, ймовірно, супроводжується зниженням темпів утворення реактивних форм кисню. Так, встановлено, що збільшення кількості атомів йоду до двох у ряду цвітер-іонних ціанінів підвищує ефективність ерадикації *S. aureus*. Для барвників з 2–4 атомами йоду ефективність залишається майже незмінною, та зменшується у випадку гексайодованого ціаніну. При цьому монойодований гептаметинціаніновий барвник викликає найбільш виражений фотоцитотоксичний вплив на *E. coli* та *P. aeruginosa*. Додатковий позитивний

заряд, який вносить триетиламонієва група, знижує ефективність барвника щодо *S. aureus*, але покращує знищення *E. coli* та *P. aeruginosa*.

Враховуючи найкращу яскравість, фотоцитотоксичність та агрегацію, що забезпечує введення двох атомів йоду, ми синтезували новий, добре розчинний у воді, дийодований БІЧ гептаметинціаніновий барвник, **2ICy7S**, який містить 3 сульфогрупи. Далі ми зв'язали цей барвник із моноклональним антитілом трастузумаб (**Ab**), що специфічне до раку молочної залози, та оцінили спектральні властивості та Φ_Δ одержаному кон'югату, а також дослідили цей ФІТ кон'югат на моделі «голих» мишей *in vivo*, при внутрішньовенному введенні, для пригнічення росту пухлин порівняно з кон'югатом нейодованого барвника **Cy7^{TM}(Cy7^{TM}−Ab)**. У той час як стимульований антитілами імунотерапевтичний ефект **2ICy7S−Ab** можна оцінити як 1.4-кратне пригнічення росту пухлини, комбінована фотоімунотерапевтична дія приводить до 5.4-кратного пригнічення, що викликано некрозом пухлинних клітин. Йодований кон'югат **2ICy7S−Ab** демонструє в 3 рази більший квантовий вихід генерації синглетного кисню у водному середовищі порівняно з нейодованим аналогом **Cy7^{TM}−Ab**. Таким чином, атоми йоду в **2ICy7S** відіграють ключову роль у підвищеній фотоцитотоксичності кон'югату **2ICy7S−Ab**. Нейодований **Cy7^{TM}−Ab** і вільні **Ab** не виявляють статистично значущої фотоцитотоксичності для ракових клітин і діють виключно як імунотерапевтичний засіб. За відсутності сенсибілізаторів, вплив ближнього інфрачервоного світла на ріст пухлини був незначним. Також, не спостерігався вплив вільних барвників **2ICy7S** і **Cy7^{TM}**, що вводилися внутрішньовенно, на ріст пухлини. Крім терапевтичного ефекту, кон'югат **2ICy7S−Ab** забезпечує яскравий флуоресцентний сигнал, що дозволяє в режимі реального часу відстежувати розподіл кон'югату в організмі та накопичення його в пухлині. Це важливо для визначення оптимального часу для світлового опромінення і, тим самим, підвищення якості лікування. Ми очікуємо, що кон'югація **2ICy7S** або інших йодованих фотосенсибілізаторів на основі ціанінів подібної структури з широким спектром антитіл може значно розширити

різноманіття ефективних матеріалів для фотоімунотерапевтичного лікування, спрямованого на різні типи раку.

При виконанні цієї роботи *вперше*: синтезовано систематичний ряд гептаметинціанінових барвників з різною кількістю (від 1 до 6) атомів йоду або брому в термінальних гетероциклічних фрагментах; вивчено зв'язок між структурою та властивостями галогенованих гептаметинціанінових барвників щодо кількості і положення атомів галогену; встановлено, як регулювати основні властивості (Φ_{Fl} і Φ_{Δ}) для гептаметинціанінових барвників, змінюючи кількість і положення атомів галогенів; оцінено вплив кількості атомів йоду в гептаметинціанінових барвниках на фотоцитотоксичний ефект до бактерій; показано, що йодовані гептаметинціанінові барвники придатні для лікування і фотоінактивації грам-позитивних і грам-негативних бактерій; одержано кон'югат "ціаніновий барвник – моноклональне антитіло", який проявляє фотоімунотерапевтичну дію і придатний для тераностики раку.

Практична цінність результатів дослідження полягає у встановленні закономірностей для одержання БІЧ ціанінових барвників з бажаними властивостями для флуоресцентної візуалізації, діагностики та, особливо, фотодинамічної терапії та тераностики. Розроблені барвники ефективні для фотоерадикації бактерій, що дозволяє обійти проблему резистентності бактерій до антибіотиків. Одержані барвники, що містять карбоксильну групу, придатні для подальшої функціоналізації шляхом їх кон'югації з різними носіями для підвищення афінності до бажаної цілі. Так, кон'югати на основі гептаметинціанінових барвників показали високу ефективність для *in vivo* діагностики та лікуванні раку при фотоімунотерапевтичному застосуванні. Таким чином, це дослідження розширює можливості використання БІЧ ціанінових барвників.

Ключові слова: гептаметинціанінові барвники, ефект важкого атома, антибактеріальна активність, біологічна активність, гетероциклізація, флуоресценція, електронна спектроскопія, синтез, цитотоксичність, молекулярна будова, фотосенсибілізатори, антибактеріальна фотодинамічна терапія, квантовий вихід, фотоімунотерапія, флуоресцентна візуалізація.

Список опублікованих праць за темою дисертації

1. **Kobzev D**, Semenova O, Tatarets A, Bazylevich A, Gellerman G, Patsenker L. Antibody-guided iodinated cyanine for near-IR photoimmunotherapy. Dyes Pigm 2023;212:111101. https://doi.org/10.1016/j.dyepig.2023.111101. *Здобувачем зроблено кон'югат моноклональне антитіло–барвник, визначено спектрально-люмінесцентні характеристики та квантовий вихід синглетного кисню барвника та кон'югата, проведено in vivo дослідження на моделі «голих мишей» (візуалізація, рост пухлини, тощо), виконано обробку усіх результатів дослідження для представлення усіх графічних матеріалів публікації, підготовлено драфт публікації, брав участь у синтезі гептаметинціанінового барвника.*

2. Semenova O, **Kobzev D**, Yazbak F, Nakonechny F, Kolosova O, Tatarets A, Gellerman G, Patsenker L. Unexpected effect of iodine atoms in heptamethine cyanine dyes on the photodynamic eradication of Gram-positive and Gram-negative pathogens. Dyes Pigm 2021;195:109745. https://doi.org/10.1016/j.dyepig.2021.109745. *Здобувачем синтезовано частину вихідних матеріалів та флуоресцентних барвників, брав участь у підготовці написанні публікації.*

3. Konovalova IS, Shishkina SV, **Kobzev D**, Semenova O, Tatarets A. Crystal structures and Hirshfeld analysis of 4,6-dibromoindolenine and its quaternized salt. Acta Crystallogr Sect E Crystallogr Commun 2021;77:1203−7. https://doi.org/10.1107/S2056989021011385. *Здобувачем синтезовано досліджувані речовини.*

4. Bokan M, Nakonechny F, Talalai E, **Kobzev D**, Gellerman G, Patsenker L. Photodynamic effect of novel hexa-iodinated quinono-cyanine dye on *Staphylococcus aureus*. Photodiagnosis Photodyn Ther 2020;31:101866. https://doi.org/10.1016/j.pdpdt.2020.101866. *Здобувачем синтезовано вихідні матеріали, брав участь у підготовці публікації.*

5. **Кобзев Д.В.**, Татарець А.Л. Галогеновмісні гептаметинціанінові барвники для медико-біологічних застосувань. XIV Всеукраїнська конференція молодих вчених, студентів та аспірантів з актуальних питань хімії (CYS2023), 10−12 жовтня 2023 р., Харків, Україна. − С. 41. *Здобувачем синтезовано сполуки, що досліджувалися проведено спектральні та біологічні дослідження.*

6. **Kobzev D**, Semenova O, Tuchinsky H, Tatarets A, Gellerman G, Patsenker L. Antibody-guided iodinated NIR cyanine for fluorescently monitored photoimmunotherapy. 5th International Caparica Conference on Chromogenic and Emissive Materials (IC3EM2022), 3-7 July, 2022, Caparica, Portugal. − P-233. *Здобувачем проведено синтез кон'югатів, а також спектральні та біологічні дослідження.*

7. **Kobzev D**, Semenova O, Tatarets A, Gellerman G, Patsenker L. Breast cancer photoimmunotherapeutic treatment with novel antibody-guided iodinated photosensitizer. International Scientific-Practical Conference Georgian Scientific Pharmacy: Past and Present (ISPC-2022), 1-2 October, 2022, Tbilisi, Georgia. − P-67. *Здобувачем проведено синтез кон'югатів, а також спектральні та біологічні дослідження.*

8. Semenova O, **Kobzev D**, Yazbak F, Nakonechny N, Tatarets A, Gellerman G, Patsenker L. Delivery of iodinated heptamethine indocyanine photosensitizing drugs to gram-positive and gram-negative pathogens for antimicrobial photodynamic therapy (APDT), ICRS-PAT Joint Workshop, 3-7 October, 2021, Ma'alot-Tarshiha, Israel. − P-30. *Здобувачем синтезовано барвники та вихідні сполуки.*

9. **Kobzev D**, Semenova O, Obukhova O, Khabuseva S, Kolosova O, Stepanenko O, Tatarets A. Influence of heavy halogen atoms on spectral properties and quantum yields of heptamethine cyanine dyes, XII International Conference Electronic Processes in Organic and Inorganic Materials (ICEPOM-12), 1−5 June

2020, Kamianets-Podilskyi, Ukraine. − P. 21. *Здобувачем проведено синтез сполук та спектральні дослідження.*

10. **Kobzev D**, Semenova O, Tatarets A. Photostability and spectral properties of heptamethinecyanine dyes with substitutions in the polymethine chain, Central European Conference on Photochemistry (CECP-2020), 9−13 February 2020, Bad Hofgastein, Austria. − P. 74. *Здобувачем проведено спектральні дослідження.*

ABSTRACT

Kobzev D.V. Long-wavelength halogenated fluorescent polymethine dyes for biomedical applications. – Qualifying scientific work, the manuscript.

Thesis for the degree of Doctor of Philosophy in programme subject area 102 Chemistry. – State Scientific Institution "Institute for Single Crystals" of National Academy of Sciences of Ukraine, Kharkiv, 2023.

Nowadays fluorescent research methods in the biological and medical fields and clinical diagnosis have become widespread. Being the main elements for the implementation of any fluorescent research method, fluorescent compounds have long been used as diagnostic tools. But with the development of personalized medicine requiring significant research on living cells and even organisms *in vivo* came the idea of using fluorescent dyes to provide a therapeutic effect raising a new approach in medicine – theranostics (simultaneous diagnosis and treatment of individual patients). To obtain a fluorescent signal or a therapeutic effect from such molecules, they must absorb light. It should be noted that only long-wavelength light (600–900 nm) in the so-called "optical window" is poorly absorbed by biological macromolecules, water, and other components of bioobjects and has little effect on the processes occurring in the body. It is clear that the imposition of such restrictions on the spectral region of fluorescent dyes significantly reduces their diversity. Moreover, any fluorescent dye must have the following properties:

➢ high extinction coefficient and fluorescence quantum yield;

➢ sufficient solubility in water and physiological issues;

➢ reasonable photo- and chemical stability.

Year after year above requirements for fluorescent dyes become stricter. Thus, obtaining new bright long-wavelength dyes that can be used for both diagnostic purposes and treatment is a pressing task today.

Cyanines are the most promising dye class due to the considerable flexibility of their spectral, photophysical, and photochemical properties. Heptamethine cyanine dyes have very low phototoxicity and they fit well to the near-infrared (NIR) "optical

window", which is why they are widely used as diagnostic tools. For instance, Indocyanine green is used in *in vivo* diagnostics and surgery. In addition to their use as fluorescent markers, heptamethine cyanine dyes can be used as sensitizers for photodynamic therapy (PDT) applications. However, the low phototoxicity of cyanines hampers their treatment applications. For that purpose, a known way to increase the phototoxicity of a dye is to incorporate heavy atoms into the dye structure. In the literature, however, the influence of heavy halogen atoms such as bromine and iodine on the spectral and photochemical properties of heptamethine cyanines remains poorly studied.

The main goal of this research was the development of novel halogenated fluorescent heptamethine cyanine dyes to explore heavy atom impact on these dyes to develop materials for theranostics, photodynamic therapy (PDT), and photoimmunotherapy (PIT) applications.

To achieve the main goal of this work, we synthesized a set of NIR cyanine dyes with iodine, bromine, and chlorine atoms as well as evaluated their spectral properties. The most exceptional is the fluorescence quantum yield (Φ_{Fl}) and lifetime data, where we observe Φ_{Fl} significant enhancement (up to 35%) and the fluorescence lifetime increase caused by the halogenation of the dyes. In general, bromine atoms have a higher positive impact on Φ_{Fl} of the dyes than iodine atoms. Then, we demonstrate that the halogen-promoted singlet oxygen quantum yield Φ_Δ enhancement is not that obvious and depends not only on the amount but also on the position where this halogen is present in the heptamethine cyanine dyes. Thus, **4,6I$_4$-HITC** dye containing 4 iodine atoms in positions 4,6 of indolenine moieties has 1.5 times lower Φ_Δ compared to **5I$_2$-HITC** with 2 iodine atoms. In particular, we observe that while iodine atoms strongly (up to 8.4 times) increase the singlet oxygen generation (Φ_Δ) of the heptamethine cyanines, bromine atoms insignificantly affect Φ_Δ. It is possible to reduce Φ_Δ even below **HITC** with the incorporation of chlorine atoms. We make a hypothesis assuming that the incorporation of heavy atoms leads to the restriction of rotation of indolium moieties around the polymethine chain, thus increasing $\Phi_{Fl,}$ fluorescence lifetime, and even Φ_Δ for **I$_6$-HITC** and **4,6I$_4$-HITC** compare to **HITC**. In general, we

show a way to adjust the key properties (Φ_{Fl} and Φ_{Δ}) for heptamethine cyanines changing the amount and positions of halogen atoms.

Then, based on the fact that iodine atoms more significantly increase Φ_{Δ} of heptamethine cyanines, a series of NIR heptamethine cyanine dyes containing up to six iodine atoms and an aliphatic carboxylic group is synthesized to investigate their spectral properties and ability for photocytotoxicity on *S. aureus*, *E. coli* and *P. aeruginosa* pathogens in APDT. The increasing of the number of iodine atoms has an unexpected and ambiguous photocytotoxic effect on these bacteria, which is connected with two opposing factors: (1) increase of the intersystem crossing and the rates of reactive species generation, and (2) dye aggregation causing the reduced dye uptake that, supposedly, is followed by the decreased rates of reactive species generation. As a result, the increase of the number of iodine atoms up to two in the series of zwitterionic cyanines increases the efficacy of *S. aureus* eradication; then the efficacy remains almost unchanged for the two-, three- and four-iodinated dyes and diminishes in the case of the hexa-iodinated cyanine. At the same time, the mono-iodinated heptamethine cyanine causes the most pronounced photocytotoxic effect on *E. coli* and *P. aeruginosa*. An additional positive charge contributed by a triethylammonium group decreases the efficacy of the dye towards *S. aureus* but improves the eradication of *E. coli* and *P. aeruginosa*.

Considering the best brightness, photocytotoxicity and taking into account the aggregation facilitated by two iodine atoms, we synthesize novel, highly water soluble (containing 3 sulfo groups), NIR, diiodinated heptamethine cyanine dye, **2ICy7S**, conjugate this dye with the breast cancer-specific monoclonal antibody trastuzumab, evaluate its spectral properties and Φ_{Δ}, and investigate the obtained PIT conjugate in the mouse xenograft model to suppress tumor growth upon intravenous (IV) injection *versus* the parent, non-iodinated **Cy7^{TM}−Ab** conjugate. While the antibody-stimulated immunotherapeutic effect of **2ICy7S−Ab** can be estimated as 1.4-fold tumor growth suppression, the combined photoimmunotherapeutic action results in 5.4-fold suppression caused by tumor cell necrosis. The iodinated **2ICy7S−Ab** conjugate demonstrates a 3-fold increased quantum yield of singlet oxygen generation in aqueous

media compared to the non-iodinated counterpart, **Cy7^{TM}−Ab**. Thus, the iodine atoms in **2ICy7S** play a key role in the augmented photocytotoxicity of the **2ICy7S−Ab** conjugate. The non-iodinated **Cy7^{TM}−Ab** and free **Ab** do not show statistically significant photocytotoxicity on cancer cells and act solely as an immunotherapeutic agent. In the absence of sensitizers, the impact of NIR light on the tumor growth is negligible and also no effect of IV administrated free **2ICy7S** and **Cy7^{TM}** dyes on the tumor growth is observed. The **2ICy7S−Ab** conjugate provides a bright fluorescent signal enabling real-time monitoring of the conjugate distribution in the body and accumulation in the tumor. This is important for recognizing the optimal time for light irradiation and thus improving the quality of treatment. We anticipate that the conjugation of **2ICy7S** or other iodinated cyanine-based photosensitizers of a similar structure with a wide range of antibodies can gradually expand the scope of efficient materials for photoimmunotherapeutic treatment aimed at different types of cancer.

In this work *for the first time* we synthesized heptamethine cyanine dyes with different numbers (from 1 to 6) of iodine or bromine atoms in terminal heterocyclic moieties; studied the structure-properties relationships of halogenated heptamethine cyanine dyes with respect to the amount and positions of halogen atoms; set how to adjust the key properties (fluorescence quantum yield Φ_{Fl} and singlet oxygen quantum yield Φ_{Δ}) for heptamethine cyanine dyes changing the amount and positions of halogen atoms; evaluated the influence of the number of iodine atoms in heptamethines on the photocytotoxic effect on bacteria; showed that iodinated heptamethine cyanine dyes are suitable for the treatment and photoinactivation of gram-positive and gram-negative bacteria; introduced the use of photoimmunotherapeutic "cyanine dye – monoclonal antibody" conjugate and demonstrated its efficacy for cancer theranostics.

Practical significance of the obtained results. This study helps in the designing of NIR cyanine dyes with the desired properties for fluorescence imaging, diagnostics, and, especially, photodynamic therapies and theranostics. The developed dyes are effective for photoeradication of bacteria circumventing bacterial drug resistance. The presence of carboxylic function potentially enables further binding of these dyes to various carriers. It has been shown that conjugates based on heptamethine cyanine are

effective for *in vivo* diagnostics and cancer treatment in photoimmunotherapy applications. Thus, this study expands applications exploiting NIR cyanine dyes.

List of publications

1. **Kobzev D**, Semenova O, Tatarets A, Bazylevich A, Gellerman G, Patsenker L. Antibody-guided iodinated cyanine for near-IR photoimmunotherapy. Dyes Pigm 2023;212:111101. https://doi.org/10.1016/j.dyepig.2023.111101. *The author's personal contribution lies in the synthesis of monoclonal antibody–dye conjugate, measurement of spectral properties and quantum yields of singlet oxygen of the dye and conjugate, carrying out the in vivo research on the mouse xenograft model (imaging, tumor growth, etc.), processing of all research results to present all illustrational materials of the publication, preparation of the draft of publication, participation in the synthesis of the heptamethinecyanine dye.*

2. Semenova O, **Kobzev D**, Yazbak F, Nakonechny F, Kolosova O, Tatarets A, Gellerman G, Patsenker L. Unexpected effect of iodine atoms in heptamethine cyanine dyes on the photodynamic eradication of Gram-positive and Gram-negative pathogens. Dyes Pigm 2021;195:109745. https://doi.org/10.1016/j.dyepig.2021.109745. *The author's personal contribution lies in the synthesis of several starting materials and fluorescent dyes, measurement of spectral properties, participation in writing of the publication.*

3. Konovalova IS, Shishkina SV, **Kobzev D**, Semenova O, Tatarets A. Crystal structures and Hirshfeld analysis of 4,6-dibromoindolenine and its quaternized salt. Acta Crystallogr Sect E Crystallogr Commun 2021;77:1203−7. https://doi.org/10.1107/S2056989021011385. *The author's personal contribution lies in the synthesis of the investigated compounds.*

4. Bokan M, Nakonechny F, Talalai E, **Kobzev D**, Gellerman G, Patsenker L. Photodynamic effect of novel hexa-iodinated quinono-cyanine dye on *Staphylococcus aureus*. Photodiagnosis Photodyn Ther 2020;31:101866. https://doi.org/10.1016/j.pdpdt.2020.101866. *The author's personal contribution lies in the synthesis of starting materials and participation in writing of the publication.*

5. **Kobzev D.V.**, Tatarets A.L. Halogenated heptamethine cyanines for biomedical applications. XIV All-Ukrainian Conference of Young Scientists, Students and PhD Students on Current Chemistry Issues (CYS2023), 10−12 October, 2023, Kharkiv, Ukraine. − P. 41. *The author's personal contribution lies in the synthesis of the investigated compounds, carrying out spectral and biological studies.*

6. **Kobzev D**, Semenova O, Tuchinsky H, Tatarets A, Gellerman G, Patsenker L. Antibody-guided iodinated NIR cyanine for fluorescently monitored photoimmunotherapy. 5th International Caparica Conference on Chromogenic and Emissive Materials (IC3EM2022), 3-7 July, 2022, Caparica, Portugal. − P-233. *The author's personal contribution lies in the synthesis of the investigated conjugates, carrying out spectral and biological studies.*

7. **Kobzev D**, Semenova O, Tatarets A, Gellerman G, Patsenker L. Breast cancer photoimmunotherapeutic treatment with novel antibody-guided iodinated photosensitizer. International Scientific-Practical Conference Georgian Scientific Pharmacy: Past and Present (ISPC-2022), 1-2 October, 2022, Tbilisi, Georgia. − P-67. *The author's personal contribution lies in the synthesis of the investigated conjugates, carrying out spectral and biological studies.*

8. Semenova O, **Kobzev D**, Yazbak F, Nakonechny N, Tatarets A, Gellerman G, Patsenker L. Delivery of iodinated heptamethine indocyanine photosensitizing drugs to gram-positive and gram-negative pathogens for antimicrobial photodynamic therapy (APDT), ICRS-PAT Joint Workshop, 3-7 October, 2021, Ma'alot-Tarshiha, Israel. − P-30. *The author's personal contribution lies in the synthesis of the fluorescent dyes and starting materials.*

9. **Kobzev D**, Semenova O, Obukhova O, Khabuseva S, Kolosova O, Stepanenko O, Tatarets A. Influence of heavy halogen atoms on spectral properties and quantum yields of heptamethine cyanine dyes, XII International Conference Electronic Processes in Organic and Inorganic Materials (ICEPOM-12), 1−5 June

2020, Kamianets-Podilskyi, Ukraine. − P. 21. *The author's personal contribution lies in the synthesis of the fluorescent dyes and carrying out spectral studies.*

10. **Kobzev D**, Semenova O, Tatarets A. Photostability and spectral properties of heptamethinecyanine dyes with substitutions in the polymethine chain, Central European Conference on Photochemistry (CECP-2020), 9−13 February 2020, Bad Hofgastein, Austria. − P. 74. *The author's personal contribution lies in the carrying out spectral studies.*

TABLE OF CONTENTS

LIST OF ABBREVIATIONS

Ab	Antibody
APDT	Antimicrobial photodynamic therapy
AcOH	Acetic acid
Ac_2O	Acetic anhydride
ACN	Acetonitrile
BODIPY	Boron-dipyrromethene
^{13}C-NMR	Carbon-13 nuclear magnetic resonance
DPBF	1,3-diphenylisobenzofuran
DMF	Dimethylformamide
DIPEA	Diisopropylethylamine
DMSO	Dimethylsulfoxide
DAR	Dye-to-antibody ratio
ESI	Electrospray ionization
E. coli	*Escherichia coli*
FITC	Fluorescein isothiocyanate
FDA	Food and Drug Administration (USA)
HER2+	Human epidermal growth factor receptor 2
HITC	1,1,3,3,3,3-Hexamethylindotricarbocyanine iodide
HPLC	High-performance liquid chromatography
HRMS	High-resolution mass spectrometry
^{1}H-NMR	Proton nuclear magnetic resonance
ISC	Intersystem crossing
IV	Intravenously
ICG	Indocyanine green
IR	Infrared
LCMS	Liquid chromatography mass spectrometry
LED	Light-emitting diode
MeOH	Methanol

MS	Mass spectrometry
S. aureus	*Staphylococcus aureus*
NIR	Near-infrared
NP	Nanoparticle
NMR	Nuclear magnetic resonance
PDT	Photodynamic therapy
PIT	Photoimmunotherapy
PS	Photosensitizer
PCR	Polymerase chain reaction
PI	Propidium iodide
PBS	Phosphate buffered saline
P. aeruginosa	*Pseudomonas aeruginosa*
r.t.	Room temperature
ROS	Reactive oxygen species
SOSG	Singlet oxygen sensor green
TLC	Thin-layer chromatography
TSTU	N,N,N',N'-Tetramethyl-O-(N-succinimidyl) uronium tetrafluoroborate
TFA	Trifluoroacetic acid
UV-VIS	Ultraviolet−visible
τ	Fluorescence lifetime
ε	Extinction coefficient
$\lambda_{max}Ab$	Absorption maxima
$\lambda_{max}Em$	Emission maxima
c_{Dye}	Concentration of the dye
k_r	Radiative constant
k_{nr}	Nonradiative constant
Φ_Δ	Quantum yield of the singlet oxygen generation
Φ_{Fl}	Fluorescence quantum yield

INTRODUCTION

Nowadays fluorescent research methods in the biological and medical fields and clinical diagnosis have become widespread. Being the main elements for the implementation of any fluorescent research method, fluorescent compounds have long been used as diagnostic tools. But with the development of personalized medicine requiring significant research on living cells and even organisms *in vivo* came the idea of using fluorescent dyes to provide a therapeutic effect raising a new approach in medicine – theranostics (simultaneous diagnosis and treatment of individual patients). To obtain a fluorescent signal or a therapeutic effect from such molecules, they must absorb light. It should be noted that only long-wavelength light (600–900 nm) in the so-called "optical window" is poorly absorbed by biological macromolecules, water, and other components of bioobjects and has little effect on the processes occurring in the body. It is clear that the imposition of such restrictions on the spectral region of fluorescent dyes significantly reduces their diversity. Moreover, any fluorescent dye must have the following properties:

- high extinction coefficient and fluorescence quantum yield;
- sufficient solubility in water and physiological issues;
- reasonable photostability and chemical stability.

Year after year above requirements for fluorescent dyes become stricter. Thus, obtaining new bright long-wavelength dyes that can be used for both diagnostic purposes and treatment is a pressing task today.

Cyanines are the most promising dye class due to the considerable flexibility of their spectral, photophysical, and photochemical properties. Heptamethine cyanine dyes have very low phototoxicity and they fit well to the near-infrared (NIR) "optical window", which is why they are widely used as diagnostic tools. For instance, Indocyanine green (ICG) is used in *in vivo* diagnostics and surgery. In addition to their use as fluorescent markers, heptamethine cyanine dyes can be used as sensitizers for photodynamic therapy (PDT) applications. However, the low cytotoxicity of cyanines hampers their treatment applications. For that purpose, a known way to increase the

cytoxicity of a dye is to incorporate heavy atoms into the dye structure. In the literature, however, the influence of heavy halogen atoms such as bromine and iodine on the spectral and photochemical properties of heptamethine cyanines remains poorly studied.

The main goal of this research is the development of novel halogenated fluorescent heptamethine cyanine dyes to explore heavy atom impact on these dyes to develop materials for theranostics, photodynamic therapy (PDT), and photoimmunotherapy (PIT) applications.

To achieve the main goal of this work, we intend to carry out the following four tasks:

1. ***To synthesize and investigate spectral properties of iodinated, brominated, and chlorinated heptamethine cyanine dyes*** for the determination of structure-properties relationships with respect to the amount and positions of halogen atoms incorporated into fluorophore structure.

2. ***To obtain iodinated heptamethine cyanine photosensitizers for antimicrobial photodynamic therapy (APDT) applications***: to synthesize a series of the new iodinated heptamethine cyanine photosensitizers (PS) with varying the amount and positions of iodine atoms; to investigate their spectral properties, efficacy to generate reactive oxygen species, cell uptake, and photocytotoxicity on gram-positive (*S. aureus*) and gram-negative (*E. coli* and *P. aeruginosa*) bacterial pathogens in APDT.

3. ***To develop antibody-guided, iodinated heptamethine cyanine photosensitizer for photoimmunotherapy (PIT)***: to synthesize the new hydrophilic iodinated heptamethine cyanine sensitizer (PS), to conjugate it with trastuzumab antibody (Ab), and to investigate the obtained **PS-Ab** conjugate for photodynamic (PDT) and immunotherapy cancer treatment in the mouse xenograft model.

The object of research is the determination of the influence of halogen atoms on spectral, photophysical, and photochemical properties and on the biological impact of heptamethine cyanine fluorescent dyes.

The subject of research is the halogenated organic fluorescent dyes, in particular, heptamethine cyanine dyes modified with chlorine, bromine, and iodine atoms, and their conjugates with monoclonal antibodies.

Research methods utilized in the work include organic synthesis and bioconjugation; mass spectrometry, NMR spectroscopy for determination and confirmation of the structure of synthesized compound; thin-layer chromatography (TLC) and liquid chromatography (LC), including high-performance liquid and gel permeation chromatography (HPLC) for purification and determination of the purity of intermediates and the aimed dyes and conjugates of dyes with monoclonal antibodies; electron absorption and emission spectroscopy for all the dyes and conjugates; quantum chemical calculations; fluorescent microscopy, *in vivo* imaging and flow cytometry for *in vivo* experiments.

Scientific novelty. For the first time we:

➢ synthesized heptamethine cyanine dyes with different number (from 1 to 6) of iodine or bromine atoms in terminal heterocyclic moieties;

➢ studied the structure-properties relationships of halogenated heptamethine cyanine dyes with respect to the amount and positions of halogen atoms;

➢ set how to adjust the key properties (Φ_{Fl} and Φ_{Δ}) for heptamethine cyanine dyes changing the amount and positions of halogen atoms;

➢ evaluated the influence of the number of iodine atoms in heptamethines on the photocytotoxic effect on bacteria;

➢ showed that iodinated heptamethine cyanine dyes are suitable for the treatment and photoinactivation of gram-positive and gram-negative bacteria;

➢ introduced the use of photoimmunotherapeutic "cyanine dye – monoclonal antibody" conjugate and demonstrated its efficacy for cancer theranostics.

The author's personal contribution lies in the systematization of literature data on the dissertation topic, the synthesis, purification, and structural identification of all dyes and their conjugates with monoclonal antibodies; conducting all spectral studies, including measuring electronic absorption and fluorescence spectra, determining quantum yields of fluorescence, extinction coefficients, quantum yields of singlet

oxygen, mathematical analysis, and processing of obtained results; working with mice, including *in vivo* tumor visualization, tumor measurements, and processing of flow cytometry results. Additionally, the author participated in the preparation of materials and drafts of publications. The formulation of tasks, discussion of research results, and formulation of conclusions were performed under the guidance of the scientific advisor, Cand. Sci., Senior Researcher A.L. Tatarets.

The author expresses gratitude to the staff of SSI "Institute of Single Crystals" of the National Academy of Sciences of Ukraine: Dr. Semenova O.M. and Starko S.M. for synthesizing some starting compounds for dye synthesis, and Dr. Semenova O.M. for carrying out experiments with bacteria (*S. aureus, E. coli, P. aeruginosa*); Dr. Zhikol O.A., Dr. Konovalova I.S. and Dr. Shishkina S.V. for conducting quantum-chemical calculations and X-ray structural analysis. The author also thanks the employees of Ariel University: Ms. Tuchinsky H. for assistance in mouse experiments, including intravenous injections of conjugates, feeding mice, and isolating organs, including tumors from mice; Dr. Marks V., Dr. Teller H. for obtaining NMR spectra, and Dr. Pitussi I. for obtaining HRMS spectra.

Approbation of dissertation results: The research results were presented at conferences: 14th Ukrainian Conference of Young Scientists, Students and Post-graduate Students on Current Chemistry Issues (CYS2023), 5th International Caparica Conference on Chromogenic and Emissive Materials (IC3EM2022), 2022, Caparica (Portugal); International Scientific-Practical Conference "Georgian Scientific Pharmacy: Past and Present" (ISPC-2022), 2022, Tbilisi (Georgia); ICRS-PAT Joint Workshop, 2021, Ma'alot-Tarshiha (Israel); 12th International Conference "Electronic Processes in Organic and Inorganic Materials" (ICEPOM-12), 2020, Kamianets-Podilskyi, (Ukraine); Central European Conference on Photochemistry, CECP-2020, 2020, Bad Hofgastein (Austria).

Publications: On the dissertation topic, 10 publications were published, including 4 articles (0 in Ukrainian scientific journals, 4 in foreign periodic publications of other countries included in the international Scopus database), and 6 conference abstracts in collections of international, Ukrainian, and regional conferences.

Connection with scientific programs, plans, topics: The dissertation work was carried out at SSI "Institute of Single Crystals" of the National Academy of Sciences of Ukraine in accordance with the projects of the National Academy of Sciences of Ukraine "Functional materials for biomedical applications based on halogen-containing organic compounds" (2020, state registration number 0120U102660), "Fluorescent cyanine and squaraine dyes with halogen atoms in terminal heterocyclic fragments" (2020, state registration number 0120U101178), and "Synthesis and investigation of halogen-containing polymethine dyes and luminescents" (2022-2024, state registration number 0122U002235).

Practical significance of the obtained results. This study helps in the designing of NIR cyanine dyes with the desired properties for fluorescence imaging, diagnostics, and, especially, photodynamic therapies and theranostics. The developed dyes are effective for photoeradication of bacteria circumventing bacterial drug resistance. The presence of carboxylic function potentially enables further binding of these dyes to various carriers. It has been shown that conjugates based on heptamethine cyanine are effective for *in vivo* diagnostics and cancer treatment through photoimmunotherapy applications. Thus, this study expands applications exploiting NIR cyanine dyes.

Structure of the Work. The dissertation is presented in 143 pages and consists of an introduction, five chapters, conclusions, and a list of references (163 titles), and includes 8 schemes, 48 figures, and 4 tables. The main text of the dissertation comprises 106 pages.

CHAPTER 1

HALOGENATED LONG-WAVELENGTH FLUORESCENT POLYMETHINE DYES: FUNDAMENTAL KNOWLEDGE AND THEIR APPLICATION (LITERATURE REVIEW)

1.1 Overview of fluorescent dyes

Fluorescent dyes are molecules that move into the electronically excited singlet state upon absorption of a quantum of light of a specific wavelength (usually ultraviolet and visible region), and then, during relaxation, rapidly (~10 ns) emit photons with lesser energy [1]. Molecules that absorb energy are not always able to emit it, as they lose energy through other pathways (bonds vibration between atoms, rotation of molecules, etc.). Triplet state population either leads to radiative (phosphorescence) or non-radiative processes. These mechanisms are depicted in Jablonski diagram (Fig. 1.1).
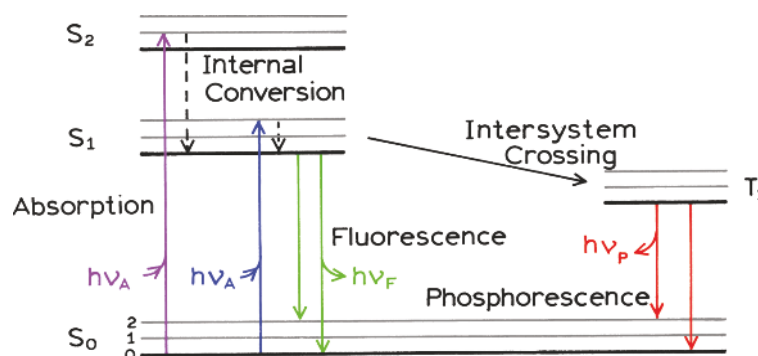
Fig. 1.1. Jablonski diagram [1].

There are several classes of chemical compounds capable of fluorescence [2]. The most well-known among them are polyaromatic hydrocarbons (anthracene, pyrenes), arylindoles [3], coumarins [4], BODIPY (boron-dipyrromethene) derivatives [5], xanthenes (fluoresceins [6], rhodamines [7]), phthalocyanines [8], and polymethines (styryls [9], squaraines [10] and cyanines [11,12]). The introduction of different substituents into the structure of fluorescent dye allows tuning the desired properties of the dye such as shifting spectral maxima, varying solubility in water and

physiological issues, altering photo- and chemical stability, and increasing affinity to certain molecules or organelles.

Nowadays, however, the ability of halogen substituents to affect the spectral and biophysical properties of fluorescent dyes is the least studied. In fact, only dyes from the fluorescein class containing halogen atoms – eosin, erythrosine, and Rose Bengal (Fig. 1.2) – are the most explored and being utilized in staining of cells and tissues [13]. However, the incorporation of halogens into these dyes significantly reduces the quantum yield of fluorescence (Φ_{Fl}) (from 92% for fluorescein to 68% for eosin (4 bromine atoms) and 14% for erythrosine (4 iodine atoms)) [14] and increases triplet state population resulting in the singlet oxygen quantum yield (Φ_{Δ}) enhancement (from 3% for fluorescein to 32% for eosin and 69% for erythrosine) [15]. It is known that the introduction of any heavy atom into the molecule leads to the fluorescence quenching of the dye due to a significant increase in spin-orbit coupling, which enhances intersystem crossing [16]. This process is called "heavy-atom effect" [17]. Not only fluoresceins but also other dye classes such as BODIPY [18], porphyrins [19,20], and anthracenes [21] behave accordingly to this phenomenon increasing Φ_{Δ} and decreasing Φ_{Fl} of these dyes. It should be noted that the chlorine atom has the least effect on Φ_{Δ} and Φ_{Fl}, while the iodine atom has the highest. Fluorine atoms, in general, slightly decrease Φ_{Δ} and Φ_{Fl} [22,23], thus, the dyes containing fluorine atoms are not the scope of this work.

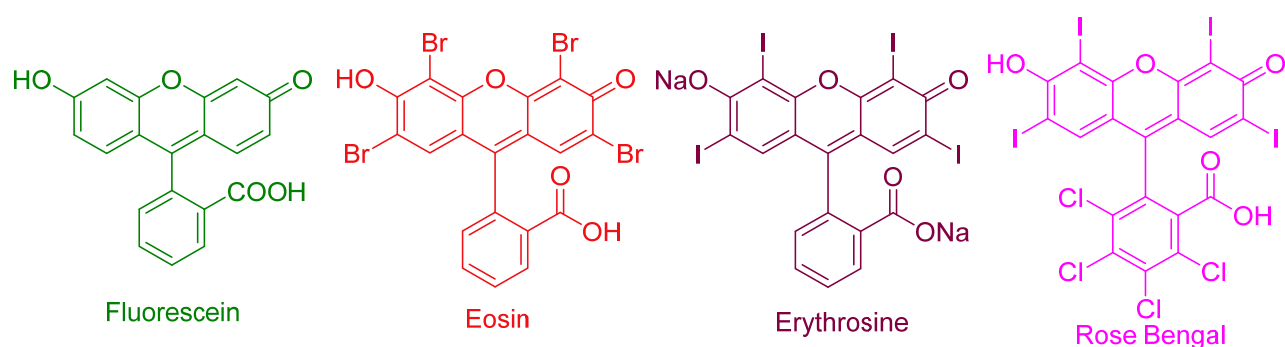**Fig. 1.2.** Structures of fluorescein, eosin, erythrosine, and Rose Bengal.

At the expense of Φ_{Fl} reduction, the incorporation of "heavy" halogen increases the quantum yield of triplet states thus sensitizing the formation of reactive oxygen species, e.g. singlet oxygen, which are cytotoxic. Therefore, such dyes become suitable for the treatment of bacterial and cancer diseases [24].

The main disadvantages of xanthene dyes are relatively short-wavelength absorption and low extinction coefficients. In contrast, polymethine fluorescent dyes (cyanines and squaraines) are more promising due to the considerable flexibility of their spectral, photophysical, and photochemical properties. Currently, polymethines are widely used in various fields: biomedical diagnostics [25,26], photonics [12], pharmacology, and medicine [27]. Nonetheless, the effect of halogen atoms on polymethine dyes has been poorly studied.

1.2 Influence of halogen atoms on the spectral-luminescent characteristics of polymethine dyes

There are several ways to introduce halogen atoms into polymethine dyes. It can be integrated into a polymethine chain, into substituents that do not contribute to the π-electron system of a dye, or into terminal heterocyclic moieties of a dye. Thereby, the impact of the halogen atom will be different depending on its position in a dye structure.

Thus, the incorporation of heavy atoms exactly into the polymethine chain of the dyes (**1.1−1.5**) (Fig. 1.3) leads to a strong blue (**1.3−1.4**) or red (**1.2** and **1.5**) spectral shift and to a significant decrease of Φ_{Fl} for all the halogenated dyes. At the same time, Φ_{Δ} of the dyes **1.3−1.4** increases in case of the presence of iodine or bromine atoms due to the heavy atom effect [28]. Fluorination in the polymethine chain (dye **1.2**), though, caused a major decrease of Φ_{Δ}, thus hampering the formation of reactive oxygen species, thereby they cannot be efficiently used for theranostics applications.

1.1-1.5

1.1: R = H (Φ_{Fl} = 24.1 %, Φ_{Δ} = 0.89 %)
1.2: R = F (Φ_{Fl} = 12.5 %, Φ_{Δ} = 0.09 %)
1.3: R = Br (Φ_{Fl} = 18.4 %, Φ_{Δ} = 4.3 %)
1.4: R = I (Φ_{Fl} = 11.4 %, Φ_{Δ} = 20 %)
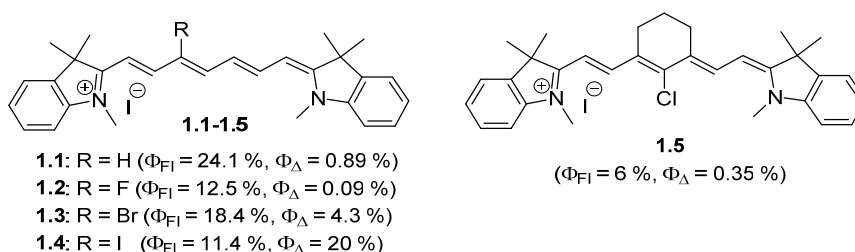
1.5
(Φ_{Fl} = 6 %, Φ_{Δ} = 0.35 %)

Fig. 1.3. Reported polymethine dyes with halogen atoms incorporated into polymethine chain and data of their fluorescence quantum yield (Φ_{Fl}) and singlet oxygen quantum yield (Φ_{Δ}) [28].

On the other hand, the presence of a halogen atom in the substituent in the polymethine chain [29] leads to insignificant spectral changes and causes a decrease of Φ_{Fl} for halogenated heptamethines (compare **1.6** with **1.7-1.11**) (Fig. 1.4). However, authors paid attention to the increase of fluorescence lifetime (τ) with increasing halogen atomic number and called this "anomalous heavy atom effect", explaining longer lifetimes with heavier atoms by restricting conformational changes through steric interactions (vibration and rotation) [29].
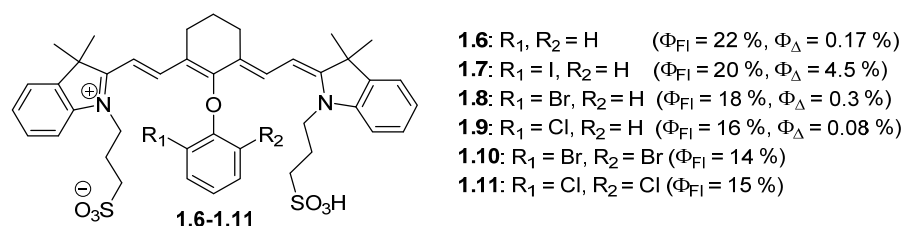

1.6: R_1, R_2 = H   (Φ_{Fl} = 22 %, Φ_Δ = 0.17 %)
1.7: R_1 = I, R_2 = H   (Φ_{Fl} = 20 %, Φ_Δ = 4.5 %)
1.8: R_1 = Br, R_2 = H (Φ_{Fl} = 18 %, Φ_Δ = 0.3 %)
1.9: R_1 = Cl, R_2 = H (Φ_{Fl} = 16 %, Φ_Δ = 0.08 %)
1.10: R_1 = Br, R_2 = Br (Φ_{Fl} = 14 %)
1.11: R_1 = Cl, R_2 = Cl (Φ_{Fl} = 15 %)

Fig. 1.4. Reported polymethine dyes with halogen atoms in the substituent in the polymethine chain and data of their Φ_{Fl} and Φ_Δ [29].

It should be noted that the most controversial is the influence of halogen atoms incorporated into the terminal heterocyclic moieties of heptamethine cyanines. The halogen impact on spectral and photochemical properties of the polymethines has been briefly investigated and limited only with dihalogenated and tetrahalogenated dyes. In general, the appearance of halogen in terminal heterocycle has a minor effect on absorption and emission spectra (up to ~10 nm shift), while Φ_{Fl} and Φ_Δ changes were much more dramatic (Fig. 1.5).

IR783: R_1, R_2 = H   (Φ_{Fl} = 11 %)
1.12: R_1 = H, R_2 = I (Φ_{Fl} = 0.22 %, Φ_Δ = 66 %)
1.13: R_1 = I, R_2 = H (Φ_{Fl} = 0.009 %, Φ_Δ = 44 %)

1.14
(Φ_{Fl} = 48 %, Φ_Δ = 75 %)

1.15: R_1 = H (Φ_{Fl} = 31 %)
1.16: R_1 = Cl (Φ_{Fl} = 34 %)
1.17: R_1 = Br (Φ_{Fl} = 35 %)

1.18: R = H (Φ_{Fl} = 37 %)
1.19: R = Cl (Φ_{Fl} = 47 %)
1.20: R = Br (Φ_{Fl} = 47 %)
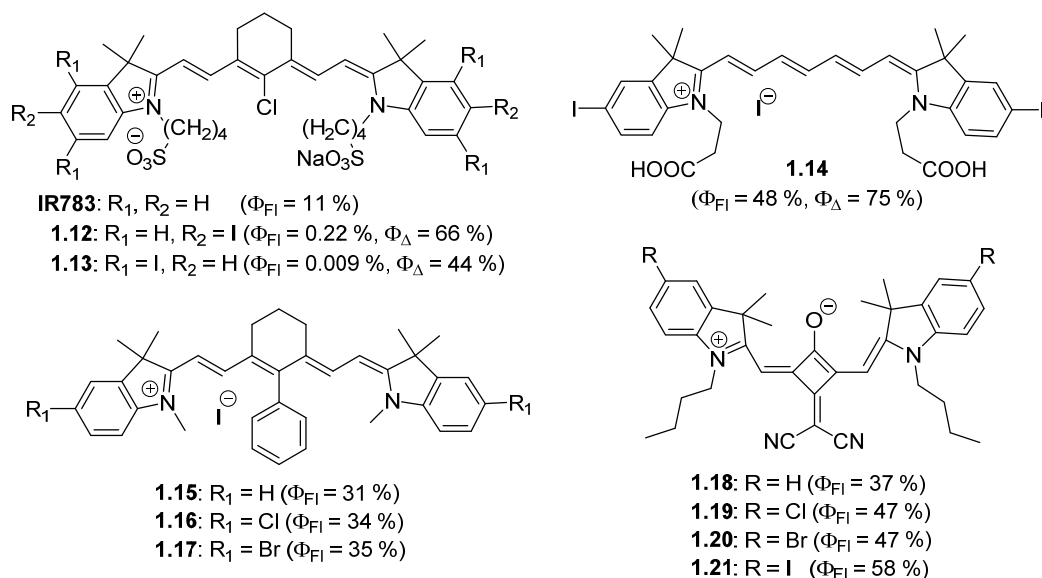**1.21**: R = I (Φ_{Fl} = 58 %)

Fig. 1.5. Reported polymethine dyes with halogen atoms incorporated into terminal heterocyclic moieties of cyanines and data of their Φ_{Fl} and Φ_Δ [31−36].

Thus, some authors [30−32] stated that the Φ_{Fl} significantly decreased for iodinated heptamethines (**1.12-1.14**, Fig. 1.5) compared to common references (**Cy7^{TM}** and Indocyanine green, **ICG**), while other authors [33] observed slight enhancement of Φ_{Fl} for halogenated heptamethines (**1.16-1.17**, Fig. 1.5) compared to non-halogenated dye (**1.15**). This corresponds with the study [34] of another class of polymethine dyes, squaraines (**1.18-1.21**, Fig. 1.5), that revealed a significant enhancement of Φ_{Fl} upon the increase of halogen substituent atomic number. The authors explained the anomalous effect of the heavy atom by the transfer of electron density from halogens to the chromophore nucleus (+M effect), which becomes more pronounced with increasing polarizability of halogen substituents (−I effect). Data on changes in Φ_{Δ} are even less explored. Thus, it is noted that iodine atoms significantly increase Φ_{Δ} (up to 7.9 times) for compounds **1.12-1.14** compared to non-halogenated analog (**IR783**) and **ICG**. But in our opinion these Φ_{Δ} are confusing and overweighted, because it is not clear what is the real value of Φ_{Δ} being used for standard (**ICG**) upon calculation [30,31]. Thus, it is stated that for compound **1.12** Φ_{Δ} equals 66% in PBS, which is 7.9 times higher than **ICG** [30]. However, other sources state that Φ_{Δ} equals only 0.2% in PBS [35] and 0.8% in methanol [36] for **ICG**, which clearly contradicts the above-mentioned data.

Thus, the existing spectral-luminescent data concerning halogen influence on polymethine dyes are insufficient and vague. ***Therefore, a systematic study of the influence of halogen atoms present in th e terminal heterocyclic moieties of heptamethine dyes on their spectral properties is necessary.***

1.3 Halogenated polymethines for biomedical applications

1.3.1 Halogenated polymethines for medical diagnostics and bioimaging

Bioimaging has become an indispensable tool in modern biology and medicine, allowing researchers to visualize and study biological structures and processes at various scales, from the molecular to the whole organism. Among the various imaging modalities available, fluorescence-based imaging stands out for its non-invasive nature and high sensitivity. Due to their versatility, low toxicity, and high extinction

coefficients, NIR polymethines have found applications in a wide range of bioassays and bioimaging techniques, including fluorescence microscopy [26,37−39], flow cytometry [37], fluorescence resonance energy transfer (FRET) assays [25], and molecular imaging [25−27,37−40]. They are also used in tracking and monitoring cellular processes, such as receptor-ligand interactions, gene expression, and protein localization [41,42]. Many NIR polymethines, such as approved by Food and Drug Administration (FDA) **ICG** and **Pafolacianine**, are biocompatible and have low cytotoxicity, making them suitable for use in *in vivo* live-cell imaging studies and surgery (Fig. 1.6) [43−46].
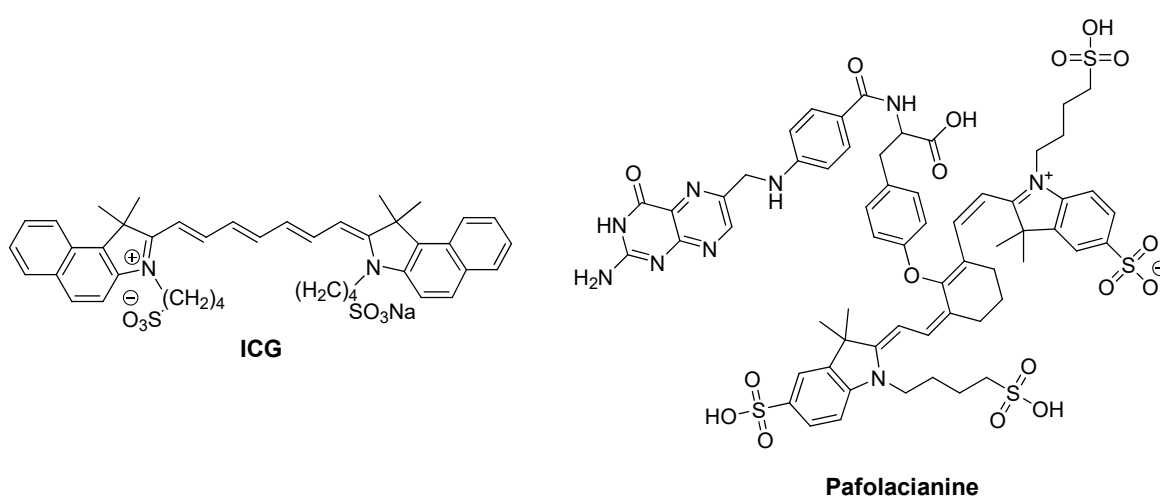
Fig. 1.6. Reported FDA-approved polymethine dyes (**ICG** and **Pafolacianine**).

Polymethine dyes can also be conjugated to various biomolecules (e.g., antibodies, peptides, or nucleic acids) insignificantly compromising the biological activity of the target molecule [42,47].

Halogenated polymethines offer the same benefits as their non-halogenated counterparts and exhibit potential for bioimaging applications, although they remain relatively underexplored. In particular, chlorine-containing NIR dyes of IR series are widely used in tumor imaging (Fig. 1.7) [36,40,37].

Fig. 1.7. Structures of **IR780**, **IR783**, **IR808**, and **IR820** dyes.

Brominated cyanine dye AlexaFluor680 (Fig. 1.8) is suggested to use for tissue distribution studies and protein pharmacokinetics [48], however, authors recommended using it with low dye-to-protein ratios (~0.3).
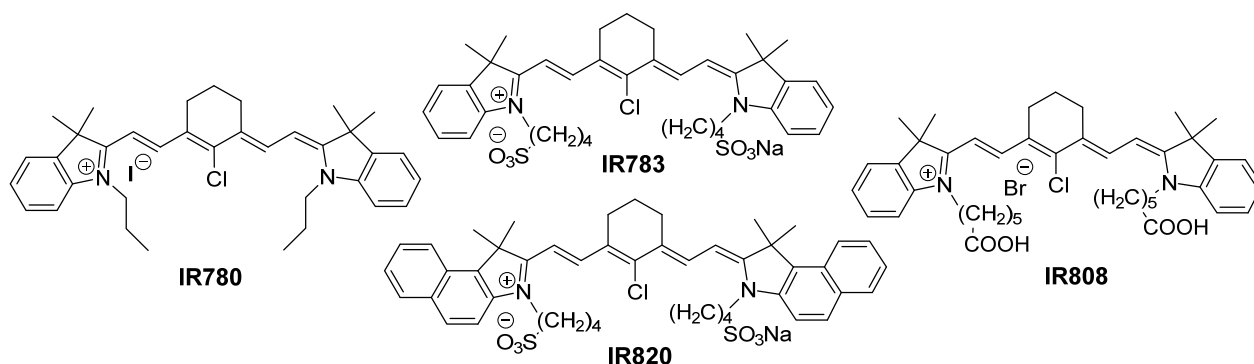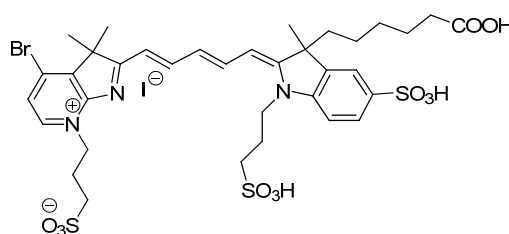

Fig. 1.8. AlexaFluor680 structure.

However, the main focus of current research on bromine- and iodine-containing NIR polymethines is on the use of such dyes as theranostic agents facilitating both *in vivo* imaging and photodynamic therapy [30,31,49]. This aspect will be discussed further in the next chapters 1.3.2 and 1.3.3.

1.3.2 Halogenated polymethines as photosensitizers for photodynamic therapy and bacterial treatment

The new treatment modality employing the heavy atom effect relates to so-called **photodynamic therapy (PDT)**. This method is useful to treat cancer [50−54], bacterial infections (antimicrobial PDT termed APDT [55,56]), and viral diseases [56] among some others [57−59]. This approach is of great importance due to its non-invasiveness and minimal side effects on normal tissues. PDT consists in the administering of a *photosensitizer* to a required region of the body, followed by its light

irradiation [60−63] to generate reactive species that kill cells in the vicinity, in particular, cancer cells and bacteria (Fig. 1.9).
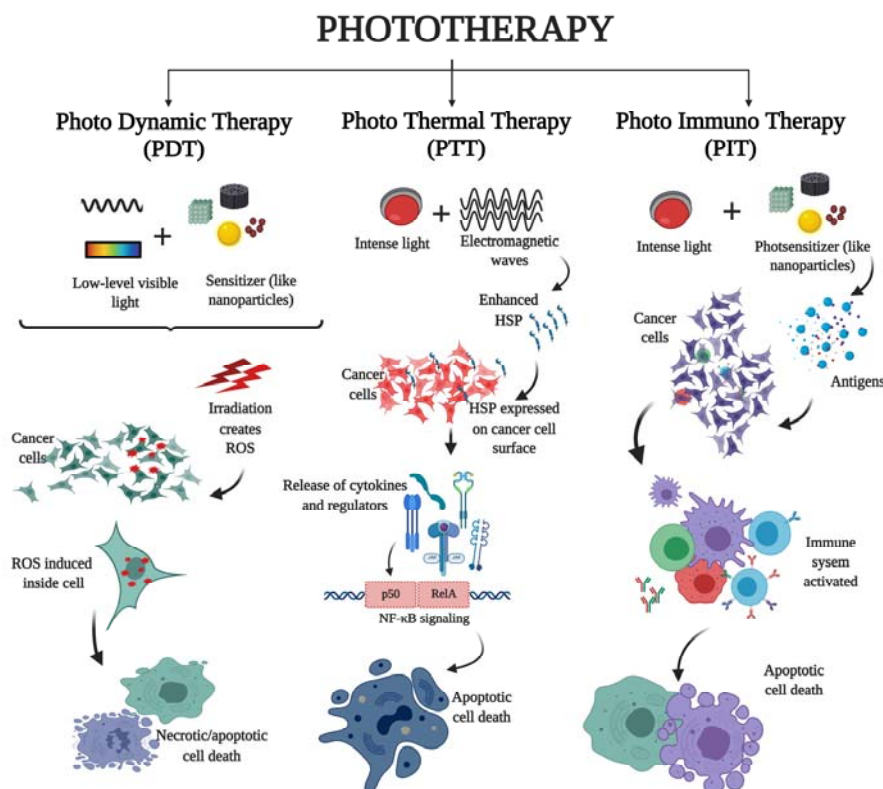
Fig. 1.9. Mechanisms of apoptosis or necrosis induction in cancer cells by employing photosensitizers (photodynamic therapy, PDT) or their conjugates with immune agents, such as antibodies (photoimmunotherapy, PIT) [64].

Photosensitizers are, in general, organic dyes [65,66] or nanoparticles [61,62]. As a result of the light exposure, sensitizing molecules pass to the first excited singlet state and then due to intersystem crossing turn into the long-lived triplet state, which is responsible for the photochemical reactions yielding cytotoxic species such as singlet oxygen ($^1O_2$), superoxide anion ($O^{2-\bullet}$), hydroxyl radical ($^\bullet OH$), hydrogen peroxide (H_2O_2), and organic radicals among others [67]. Thus, the efficient population of the triplet state plays an important role in their cytotoxicity. The probability of intersystem crossing can be increased by the introduction of heavy atoms in the sensitizer molecule, which facilitates the generation of reactive oxygen species (ROSs) and other cytotoxic products (Fig. 1.10).

Fig. 1.10. Type I and type II PDT mechanisms [68].

Most of the PDT photosensitizers approved by the FDA are porphyrin-based dyes that predominantly absorb light in the short wavelength range but insufficien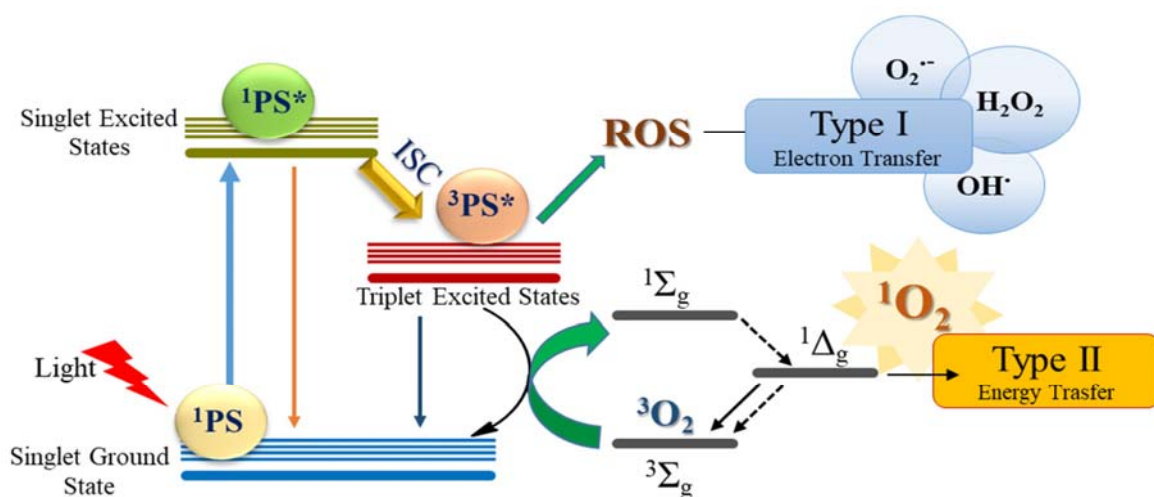tly absorb light in the biologically transparent and, thus, therapeutically important red and near-infrared (NIR) spectral region [69,70]. The extinction coefficients (ε) of these PSs in the red region are, however, relatively low, (e.g. 3,500 $M^{-1}cm^{-1}$ for Photofrin [71], 30,000 $M^{-1}cm^{-1}$ for Foscan, 42,000 $M^{-1}cm^{-1}$ for Lutrin [72], and 55,000 $M^{-1}cm^{-1}$ for Chlorin e6 [73], which is a serious limitation for their clinical applications, in particular, in deeper tumor and metastases treatment [72,74].

In recent years, special attention was paid, therefore, to non-porphyrin-based PSs such as phthalocyanines [75−77] and cyanines [78−80]. Compared to porphyrins, heptamethine cyanine dyes such as **Cy7** exhibit much stronger absorption in the longer-wavelength (NIR) region with extinction coefficients in the same order as phthalocyanines, i.e. about 200,000−250,000 $M^{-1}cm^{-1}$. Due to the bright fluorescence, low cytotoxicity, and minor phototoxicity, these dyes are widely used as reporters in numerous biomedical applications including *in vivo* imaging [40−39,50]. Although the phototoxicity of cyanines is relatively low, their ability for effective NIR light absorption makes them promising structures for the development of highly efficient PSs. A well-known example of heptamethine is **ICG** (ε = 230,000 $M^{-1}cm^{-1}$) [81], which has been FDA-approved for both *in vivo* diagnostics and treatment of several types of cancer [43−45].

To date, there is a growing interest in *halogenated* cyanines as favorable photosensitizers [30−32,82]. The incorporation of *heavy atoms*, such as iodine and bromine, is known to lead to an increase in the probability of intersystem crossing (ISC) from the singlet to the triplet state due to enhanced spin-orbit coupling (Fig. 3) resulting in the elevated rates of cytotoxic species generation [83], in particular, singlet oxygen ($^1O_2$). The singlet oxygen quantum yield (Φ_Δ) serves as a preliminary indicator for an increase in dye phototoxicity. A series of publications have demonstrated that Φ_Δ of the iodinated heptamethines is several times higher compared to their non-halogenated counterparts, **Cy7** and **ICG**, making these dyes promising PSs [30−32]. For instance, the introduction of iodine atoms causes a noticeable increase in the ability of cyanine dyes for photo-killing gram-positive and gram-negative pathogenic bacteria [84,85].

1.3.3 Halogenated polymethines for targeted drug delivery and theranostics

In principle, halogenated polymethine photosensitizers can act simultaneously as the cytotoxic drug and as the fluorescent reporter for cancer diagnostics and treatment. However, current PSs suffer not only from insufficient efficacy, in particular, upon photoexcitation within the NIR spectral range (as we discussed above), but also from lack of specificity to targeted abnormal cells and side effects. Similar to the conventional drugs, this issue can be solved by the conjugation of PSs with target-specific carriers for targeted drug delivery, which improves the safety of treatment [86−88].

Carriers are molecules, groups, or species facilitating effective transportation of drugs to the targeted site [89]. Ideally, carriers should be highly specific to the target, nontoxic, stable during circulation in the bloodstream to mitigate drug side effects until a carrier reaches the target, and biodegradable, i.e. decompose in the organism avoiding accumulation that may lead to cytotoxicity [89]. Also, carriers should not trigger immune response in the bloodstream [90].

Up to now, a number of different kinds of carriers have been developed to target these abnormal cells. As the ***cancer-specific carriers***, antibodies [91], peptides [92], liposomes [93], dendrimers [94], hydrogels [95], nanoparticles (NPs such as quantum

dots [96], magnetic NP [97], inorganic NP [98]), and polymers [99] are used. *Antibodies* have certain advantages over other carriers due to their high affinity and specificity to many antigens of interest [91,100]. Antibodies are not recognizable as a threat by the immune system (e.g. humanized antibodies [101]), and have long circulatory half-life in the bloodstream [91]. In addition, antibodies are fully biodegradable [102]. Importantly, antibodies act not only as carriers but also as *immunotherapeutic agents*, which is due to their ability to block receptor-ligand interactions, involve proteins and cells of the innate immune system and, in doing so, mediate complement-dependent cytotoxicity, antibody-dependent cellular cytotoxicity, and antibody-dependent cellular phagocytosis [91]. Thus, antibodies work simultaneously as immunotherapeutic agents to stimulate the immune system to attack tumors [103−105] and as the carriers for targeted photosensitizer delivery to specific cancer cells [106−108].

Arming PSs with tumor-specific antibodies to yield **PS−Ab** conjugates ensures selective delivery of the PSs to cancer cells, which increases treatment efficacy and reduces side effects on normal organs [109,110].

Importantly, the conjugation of PSs with immunotherapeutic agents such as antibodies expands PSs applications to **photoimmunotherapy** (**PIT**). PIT synergistically combines two different modalities: photodynamic therapy (PDT) [109] with immunotherapy, based on the modulation of the immune system with certain compounds (e.g. antibodies [111], antibody-drug conjugates [112], cytokines [113], and cells [114,115]).

Some requirements for the targeting PSs used for PIT differ from those for the conventional, non-targeting, dyes. First, the targeting photosensitizers must be equipped with *reactive groups* enabling their conjugation with a carrier. Notably, mono-reactive dyes containing *one* reactive group are preferable to the bis- and poly-reactive dyes because they prevent cross-linking, where two or more molecules are connected with each other through the dye bridge. Second, the targeting PSs should be *hydrophilic* to reduce their aggregation on a carrier [116], while the conventional sensitizers are relatively *lipophilic*, which improves their uptake by malignant cells [72]. The reason is

that, in general, the dye aggregation in solutions or when bound to a carrier decreases the extinction coefficients, fluorescence quantum yields, and the yields of the cytotoxic species generation [11,117−119]. A known method for avoiding this issue consists in the introduction of hydrophilic moieties such as negatively charged sulfonic [116,119] or positively charged trialkylammonium groups [120].

The above requirements imply the synthesis of asymmetric dyes, which is possible but difficult to realize with porphyrins or phthalocyanines. This is likely the reason why **IRdye700DX**, the sole commercially accessible phthalocyanine derivative, has been extensively studied as the photosensitizer for photoimmunotherapy thus far. [121−125]. Despite the synthesis of appropriately functionalized cyanines is a more straightforward process, which is an additional advantage of these dyes, they have not been investigated for PIT applications yet.

Importantly, as organic dyes, photosensitizers can provide fluorescent signal for visualization and monitoring of their distribution in the body, accumulation in the targeted tissue, and thus for diagnostics.

To conclude the most challenging task for theranostics applications including PIT is to develop suitable photosensitizers simultaneously having a reactive group for binding to a target-specific carrier such as an antibody, high cytotoxicity upon light exposure, sufficient hydrophilicity to avoid aggregation, and reasonable brightness for bioimaging.

1.4 Summary to chapter 1

Polymethine dyes exhibiting high extinction coefficients, fluorescence quantum yields, and brightnesses within the NIR region are widely used as reporters in many biomedical assays, imaging applications, and as theranostics agents. The development of a novel class of fluorophores, halogenated polymethine dyes, potentially allows us to expand the variety of available fluorophores capable of either visualization and/or therapeutic effect. For that purpose, it is important to understand the impact of halogen atoms on the spectral-luminescent properties. However, the existing spectral-luminescent data on the effect of halogen atoms on polymethine dyes are scant

and vague. Therefore, a systematic study of the influence of halogen atoms on the spectral properties of polymethine dyes is crucial for the fine-tuning of such dyes.

Due to intensive absorption in the NIR, these dyes are considered promising photosensitizers (PSs) for PDT and APDT. However, the low phototoxicity of cyanines is a major limitation for their photodynamic therapy utility. One of the ways to enhance the phototoxicity of polymethines is the incorporation of heavy atoms. Besides, increased phototoxicity of the dyes is only one of the requirements for more sophisticated applications, such as targeted drug delivery and theranostics. Thus, the most challenging task for photoimmunotherapy is to develop suitable PSs simultaneously bearing a reactive group for binding to a target-specific carrier such as an antibody and having high cytotoxicity upon light irradiation, sufficient hydrophilicity to avoid aggregation and reasonable brightness for bioimaging. Although the *halogenated cyanines* may expand the scope of current PSs, there is an explicit lack of research in this field. Thereby, there is a need for the development of new effective photosensitizers and antibody−PS conjugates for APDT, PIT, and theranostics applications.

CHAPTER 2
SYNTHESIS OF HALOGENATED HEPTAMETHINE CYANINE DYES AND THEIR INTERMEDIATES

This chapter focuses on the development of an efficient synthetic pathway towards the synthesis of heptamethine cyanine dyes containing halogen atoms in terminal heterocyclic moieties, including the synthesis and structure confirmation of all the intermediates.

2.1 Synthesis of starting materials for heptamethine cyanine dyes

Halogenated phenylhydrazines **2.3b-f** were formed by a one-pot diazotization reaction of corresponding anilines **2.1b-f** with $NaNO_2$ in sulfuric acid (nitrosylsulfuric acid) or in 20% aqueous HCl followed by the reduction of obtained diazonium salts **2.2b-f** with tin(II) chloride in HCl (Scheme 2.1). Phenylhydrazinium salts (**2.3b-f**) precipitated out of the reaction mixture during the reaction. Precipitate was filtered off, washed with 1 M aqueous solution of HCl and water, dried, and then used without additional purification.
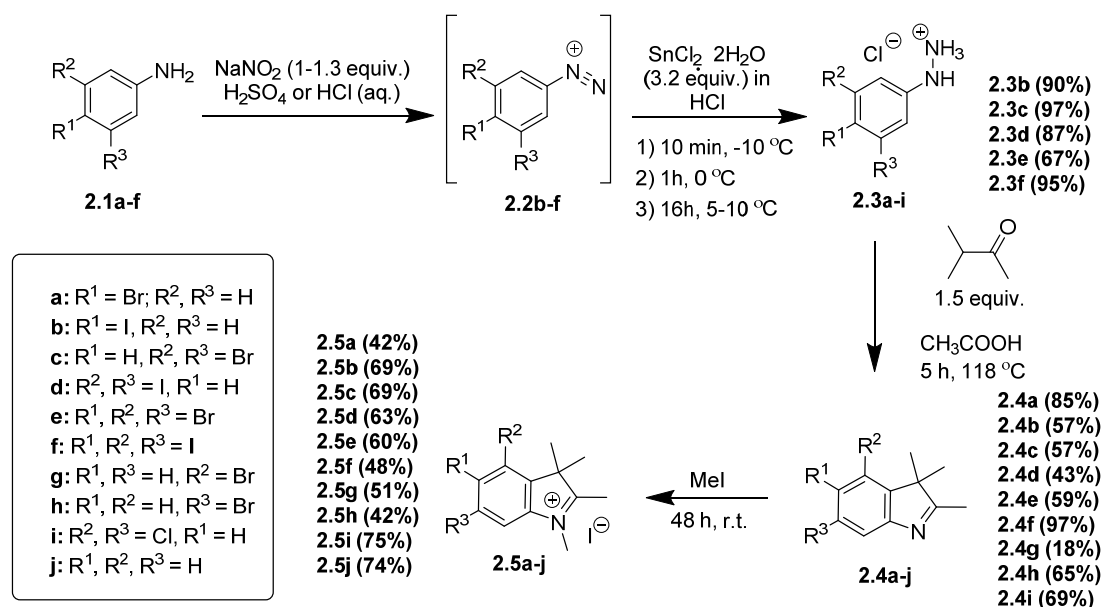
Scheme 2.1. Synthetic route toward indolenines quaternized with iodomethane.

It is worth mentioning that diazotization of 4-iodoaniline (**2.1b**) was carried out in aqueous HCl resulting in a high synthetic yield (90%). However, the attempt to

perform diazotization of less reactive 3,4,5-tribromoaniline (**2.1e**) in the same conditions resulted in a reduced yield (67%). Therefore, we employed stronger conditions, carrying out the diazotization reaction in anhydrous sulfuric acid instead of aqueous HCl for other halogenated anilines (**2.1c**, **2.1d**, **2.1f**), to obtain corresponding halogenated phenylhydrazines in good yields (87−97%). The structures of phenylhydrazines **2.3b-f** were confirmed by ^{1}H-NMR and ESI-MS analysis. Other halogenated phenylhydrazines (**2.3a**, **2.3g**, and **2.3i**) were commercially available and purchased from *TCI* chemicals.

Heterocyclization of halogenated phenylhydrazines **2.3a-i** with 3-methyl-2-butanone was performed in acetic acid under reflux for 5 hours. To purify the product, acetic acid was evaporated, and the residue was treated with 5% aqueous Na_2CO_3 to get pH around 9, and then product was extracted with benzene. The organic layer was collected, evaporated, and dried to yield halogenated indolenines **2.4a-i** in moderate to high synthetic yields (43−97%). It should be noted that indoles **2.4g** and **2.4h** were obtained as the mixture upon heterocyclization of 3-bromophenylhydrazine **2.3g**. To isolate both products from the mixture, we performed preparative column chromatography on Silica gel 60 followed by chromatography on RP-18 resin. Silica gel 60 column (CHCl$_3$−MeOH or ethyl acetate−hexane) and RP-18 column with commonly used solvents (ACN or MeOH−H$_2$O + 0.1% acetic acid) did not allow us to separate these products. Therefore, we selected the appropriate solvent mixture for RP-18 column (ACN−water (+0.05% acetic acid)−ethyl acetate from 45:50:10 to 65:25:20, v./v./v.) for the isolation of both **2.4g** and **2.4h** products in 18% and 65% synthetic yields, respectively.

Structures of indoles **2.4a-i** were confirmed by ^{1}H-NMR analysis, where two new singlet signals from methyl groups at 2.25−2.18 ppm and 1.39−1.22 ppm appeared. Also, changes in aromatic protons positions were substantial due to cyclization. For instance, 5-iodo-2,3,3-trimethyl-3*H*-indole **2.4b** had the singlet signals at 7.80 and doublets at 7.60 and 7.23 ppm of aromatic protons (Fig. 2.1) compared to doublet signals at 7.58 and 6.81 ppm for 4-iodophenylhydrazine (**2.3b**).
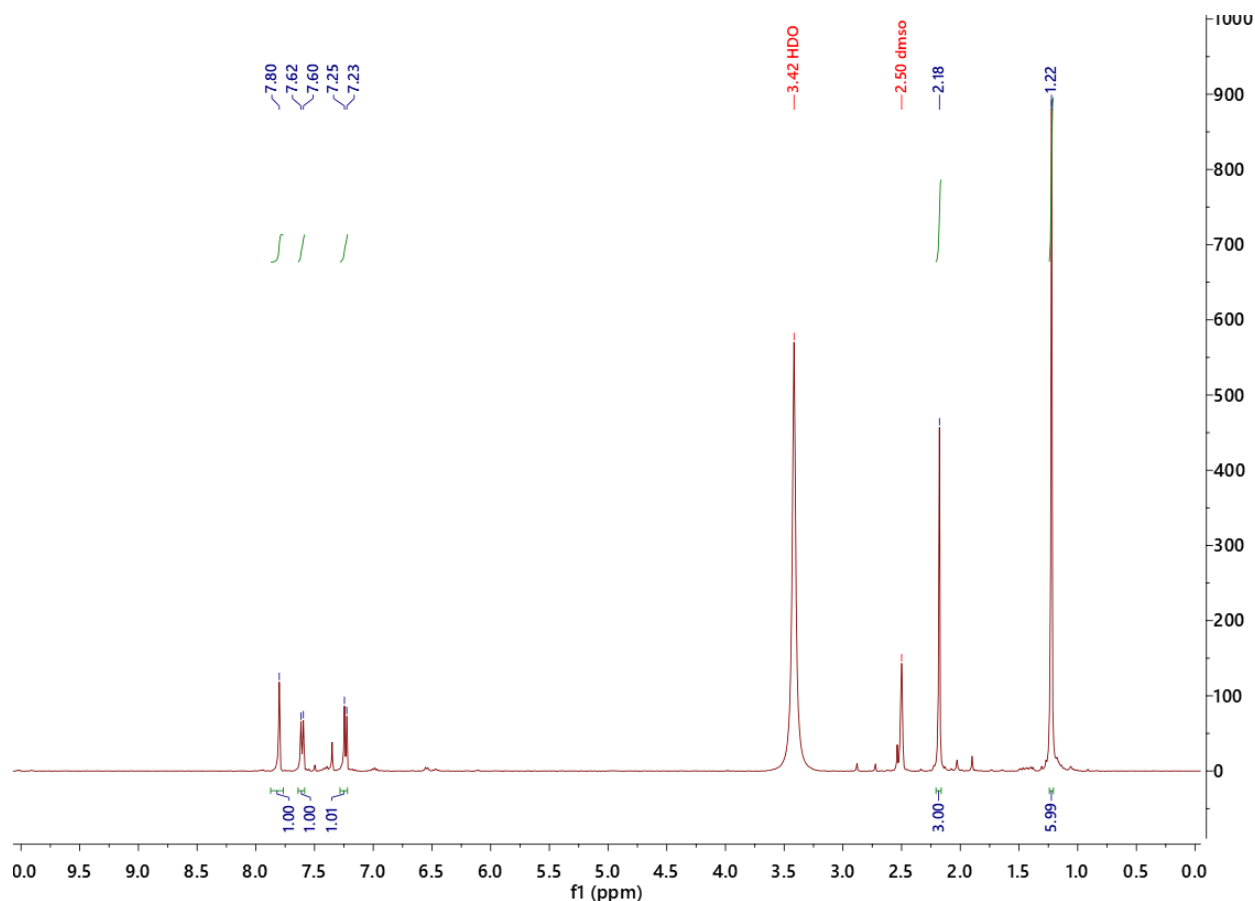
Fig. 2.1. ^{1}H-NMR of 5-Iodo-2,3,3-trimethyl-3*H*-indole (**2.4b**) in DMSO-*d₆*.

Indoles **2.4g** and **2.4h** also can be clearly characterized by ^{1}H-NMR. 4-Bromo-2,3,3-trimethyl-3*H*-indole **2.4g** has 2 doublets at 7.46, 7.36 ppm and triplet at 7.25 ppm, while 6-bromo-2,3,3-trimethyl-3*H*-indole **2.4h** has 2 doublets at 7.41, 7.38 ppm and singlet at 7.61. 2,3,3-Trimethyl-3*H*-indole **2.4j** was commercially available and purchased from *TCI* chemicals.

N-alkylation of the indoles **2.4a-j** was carried out over 48 h at room temperature (r.t.) with the excess of iodomethane (MeI), which was used as the reagent and the solvent. The reaction mixture, which solidified during this time, was triturated with diethyl ether and dried to provide quaternizated salts **2.5a-i** in moderate yields (42−75%). Structures of indolenines **2.5a-j** were confirmed by ^{1}H-NMR spectrum, where a new singlet signal, corresponding to the N<u>CH</u>₃ group appeared at 3.95-3.91 ppm, as it is shown for 5-iodo-1,2,3,3-tetramethyl-3*H*-indol-1-ium iodide **2.5b** (Fig. 2.2) [126].
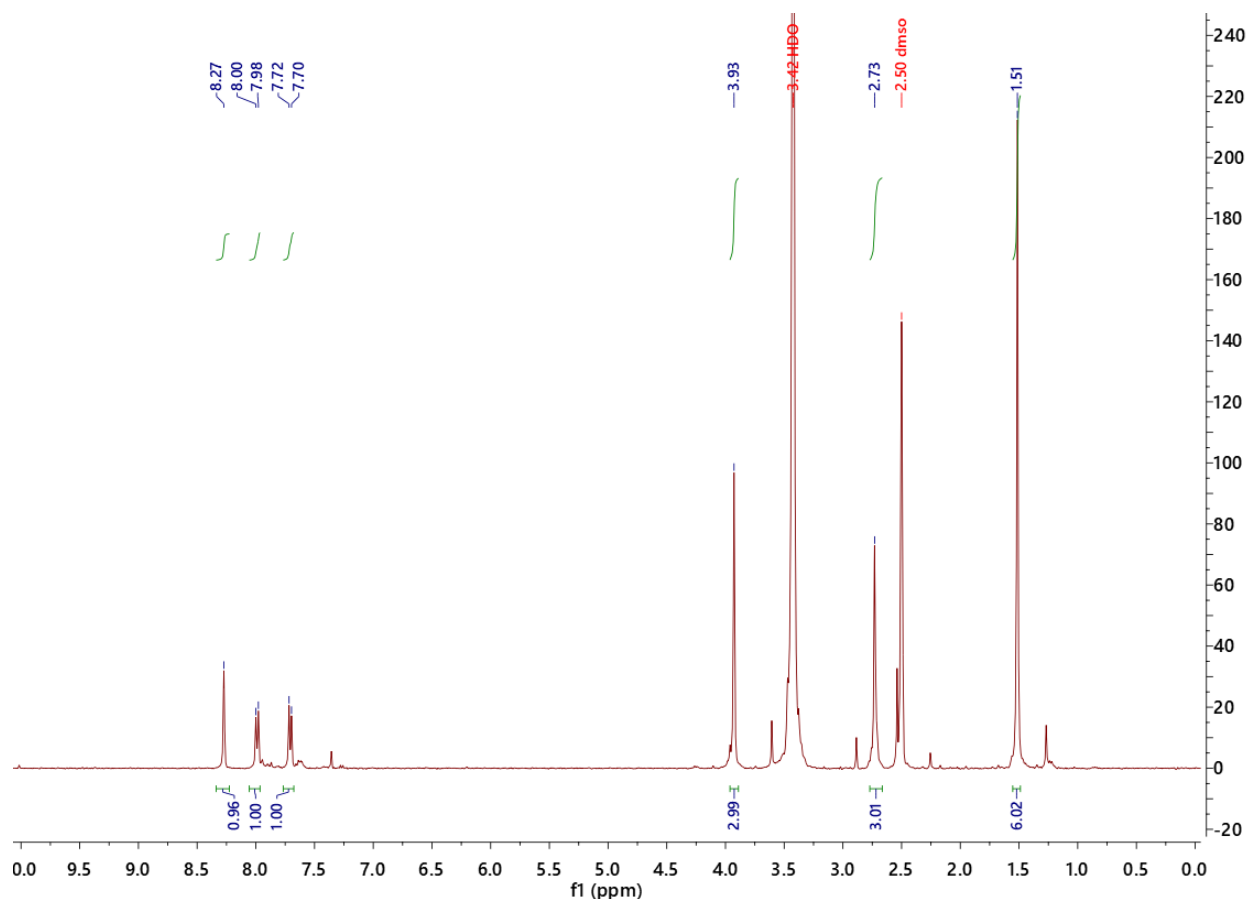
Fig. 2.2. ^{1}H-NMR of 5-iodo-1,2,3,3-tetramethyl-3H-indol-1-ium iodide **2.5b** in DMSO-d_6.

In order to receive indolenines containing carboxylic acid group, N-alkylation of the indolenines **2.4b**, **2.4f**, and **2.4j** was carried out with the excess of 6-bromohexanoic acid (Scheme 2.2) in the absence of solvent.
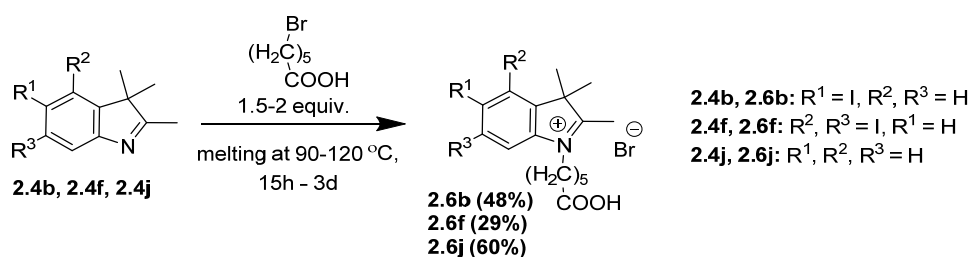
Scheme 2.2. Synthesis of the indolenines quaternized with 6-bromohexanoic acid.

We found out that melting of indolenines with 6-bromohexanoic acid provided the best synthetic yields among other tested reaction conditions, such as heating in solvents (acetonitrile or benzene). Nonetheless, time and temperature were dependent

on the compound. Thus, non-halogenated compound **2.6j** was obtained in moderate yield (60%) at 120 °C over 15 h. However, melting of iodinated indoles **2.4b** or **2.4f** with 6-bromohexanoic acid at that temperature (120 °C) resulted in partial elimination of iodine atom. To avoid this issue, we decreased the reaction temperature to 90 °C and increased time to 2−3 days to obtain **2.6b** or **2.6f** in 48% and 29% yields, respectively. Viscous products were washed 3 times with benzene, then with acetone, and dried to receive powder of **2.6b**, **2.6f**, **2.6j** and used them as is for further synthesis.

Similarly to previous alkylated indolenines, **2.6b, 2.6f,** and **2.6j** were confirmed by ^{1}H-NMR spectrum, where a new triplet at 4.45-4.41 ppm, corresponding to the NC$\underline{H}_2$ group appeared, as well as other peaks corresponding to methylene protons (C$\underline{H}_2$-COOH) at 2.23-2.20 ppm.

In order to receive indolenines containing triethylammonium moiety, *N*-alkylation of the indole **2.4b** was carried out with the 3-bromo-*N,N,N*-triethylpropan-1-aminium bromide in acetonitrile at reflux over 2 days to give desired product **2.7** (Scheme 2.3).
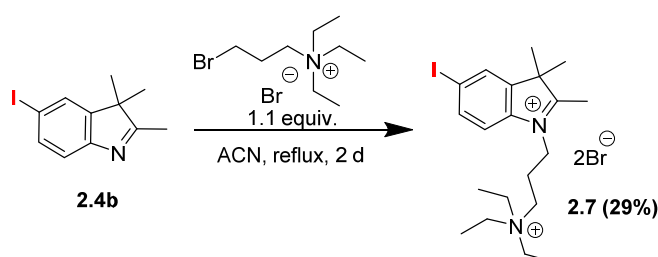

Scheme 2.3. Synthesis of the 5-iodo-2,3,3-trimethyl-1-(3-(triethylammonio)propyl)-3H-indol-1-ium dibromide **2.7**.

Compound **2.7** was obtained in 29% yield by precipitation from the reaction mixture with benzene, washing with diethyl ether, and drying. ^{1}H-NMR spectrum of compound **2.7** showed multiplet signal at 3.25 ppm and triplet at 1.18 ppm corresponding to triethylammonium group.

In order to receive indolenines containing sulfo group, which imparts high water-solubility to an organic compound, *N*-alkylation of the indole **2.4d** was carried out with the 1,3-propane sultone in toluene at reflux over 15 h (Scheme 2.4).
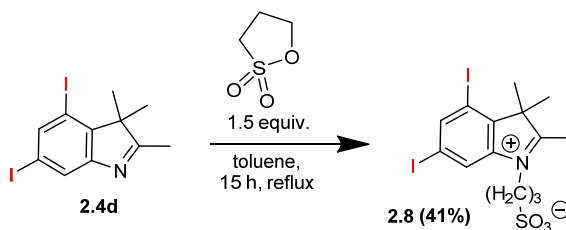
Scheme 2.4. Synthesis of the 3-(4,6-diiodo-2,3,3-trimethyl-3H-indol-1-ium-1-yl)propane-1-sulfonate **2.8**.

The resulting viscous precipitate was filtered, dissolved in methanol, and precipitated with diethyl ether. Reprecipitation step was repeated several times till the product became powder. Then, the product was dried to obtain 3-(4,6-diiodo-2,3,3-trimethyl-3H-indol-1-ium-1-yl)propane-1-sulfonate (**2.8**) in 41% yield. The structure was confirmed by ^{1}H-NMR (Fig. 2.3) indicating characteristic signals: triplet at 4.59 ppm of N$\underline{CH_2}$ and triplet at 2.62 ppm of $\underline{CH_2}SO_3^-$.
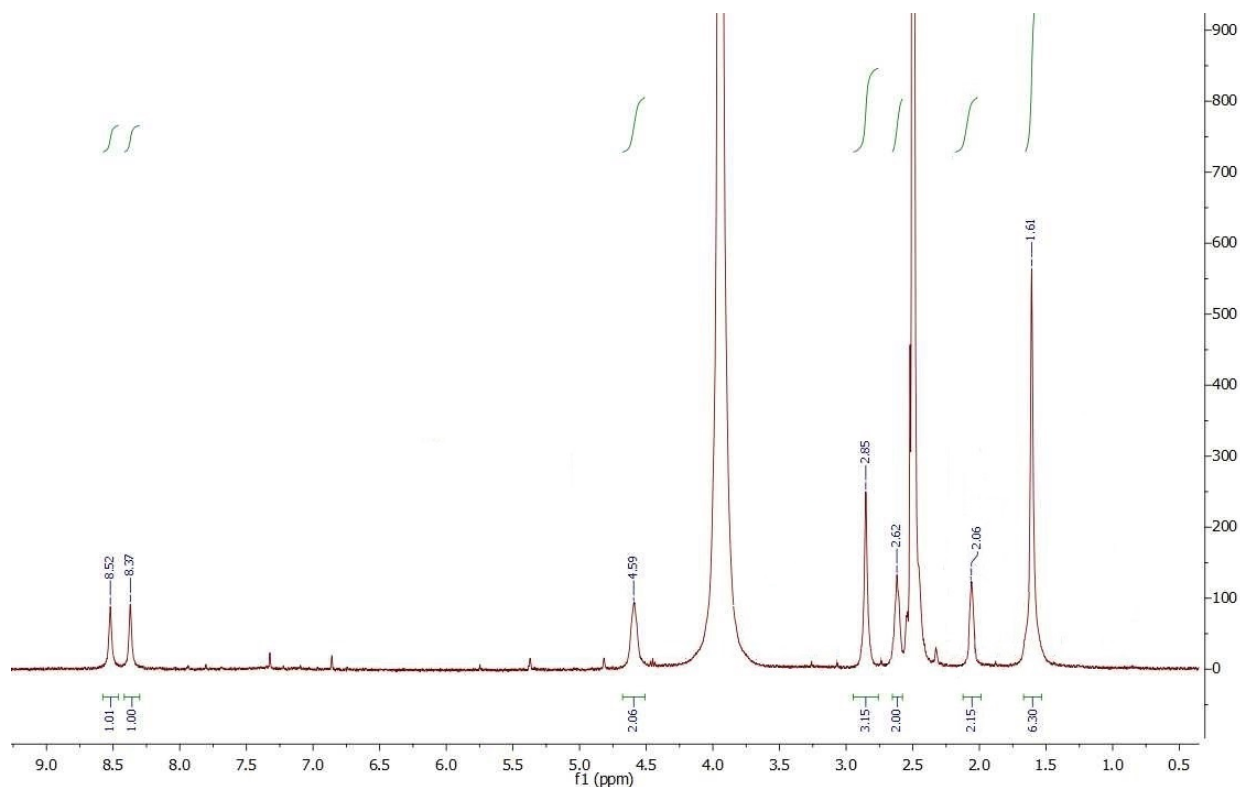
Fig. 2.3. ^{1}H-NMR of compound **2.8** in DMSO-d_6.

Additionally, we confirmed the structure of **2.8** by ^{13}C-NMR, which was done in TFA-*d* due to insufficient compound solubility in other solvents. As expected, carbons conjugated with iodine atoms demonstrated chemical shifts at 95.44 ppm and 91.70 ppm, while other aromatic carbons were in the range of 201.46–126.56 ppm.

The molecular structures of 4,6-dibromo-2,3,3-trimethyl-3H-indole (**2.4c**) and 4,6-dibromo-1,2,3,3-tetramethyl-3H-indol-1-ium iodide (**2.5c**) were also confirmed by X-ray diffraction analysis (Fig. 2.4) [127].

2.4c   **2.5c**
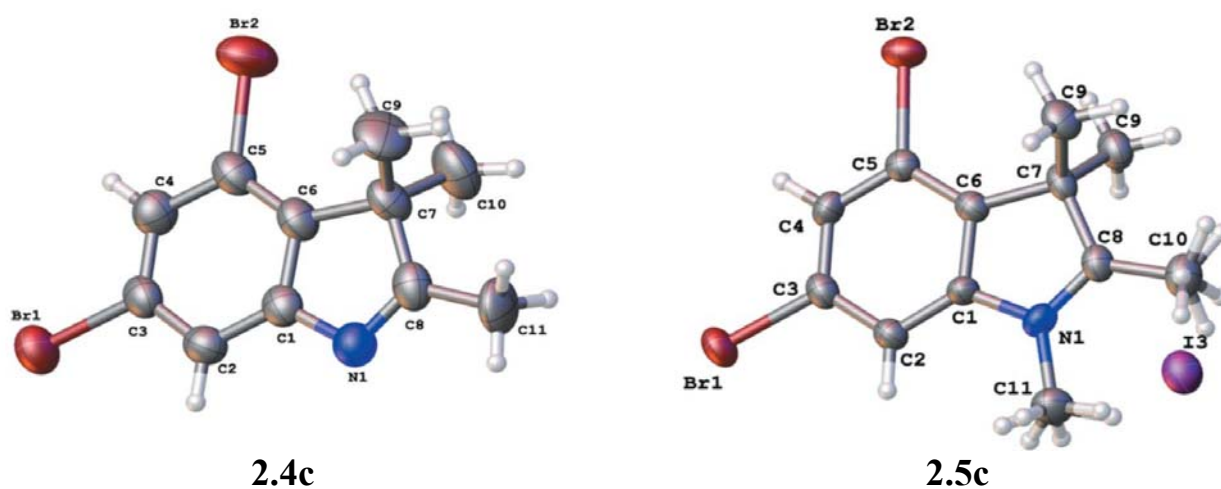
Fig. 2.4. Molecular structure of compounds **2.4c** and **2.5c** by X-Ray diffraction analysis [127].

Light-brown crystals of **2.4c** were obtained after recrystallization from acetonitrile, while beige crystals of **2.5c** were obtained as the result of the synthesis of **2.4c** with the excess of iodomethane in benzene solution. In the crystal, 4,6-dibromo-2,3,3-trimethyl-3H-indole (**2.4c**) exists as one neutral molecule in the asymmetric unit (Fig. 2.8). The quaternized molecule **2.5c** exists as a salt with an iodine anion in the crystal phase (Fig. 2.8). All atoms of the quaternized cation **2.5c**, with exception of the C9 atom and the hydrogen atoms of the C10—H3 and C11—H3 methyl groups are located in a special position relative to the symmetry plane. In compound **2.5c**, the positive charge is localized on the nitrogen atom, which is caused by its quaternization. The N1—C11 bond is shortened to 1.460 (10) Å in comparison with the mean value of 1.485 Å for an N—Csp^3 bond [128].

For the synthesis of halogenated non-symmetrical hydrophilic and reactive cyanine dye, it was necessary to obtain corresponding non-halogenated indolenine containing sulfonic acid and carboxy group. We started from commercially available 4-hydrazinobenzenesulfonic acid (**2.3k**), which was reacted with 7-methyl-8-oxononanoic acid in acetic acid at reflux for 3 h to yield 6-(2,3-dimethyl-5-sulfo-3H-indol-3-yl)hexanoic acid in a good yield (**2.4k**). After evaporation of acetic acid, the product was triturated with diethyl ether and filtered off. Obtained **2.4k** was dissolved in methanol and alkalized with a methanolic solution of potassium hydroxide to get potassium salt of **2.4k**, which further quaternized with 1,3-propane sultone in sulfolane at reflux for 5 h (Scheme 2.5).
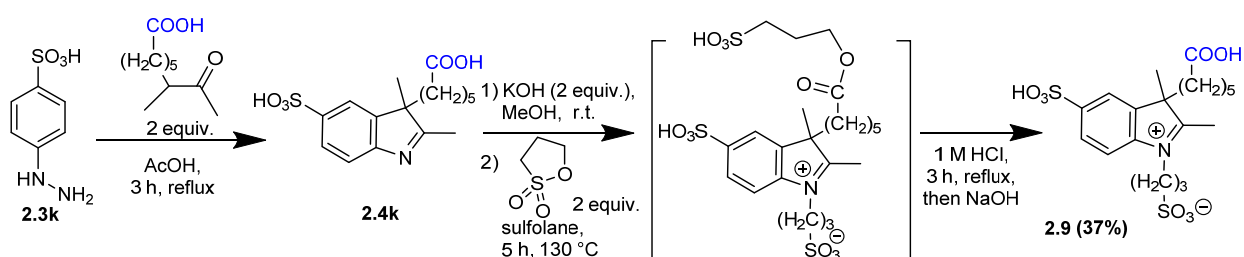
Scheme 2.5. Synthetic pathway of 3-(3-(5-carboxypentyl)-2,3-dimethyl-5-sulfo-3H-indol-1-ium-1-yl)propane-1-sulfonate (**2.9**).

We observed that during this reaction not only *N*-alkylation but also esterification of the carboxylic group during the reaction was occurred. Therefore, we performed acidic hydrolysis in 1 M aqueous HCl at reflux for 3 h to hydrolyze ester moiety. Then, the reaction mixture was neutralized with NaOH and purified on RP-18 column using water as eluent to obtain 3-(3-(5-carboxypentyl)-2,3-dimethyl-5-sulfo-3H-indol-1-ium-1-yl)propane-1-sulfonate (**2.9**) in 37% synthetic yield. The structure of compound **2.9** was confirmed by ^{1}H-NMR (Fig. 2.5) and ^{13}C-NMR, as described in chapter 5.
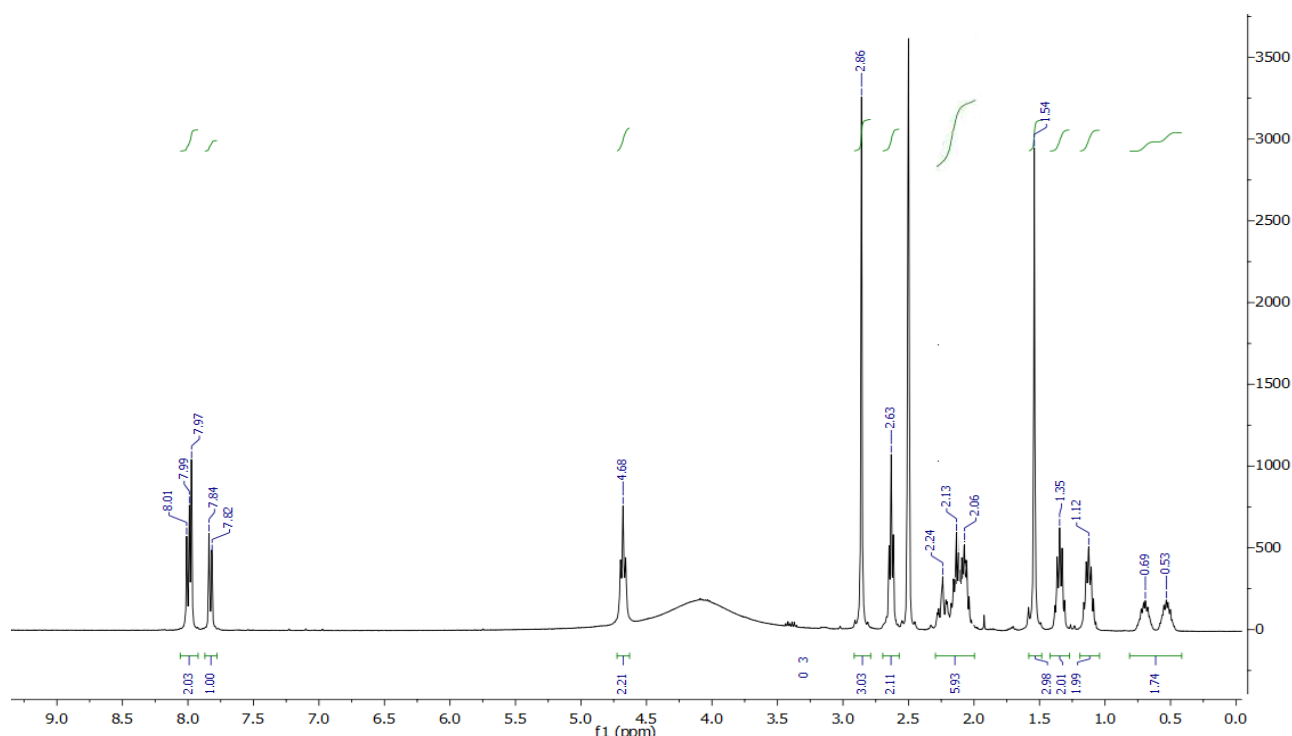
Fig. 2.5. ^{1}H-NMR of compound **2.9** in DMSO-d_6.

2.2 Synthesis of halogenated heptamethine cyanine dyes

We synthesized symmetrical cyanine dyes of **xHal$_n$-HITC** series with various quantities of iodine, bromine, and chlorine atoms by the route outlined in Scheme 2.6.

2.5a, 5Br$_2$-HITC: R^1 = Br; R^2, R^3 = H **(58%)**
2.5b, 5I$_2$-HITC: R^1 = I, R^2, R^3 = H **(50%)**
2.5c, 4,6Br$_4$-HITC: R^1 = H, R^2, R^3 = Br **(48%)**
2.5d, 4,6I$_4$-HITC: R^2, R^3 = I, R^1 = H **(55%)**
2.5e, Br$_6$-HITC: R^1, R^2, R^3 = Br **(82%)**
2.5f, I$_6$-HITC: R^1, R^2, R^3 = I **(32%)**
2.5g, 4Br$_2$-HITC: R^1, R^3 = H, R^2 = Br **(33%)**
2.5h, 6Br$_2$-HITC: R^1, R^2 = H, R^3 = Br **(64%)**
2.5i, 4,6Cl$_4$-HITC: R^2, R^3 = Cl, R^1 = H **(48%)**
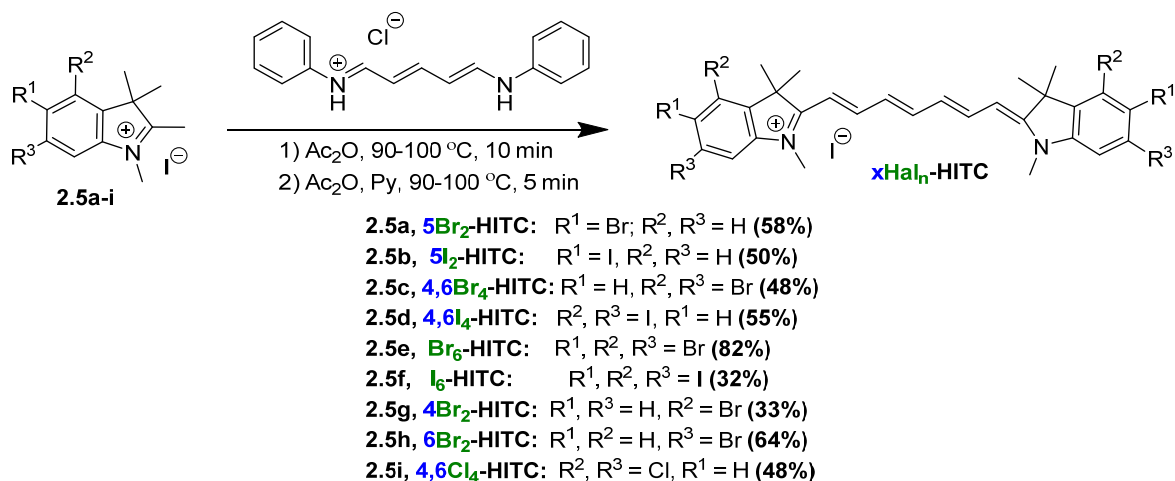
Scheme 2.6. Synthesis of halogenated symmetrical heptamethine cyanine dyes.

The indolinium salts **2.5a-j** were heated at 90−100 °C with glutaconaldehyde dianilide hydrochloride in acetic anhydride during 10 min. Then, the reaction mixture was cooled to 50 °C, following by the addition of pyridine (3 mL) and heating at

90-100 °C during 5 min, resulting in the formation of the product. The reaction mixture was precipitated with ether, filtered off, and washed with ether. The crude product was dissolved in chloroform and column-purified on Silica gel 60 using 1−20% methanol-chloroform as eluent. Fractions from the column were monitored by LCMS. The fraction containing the dye was collected, evaporated, washed with ether, and vacuum-dried to yield target **xHal$_n$-HITC** cyanine dyes in moderate yields (32−82%).

To this end, we synthesized a series of novel halogenated heptamethine cyanine dyes **xHal$_n$-HITC** containing bromine (**4Br$_2$-HITC, 5Br$_2$-HITC, 6Br$_2$-HITC, 4,6Br$_4$-HITC, Br$_6$-HITC**), iodine (**5I$_2$-HITC, 4,6I$_4$-HITC, I$_6$-HITC**) or chlorine atoms (**4,6Cl$_4$-HITC**) at both terminal indolenine moieties. All these dyes possess a methyl group attached to the nitrogen of both indolenine moieties.

For the synthesis of unsymmetrical iodinated cyanines, we applied a one-pot sequential reaction of *N*-[5-(phenylamino)-2,4-pentadienylidene]aniline hydrochloride with the first and then the second quaternized indolenine (Scheme 2.7) [129].
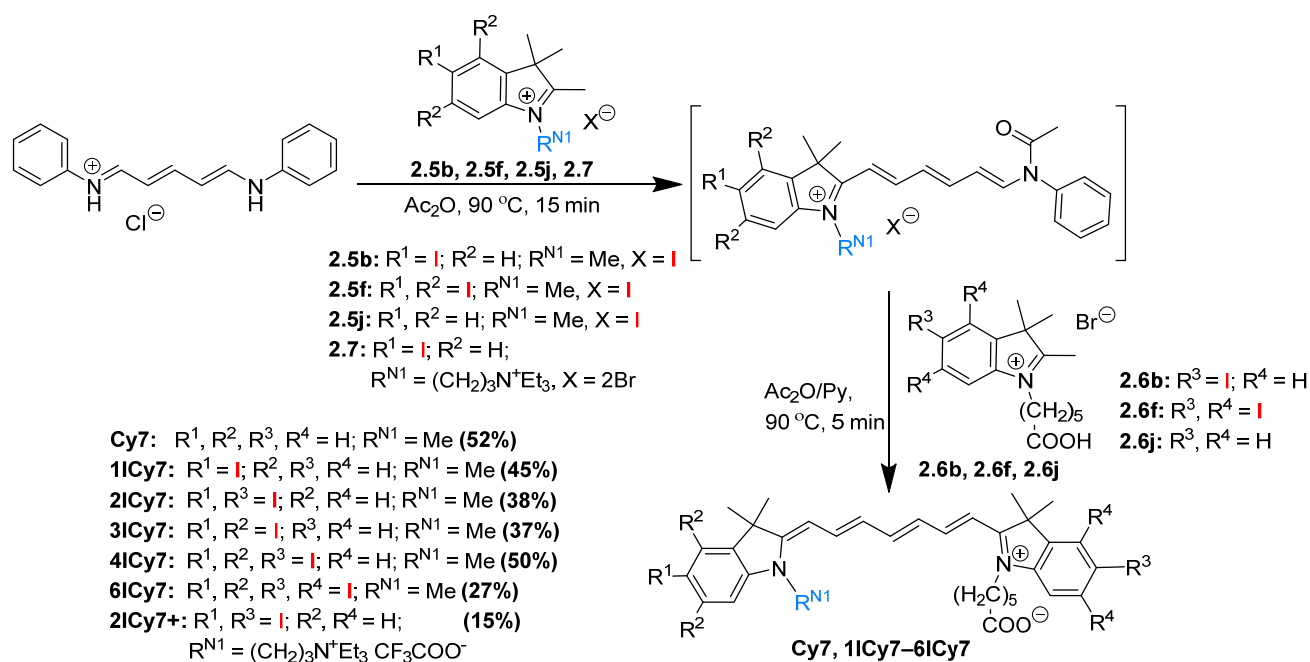
Scheme 2.7. Synthesis of heptamethine cyanine dyes.

In the first step, the starting aniline was condensed in acetic anhydride with the first indolenine molecule **2.5b**, **2.5f**, **2.5j** or **2.7** at 90 °C over 15 min to form a corresponding *N*-phenylacetamide derivative, which was further reacted with the

second molecule, *N*-carboxypentyl indolenine **2.6b**, **2.6f** or **2.6j** in the presence of pyridine at 90 °C over 5 min, resulting in the formation of the product. Similarly to symmetrical dyes, reaction mixtures were precipitated and washed with ether, then the crude products were column-purified on Silica gel 60 using 1−10% methanol-chloroform to give the dyes **Cy7** and **1ICy7−6ICy7** in moderate yields (27−52%). We found that positively charged **2ICy7+** dye cannot be efficiently purified on Silica gel 60 column, thereby it was purified on RP-18 column using acetonitrile−water + 0.05% TFA as eluent to give **2ICy7+** in 15% yield. We assume that the counterion for this dye changed from bromine to trifluoroacetate.

Thus, we synthesized a series of indolenine-based heptamethine cyanine dyes of the asymmetric structure containing no iodine (**Cy7**) as well as one (**1ICy7**), two (**2ICy7**), three (**3ICy7**), four (**4ICy7**) and six (**6ICy7**) iodine atoms. These dyes possess a carboxypentyl group attached to the nitrogen of one indolenine moiety and the methyl group at the second indolenine nitrogen. When the carboxylic group is deprotonated, these dyes exist in zwitterionic form. Furthermore, one of the dyes (**2ICy7+**) bears an additional positive charge provided by the quaternized propyl triethylammonium group substituting *N*-methyl.

Similarly to hydrophobic nonsymmetrical dyes, the hydrophilic iodinated **2ICy7S** dye was synthesized by a one-pot sequential reaction of *N*-[5-(phenylamino)-2,4-pentadienylidene]aniline hydrochloride with the first and then the second quaternized indolenine (Scheme 2.8).

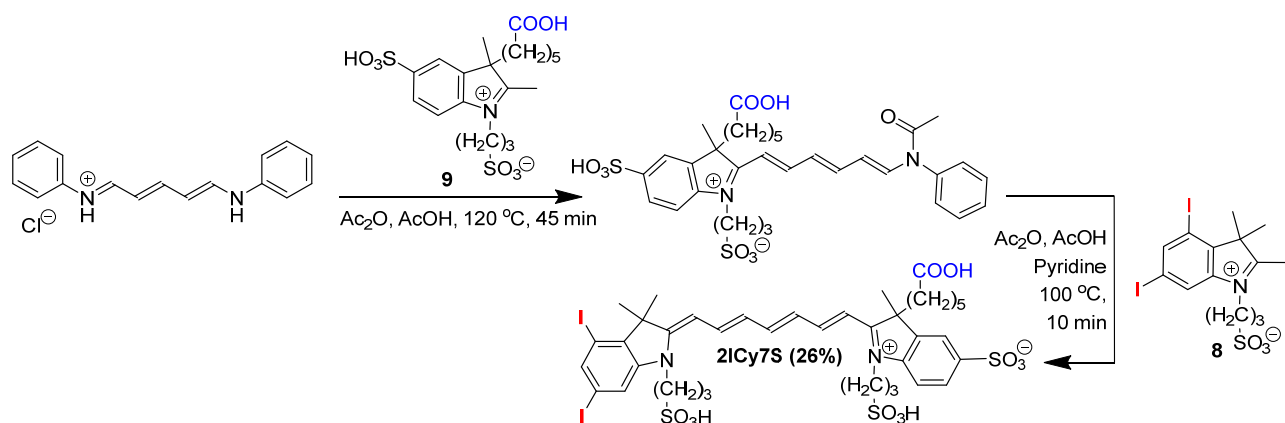**Scheme 2.8**. Synthesis of the **2ICy7S** dye.

However, worse reactivity of *N*-[5-(phenylamino)-2,4-pentadienylidene]aniline with hydrophilic indolenine **2.8** compared to hydrophobic indolenines (**2.5b, 2.5f, 2.5j** or **2.7**) required more harsh reaction conditions. Moreover, we observed the formation of a substantial amount of undesired symmetrical dye in acetic anhydride as the solvent even without pyridine addition. Thus, in the first step the condensation of *N*-[5-(phenylamino)-2,4-pentadienylidene]aniline with the carboxypentyl indolenine **2.9** was performed in the mixture of acetic anhydride and acetic acid (1:1) at 120 °C over 45 min to form the intermediate *N*-phenylacetamide derivative. The mixture of acetic anhydride and acetic acid (1:1) allowed us to significantly slow down the formation of symmetrical dye. Then, the *N*-phenylacetamide derivative reacted with iodinated indolenine **2.8** in the presence of pyridine at 100 °C for 10 min. Then reaction mixture was precipitated with ether, filtered off, washed with ether, dissolved in water, and column-purified on RP-18 using 0−30% acetonitrile−water+0.05% acetic acid as eluent to yield **2ICy7S** in moderate yield (26% after column purification).

Thereby, we synthesized a highly hydrophilic unsymmetrical indolenine-based heptamethine cyanine dye **2ICy7S** comprising 1) two iodine atoms in terminal indolenine moiety; 2) two sulfo groups attached to the nitrogen of both indolenine moieties and one sulfo group in terminal indolenine moiety; 3) carboxypentyl group attached to position 3 of indolenine moiety, which was further used for activation with *N*-hydroxysuccinimide and subsequent bioconjugation.

Molecular structure and purity for all the cyanines were confirmed by ^{1}H-NMR, ^{13}C-NMR, LCMS, and HRMS, and detailly presented in chapter 5, and it was done in a similar way for all the cyanines. For instance, ^{1}H-NMR chemical shifts for cyanine **5I$_2$-HITC** (Fig. 2.6) at 7.96, 7.73, 7.19 ppm related to aromatic ring protons and at 7.86, 7.76, 6.54, 6.30 ppm to polymethine chain protons. To discern these protons, we paid attention to spin-spin coupling, where aromatic protons had typically 7.4−8.5 Hz and polymethine chain protons had typically 12.1−13.8 Hz.
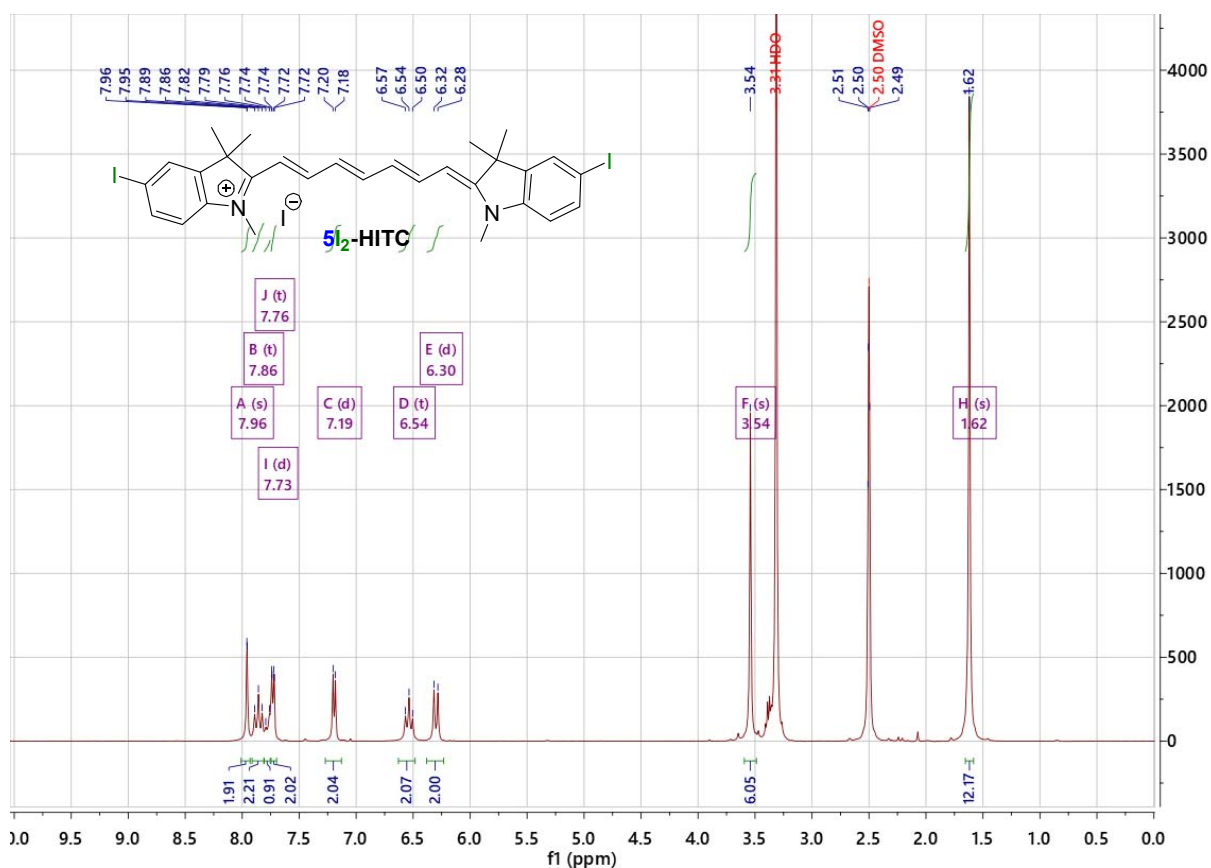
Fig. 2.6. ^{1}H-NMR of cyanine **5I$_2$-HITC** in DMSO-d_6.

Chemical shifts of aliphatic protons were found in typical regions. Thus, singlets of NC$\underline{H_3}$ and C3($\underline{CH_3})_2$ protons for **5I$_2$-HITC** were present at 3.54 ppm and 1.62 ppm, respectively (Fig. 2.6). For **Cy7**, **1ICy7−6ICy7**, and **2ICy7+** dyes, NC$\underline{H_2}$ triplet was observed at 4.08-3.86 ppm, and other peaks corresponding to the pentacarboxylic acid moiety, such as $\underline{CH_2}$-COOH at 2.30-2.22 ppm or methylene groups -$\underline{CH_2}$- at 1.80-1.40 ppm (e.g., **2ICy7**, Fig. 2.7) were detected in ^{1}H-NMR spectra.
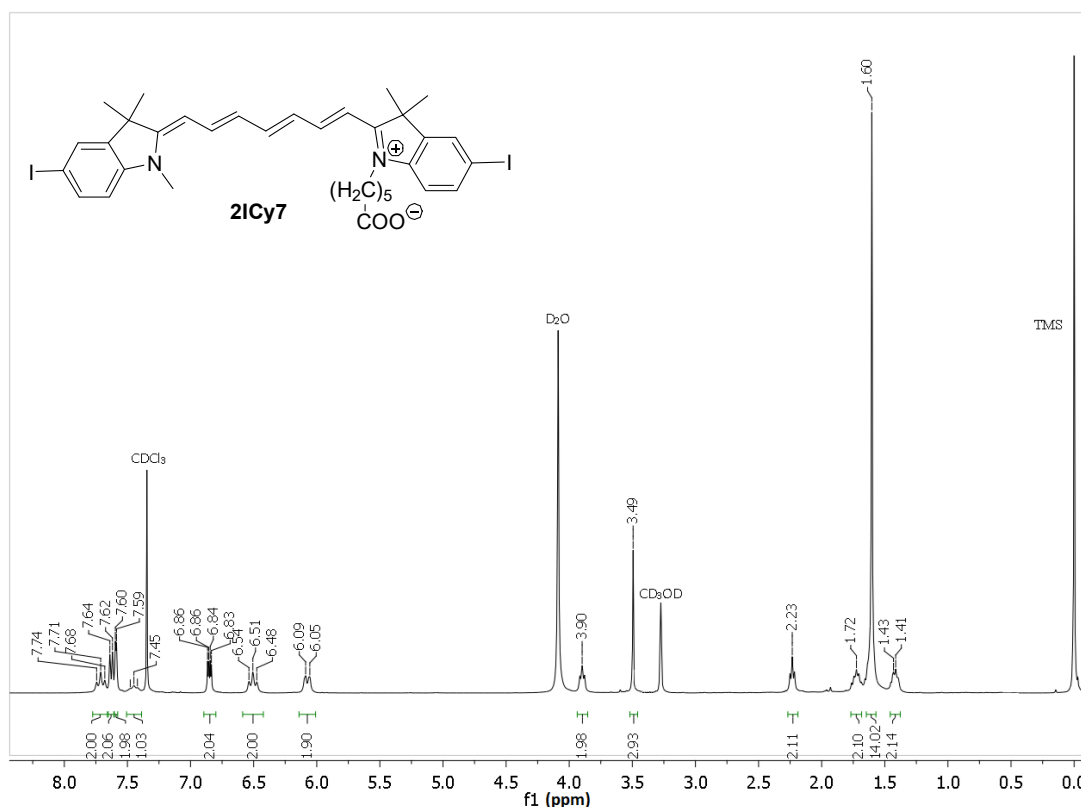
Fig. 2.7. ^{1}H-NMR spectrum of **2ICy7** in CDCl$_3$−CD$_3$OD.

^{1}H-NMR spectrum of **2ICy7S** shown in Fig. 2.8 does not contradict the proposed structure. The characteristic signal of C3(<u>CH$_3$</u>)$_2$ is revealed at 1.71 ppm, while C3(<u>CH$_3$</u>) of the other indolenine appears at 1.64 ppm.

The spectral purity of all synthesized dyes was determined by LCMS analysis, where only one peak on the chromatogram at 254 nm was detected. The mass spectrum of this peak corresponded to the theoretically calculated mass-to-charge (*m/z*) value of the dye. As an example, LCMS for **5I$_2$-HITC** dye (Fig. 2.9) showed one peak at 7.757 min and *m/z* of the compound in this peak was 661.1, which is in good agreement with the theoretical value (661.1).
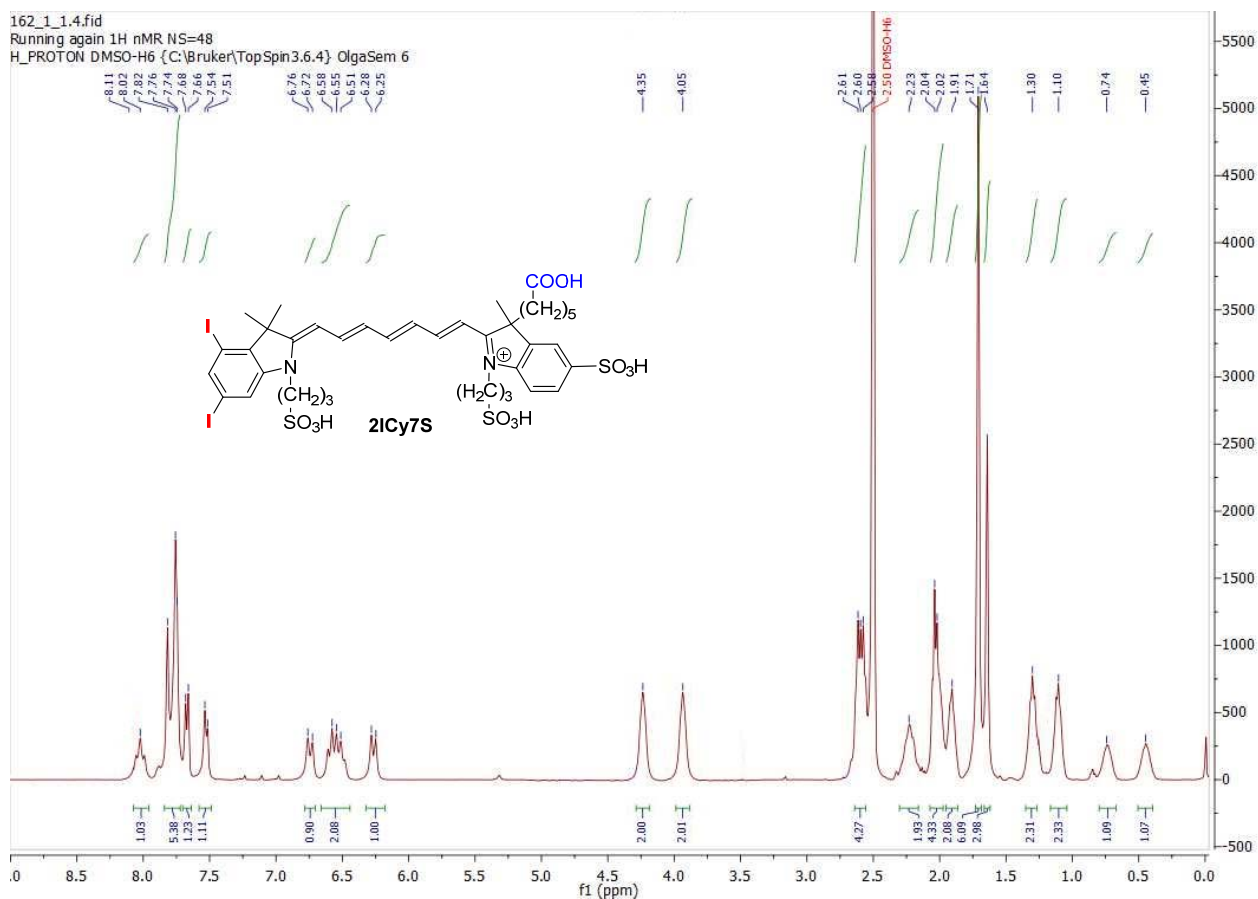
Fig. 2.8. ^{1}H-NMR of cyanine **2ICy7S** in DMSO-d_6.
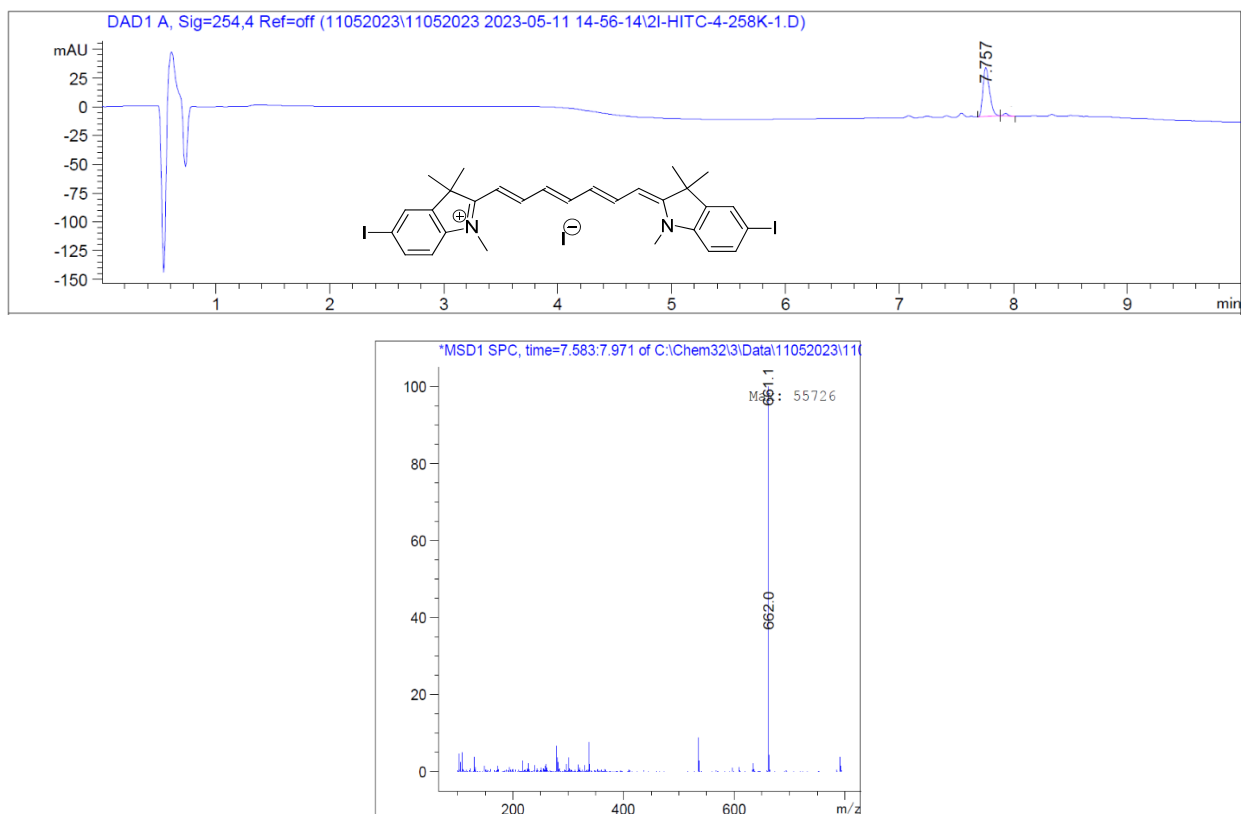
Fig. 2.9. LCMS spectrum of **5I$_2$-HITC**.

To more precisely estimate the exact mass of the dyes we performed HRMS analysis, which allowed us to register the *m/z* value with the high accuracy (till four decimals), and thereby, to predict the chemical formula of the compound. For instance, the HRMS analysis for **2ICy7S** showed *m/z* = 1057.0464 (Fig. 2.10), which is in good agreement with the theoretical value (1057.0426).
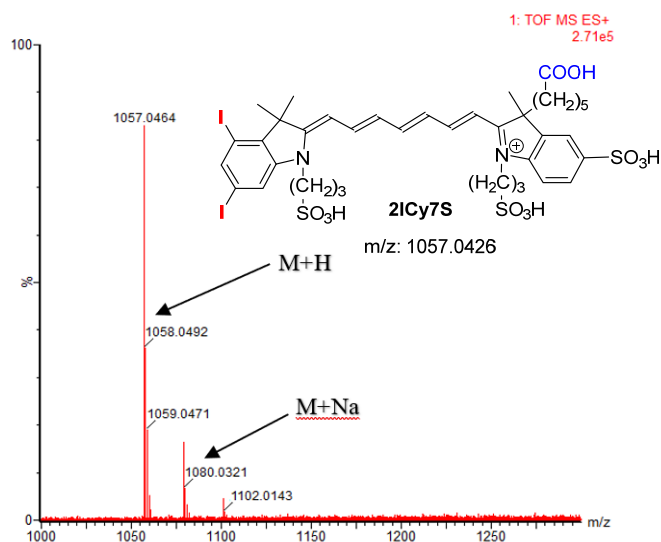
Fig. 2.10. HRMS spectrum of **2ICy7S**.

All intermediates and heptamethine cyanine dyes synthetical procedures and their full characterization by ^{1}H-NMR, ^{13}C-NMR, MS, LCMS, HRMS, and UV-VIS spectroscopy are thoroughly described in chapter 5.

2.3 Conclusions to chapter 2

The initial quaternized 2,3,3-trimethylindoleninium salts for halogenated heptamethine cyanine dyes synthesis can be obtained by multistep reaction starting from the diazotization of corresponding halogenated anilines followed by reduction with tin(II) chloride, and then heterocyclization with 3-methyl-2-butanone in acetic acid, with further *N*-alkylation by iodomethane, 6-bromohexanoic acid or 3-bromo-*N,N,N*-triethylpropan-1-aminium bromide. Better yields in the reaction of diazotization can be achieved by the use of nitrosylsulfuric acid and precise temperature control.

An efficient synthetic pathway towards the synthesis of symmetrical and unsymmetrical heptamethine cyanine dyes containing a number of different halogen atoms in terminal heterocyclic moieties is as follows: respective quaternized indoleninium salts, containing halogen substituents, are introduced into one-pot sequential reaction with *N*-[5-(phenylamino)-2,4-pentadienylidene]aniline hydrochloride with the first and then with the second quaternized indolenine. In the first step, the formation of an intermediate phenylacetamide derivative is carried out in acetic anhydride, while in the second step, the formation of heptamethine cyanine dye is initiated by the addition of pyridine. In the case of symmetrical heptamethinecyanines, the first and the second quaternized indolenine is the same compound. The synthesis of the phenylacetamide derivative in acetic anhydride is accompanied by undesired at this step symmetrical dye byproduct formation. The formation of heptamethine cyanine dye speeds up with the addition of pyridine and slows down with acetic acid addition to acetic anhydride

However, in the case of the synthesis of unsymmetrical cyanines, this side reaction is undesired since it reduces the yield of the target product. Therefore, to hamper this side reaction, acetic acid is suggested to be used on the first step to increase overall yield.

CHAPTER 3

INFLUENCE OF HALOGEN ATOMS IN TERMINAL HETEROCYCLE ON SPECTRAL PROPERTIES OF HEPTAMETHINE CYANINE DYES

This chapter focuses on the thorough investigation of the effect of the introduction of heavy halogen atoms in terminal indolenine heterocycle on spectral-luminescent properties of long-wavelength heptamethine cyanine dyes, as well as the relationship between structure and spectral properties, and, especially, with the fluorescence quantum yield Φ_{Fl} and the singlet oxygen quantum yield Φ_Δ.

For the determination of structure-properties relationships with respect to the amount and position of halogen atom substituent incorporated into fluorophore structure, we investigated spectral properties of iodinated, brominated, and chlorinated heptamethine cyanine dyes of **xHal$_n$-HITC** series, which contain methyl substituents on positions 1 and 3 of indolenine moieties.

5Br$_2$-HITC: $R^1 = Br; R^2, R^3 = H$
5I$_2$-HITC: $R^1 = I, R^2, R^3 = H$
4,6Br$_4$-HITC: $R^1 = H, R^2, R^3 = Br$
4,6I$_4$-HITC: $R^1 = H, R^2, R^3 = I$
Br$_6$-HITC: $R^1, R^2, R^3 = Br$
I$_6$-HITC: $R^1, R^2, R^3 = I$
4Br$_2$-HITC: $R^1, R^3 = H, R^2 = Br$
6Br$_2$-HITC: $R^1, R^2 = H, R^3 = Br$
4,6Cl$_4$-HITC: $R^1 = H, R^2, R^3 = Cl$
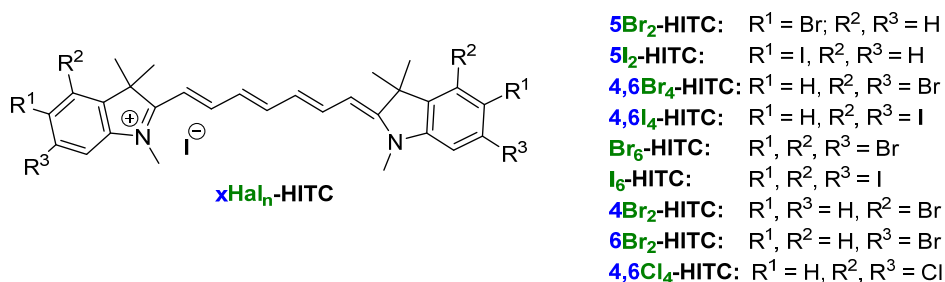
3.1 Spectral properties of xHal$_n$-HITC

The absorption and emission maxima (λ_{max}), extinction coefficients (ε), fluorescence quantum yields (Φ_{Fl}), fluorescence lifetimes (τ), and the quantum yields of the singlet oxygen generation (Φ_Δ) of the investigated dyes measured in methanol, and calculated radiative (k_r) and nonradiative (k_{nr}) rate constants are summarized in Table 3.1, while the absorption and emission spectra are shown in Fig. 3.1.

Table 3.1. Spectral characteristics of the dyes in methanol at 25 °C (λ_{ex} = 700 nm).

Dye	λ_{max}Ab nm	λ_{max}Em nm	ε, $M^{-1} \cdot cm^{-1}$	$\Phi_{Fl}^{(1)}$, %	τ, ns	$k_r^{(2)} \cdot 10^{-8}$, s^{-1}	$k_{nr}^{(3)} \cdot 10^{-8}$, s^{-1}	$\Phi_\Delta^{(4)}$, %
HITC	740	770	212,000	28.0 [130]	1.01	2.77	7.13	0.89 [28]
5Br$_2$-HITC	748	779	233,000	27.2±0.2	1.01	2.75	7.22	1.18±0.02
5I$_2$-HITC	753	783	242,000	25.6±0.1	0.96	2.67	7.75	3.43±0.03
4,6Br$_4$-HITC	740	770	216,000	37.8±0.4	1.2	3.15	5.18	0.89±0.04
4,6I$_4$-HITC	745	774	216,000	36.8±0.1	1.17	3.01	5.40	2.25±0.04
Br$_6$-HITC	748	778	247,000	36.7±0.8	1.17	3.14	5.41	1.45±0.02
I$_6$-HITC	756	788	270,000	32.1±0.5	1.07	3.00	6.35	7.51±0.14
4Br$_2$-HITC	738	767	279,000	34.0±0.4	1.15	2.96	5.74	0.85±0.02
6Br$_2$-HITC	740	770	266,000	34.8±0.5	1.10	3.16	5.93	0.92±0.06
4,6Cl$_4$-HITC	737	766	268,000	37.9±0.8	1.21	3.13	5.13	0.70±0.01

[1] **HITC** was used as reference, Φ_{Fl} = 28% in methanol [130]
[2] k_r was calculated as Φ_{Fl} / τ
[3] k_{nr} was calculated as $(1-\Phi_{Fl}) / \tau$
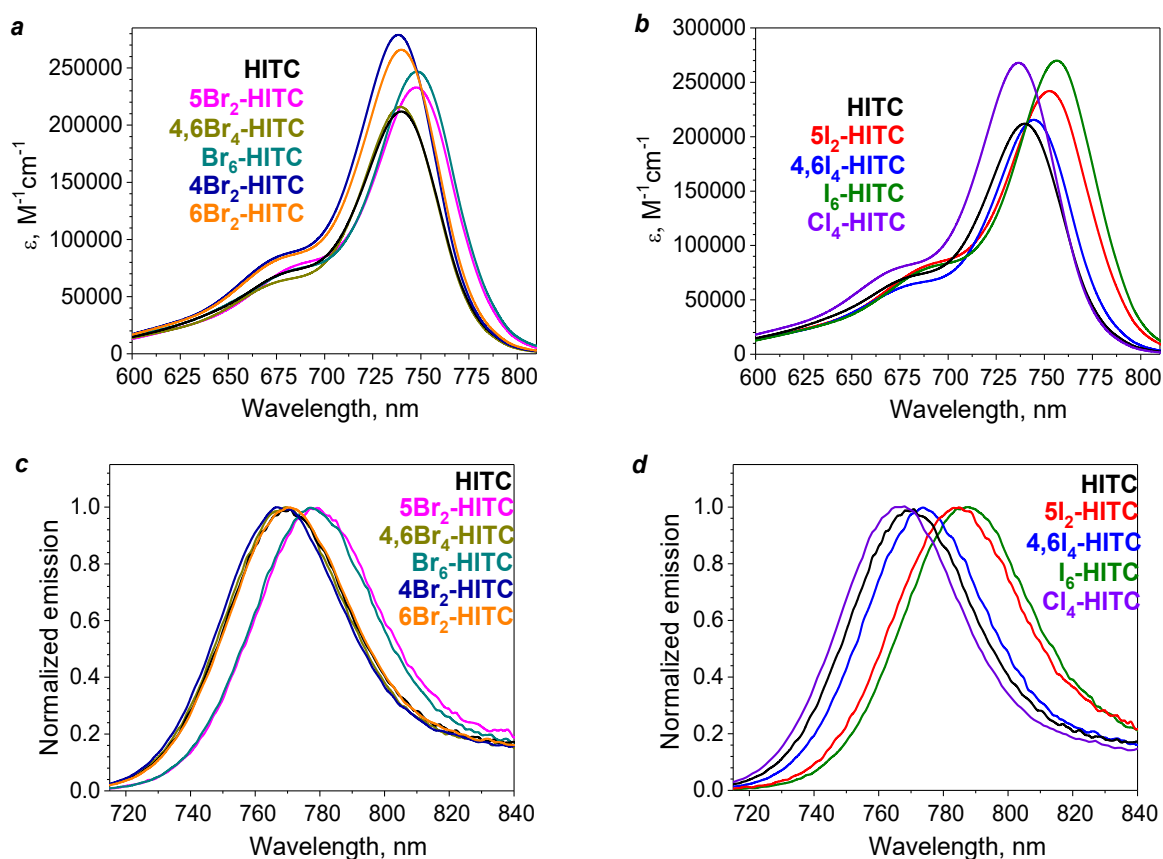[4] **HITC** was used as a reference, Φ_Δ = 0.89% in methanol [28]

Fig. 3.1. Absorption *a*, *b*) and emission *c*, *d*) spectra of **HITC** and **xHal$_n$-HITC** dyes in methanol (c_{Dye} ~ 0.5 μM).

All the dyes absorb and emit in the NIR region with high extinction coefficients ranging from 212,000 to 279,000 $M^{-1}\cdot cm^{-1}$. No signs of aggregation are found in the absorption spectra measured in methanol at dye concentration up to at least 5 µM. The introduction of bromine (**5Br$_2$-HITC**) or iodine (**5I$_2$-HITC**) atoms at position 5 of indolenine rings causes a slight bathochromic shift of about 8–9 and 13 nm, respectively, both in the absorption and emission spectra compared to the unsubstituted dye, **HITC**. The absorption maxima of the dyes with halogen atoms at positions 4 and/or 6 (**6Br$_2$-HITC**, **4,6Br$_4$-HITC**,) are either similar to that of **HITC**, or slightly red- (**4,6I$_4$-HITC**) or blueshifted (**4,6Cl$_4$-HITC, 4Br$_2$-HITC**). At the same time, the changes in the position of emission maxima for these dyes are negligible. The absorption and emission maxima of hexabromo- (**Br$_6$-HITC**) and hexaiodo- (**I$_6$-HITC**) cyanines are redshifted by 8 nm and up to 18 nm, respectively, compared to **HITC**. In general, spectra of cyanine dyes comprising iodine atoms are more redshifted compared to those for bromine-containing cyanines.

The extinction coefficients (ε) of **4Br$_2$-HITC**, **6Br$_2$-HITC**, **4,6Cl$_4$-HITC** and **I$_6$-HITC** are approximately 1.25-fold higher compared to **HITC**, while ε for **5Br$_2$-HITC**, **5I$_2$-HITC**, and **Br$_6$-HITC** are higher only in 1.10-1.16 times. As for **4,6Br$_4$-HITC** and **4,6I$_4$-HITC,** ε are similar to **HITC**.

3.3 Fluorescence quantum yield and lifetime

It is well known that the incorporation of heavy atoms into a dye structure leads to a significant decrease in its fluorescence quantum yield due to the increased probability of spin-orbit coupling [1,16]. However, the incorporation of halogen atoms into the structure of heptamethine cyanine dyes led to unexpected results. Thus, dihalogenated dyes (**5Br$_2$-HITC** and **5I$_2$-HITC**) exhibited only an insignificant Φ_{Fl} decrease compared to **HITC**. Meanwhile, tetrahalogenated dyes (**4,6Br$_4$-HITC** and **4,6I$_4$-HITC**) demonstrated a pronounced increase in Φ_{Fl} by 1.35 and 1.31 times, respectively. The further increasing number of bromines (**Br$_6$-HITC**) or iodines (**I$_6$-HITC**) showed the least Φ_{Fl} increase by 1.31 and 1.16-folds, respectively. Nonetheless, Φ_{Fl} of **Br$_6$-HITC** and **I$_6$-HITC** remained higher compared to that value

for **HITC**. It is also seen that fluorescence quantum yields for dyes with bromine atoms (**5Br$_2$-HITC**, **4,6Br$_4$-HITC**, **Br$_6$-HITC**) generally exceed those for their analogs with iodine atoms (**5I$_2$-HITC**, **4,6I$_4$-HITC**, **I$_6$-HITC**). To further expand our comprehension of structure-properties relationships, we compared the dyes with bromine substituents in positions 4 (**4Br$_2$-HITC**) and 6 (**6Br$_2$-HITC**) in terminal indolenine moieties. The values of fluorescence quantum yield seem almost the same for **4Br$_2$-HITC** and **6Br$_2$-HITC**, thus the proximity of bromine atom to 3,3-dimethyl groups of indolenine moiety in **4Br$_2$-HITC** does not affect the Φ_{Fl} and both dyes show a noticeable increase in Φ_{Fl} of about 1.2 times compared to **HITC**. It seems that Φ_{Fl} of the tetrahalogenated dye with two bromine substituents in positions 4 and 6 (**4,6Br$_4$-HITC**, 1.35-fold Φ_{Fl} increase) lays in a superposition of that effect for both **4Br$_2$-HITC** and **6Br$_2$-HITC** dyes. Dye containing more light-weighted halogen atoms like chlorine in positions 4 and 6 (**4,6Cl$_4$-HITC**), also demonstrates 1.35-fold higher Φ_{Fl} as for **4,6Br$_4$-HITC** compared to HITC, indicating the insignificant influence of the heavy atom incorporation in positions 4 and 6 on dye Φ_{Fl}.

The introduction of the heavy atom into a dye promotes not only the intersystem crossing but also shortens the fluorescence lifetime (τ) [131]. However, τ for dihalogenated dyes (**5Br$_2$-HITC** and **5I$_2$-HITC**) are almost the same as for the non-halogenated dye (**HITC**), as shown in Table 3.1. Surprisingly, τ became even longer for tetra- (**4,6Br$_4$-HITC**, **4,6I$_4$-HITC, 4,6Cl$_4$-HITC**) and hexahalogenated (**Br$_6$-HITC**, **I$_6$-HITC**) dyes.

3.4 Singlet oxygen quantum yield

The quantum yields of the singlet oxygen generation (Φ_Δ) (Table 3.1) for all the dyes were measured in methanol using 1,3-diphenylisobenzofuran (**DPBF**) [28] as a singlet oxygen scavenger. The **DPBF** absorbance at 410 nm was monitored over time and compared with that of **HITC**. Then, a plot of the absorbance at 410 nm against irradiation time was built and the Φ_Δ value was calculated using the slope of the graph.

Since heavy atoms are known to enhance spin-orbit coupling, we anticipated that the Φ_Δ will increase with an increasing number of bromine and iodine atoms. As

expected, hexaiodinated dye **I₆-HITC** showed the most pronounced 8.4-fold Φ_Δ increase compared to **HITC**. Surprisingly, Φ_Δ depends not only on the number of heavy atoms incorporated into the dye but also on the position(s) of these atoms. Thus, two iodine atoms in positions 5 of indolenine moieties (**5I₂-HITC**) affected Φ_Δ 1.5 times stronger than four iodines in positions 4,6 (**4,6I₄-HITC**) (3.43% *vs.* 2.25%). At the same time, six iodines in positions 4,5,6 (**I₆-HITC**) had a synergistic effect with $\Phi_\Delta = 7.51\%$, which is overall higher compared to **5I₂-HITC** or **4,6I₄-HITC** (3.3 and 2.2 times respectively).

Having the same trend with iodinated dyes, **Br₆-HITC** with six bromines in positions 4,5,6 had $\Phi_\Delta = 1.45\%$, which is the highest value for investigated brominated dyes, 1.6 times higher than for **HITC**. Also, two bromines in position 5 (**5Br₂-HITC**) demonstrated 1.3 times increase compared to **HITC**. All the other brominated dyes with substituents in position 4 and/or 6 (**4Br₂-HITC, 6Br₂-HITC, 4,6Br₄-HITC**) did not facilitate any Φ_Δ increase. We consider that bromine-promoted Φ_Δ increase interferes with high Φ_{Fl} for these dyes, which reduces the probability of intersystem crossing. Then, we assumed that the incorporation of chlorine atoms, which do not substantially affect intersystem crossing [14,15], would increase Φ_{Fl} at the expense of Φ_Δ. Indeed, we observed 1.35 times Φ_{Fl} increase and 1.27 times Φ_Δ decrease for **4,6Cl₄-HITC** dye containing 4 chlorine atoms in positions 4,6, compared to **HITC**.

To sum up, iodine atoms strongly (up to 8.4 times) increase the Φ_Δ of the heptamethine cyanine dyes, while bromine atoms are insignificantly affected Φ_Δ. And for the reduction of Φ_Δ of cyanine dyes, it is reasonable to incorporate chlorine atoms in positions 4 and/or 6 of indolenine moiety.

3.5 Evaluation of anomalous heavy atom effect phenomenon

The obtained results on fluorescence and singlet oxygen quantum yields contradict the common point of view concerning so-called "heavy atom effect" [1,16]. So, we imply an explanation for this phenomenon. After molecule excitation, there are two major relaxation pathways: radiative with its decay rate constant k_r and non-radiative decay characterized by a rate constant k_{nr}. Radiative decay rate constant

(k_r) solely depends on fluorescence lifetime τ and Φ_{Fl}, while k_{nr} comprises several non-radiative mechanisms. Equation 3.1 defines k_{nr} as the sum of the corresponding rates associated with non-radiative relaxation pathways [18,29].

$$k_{nr} = k_{isc} + k_{ic} + k_p + k_{sd} \tag{3.1},$$

where k_{isc} is the constant of intersystem crossing rate, k_{ic} is the constant of internal conversion rate, k_p is the constant of rate of photoisomerization and k_{sd} is the solvent-dependent rate constant, characterizing the interaction of excited dye molecules with the solvent.

Fluorescence decays of all investigated dyes corresponded with a monoexponential function, indicating that fluorescence decay appears to originate from a single emitting species and the probability of photoisomerization is negligible. Interaction of dye with the solvent (k_{sd}) is supposed to be negligible compared to k_{ic} [29] since internal conversion is the main deactivation pathway for polymethine dyes in organic solvents because of twisting of the terminal heterocyclic rings around the polymethine chain, whereby energy is dissipated mainly due to intramolecular vibration and rotation [29]. Hence, the major non-radiative energy relaxation pathways are the intersystem crossing with its rate constant k_{isc} and the internal conversion, characterized by rate constant k_{ic}. Intersystem crossing rate constant (k_{isc}) can be evaluated by two parameters: triplet lifetime (phosphorescence decay) and singlet oxygen quantum yield Φ_Δ. Due to the absence or very low level of phosphorescence, we were unable to detect phosphorescence for any of the dyes studied at room temperature to calculate precise k_{isc} values, thereby we attributed the k_{isc} increase solely with Φ_Δ increase.

In accordance with the common "heavy atom effect" incorporation of a heavy atom should decrease the radiative decay rate constant expressed by ($k_r = \Phi_{Fl} / \tau$) due to an increase in the non-radiative decay constant. As can be seen from the Table 3.1, the k_r slightly increases in the row **5I$_2$-HITC < 5Br$_2$-HITC ≈ <u>HITC</u> < 4Br$_2$-HITC < I$_6$-HITC ≈ 4,6I$_4$-HITC < 4,6Cl$_4$-HITC ≈ Br$_6$-HITC ≈ 4,6Br$_4$-HITC ≈ 6Br$_2$-HITC**, while k_{nr} significantly decreases in the in the row **5I$_2$-HITC > 5Br$_2$-HITC > <u>HITC</u> > I$_6$-HITC > 6Br$_2$-HITC > 4Br$_2$-HITC > Br$_6$-HITC ≈ 4,6I$_4$-HITC > 4,6Br$_4$-HITC >**

4,6Cl₄-HITC. Wherein the intersystem crossing rate (k_{isc}), which we attribute to the Φ_Δ changes, decreases in a row **I₆-HITC** > **5I₂-HITC** > **4,6I₄-HITC** > **5Br₂-HITC** > **HITC** ≈ **6Br₂-HITC** ≈ **4Br₂-HITC** ≈ **Br₆-HITC** ≈ **4,6Br₄-HITC** > **4,6Cl₄-HITC**, which does not coincide with the row for k_{nr} decreasing.

Thereby, in accordance with the common "heavy atom effect", k_{nr} *increases* for the dyes with bromine or iodine at position 5 of terminal indolenine fragment (**5I₂-HITC**, **5Br₂-HITC**) due to Φ_Δ (e.g. k_{isc}) increase compared to **HITC**. If the incorporation of halogen atoms leads to a decrease of k_{nr} while maintaining the high level of Φ_Δ compared to **HITC** (**I₆-HITC**, **4,6I₄-HITC**, **Br₆-HITC**) it corresponds to the anomalous heavy atom effect. In this case, a decrease in the of non-radiative decay rate can occur only due to a decrease in the rate of internal conversion k_{ic}. When k_{nr} decreases due to both k_{isc} and k_{ic} decrease it is consistent with the absence of heavy atom effect (for **4,6Cl₄-HITC**) (Fig. 3.2).
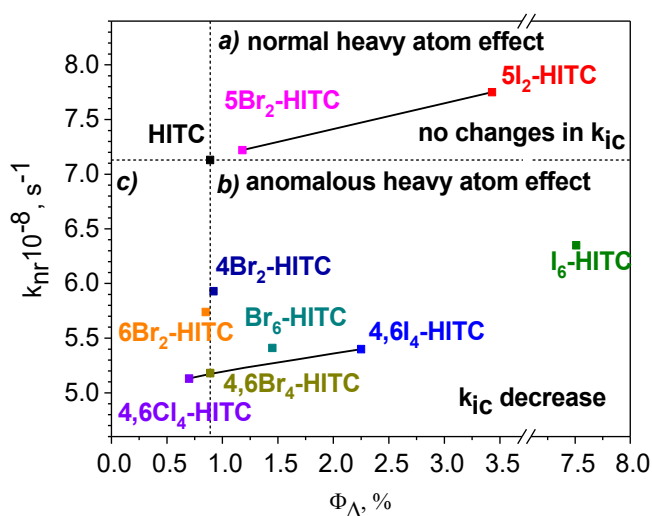
Fig. 3.2. Non-radiative decay rate k_{nr} *vs.* singlet oxygen quantum yields (Φ_Δ) of all the dyes. Region *a)* k_{nr} and Φ_Δ decrease consistently with known heavy atom effect, region *b)* k_{nr} decrease and Φ_Δ increase correspond to anomalous heavy atom effect, region *c)* k_{nr} and Φ_Δ decrease indicates no heavy atom effect, k_{nr} decreases due to k_{ic} decrease.

It is known that cyanine dyes exhibit significant energy dissipation through non-radiative pathways [29,132,133] due to the rotation of indolenine moieties around the polymethine chain (significant contribution of the k_{ic}). We suppose that the

incorporation of halogen atoms in positions 4 and/or 6 (**4,6Br$_4$-HITC**, **4,6I$_4$-HITC**, **4Br$_2$-HITC**, **6Br$_2$-HITC**, **4,6Cl$_4$-HITC**), leads to the decrease of non-radiative rate (k$_{nr}$) at the expense of internal conversion rate (k$_{ic}$) decrease due to the limitation of rotation of indolium moieties in the dyes. This also explains the increase in fluorescence quantum yield and lifetime for the **4,6Br$_4$-HITC**, **4,6I$_4$-HITC**, **4Br$_2$-HITC**, **6Br$_2$-HITC**, **4,6Cl$_4$-HITC** simultaneously with an increase in Φ_Δ for **I$_6$-HITC**, **4,6I$_4$-HITC** and **Br$_6$-HITC**.

3.6 Quantum chemical calculations

Quantum chemical calculations of the brominated dyes were carried out to explain structure-related possibilities leading to Φ_{Fl} increase concerning energy relaxation on a quantum chemical level like reversed intersystem crossing, when singlet energy level (S$_1$) and triplet energy level (T) are close by to each other [134] or competition in deactivation channels when a number of triplet states have lower energy than S$_1$ [135]. The calculation of energy levels of the brominated dyes (**5Br$_2$-HITC**, **4,6Br$_4$-HITC**, **Br$_6$-HITC**) showed that triplet energy levels T$_2$ are too far from the lowest excited singlet energy level S$_1$ to interfere with its vibrational levels, and energy relaxation pathways (fluorescence, ISC, phosphorescence) should have maintained similar trend for all the dyes (Fig. 3.3).
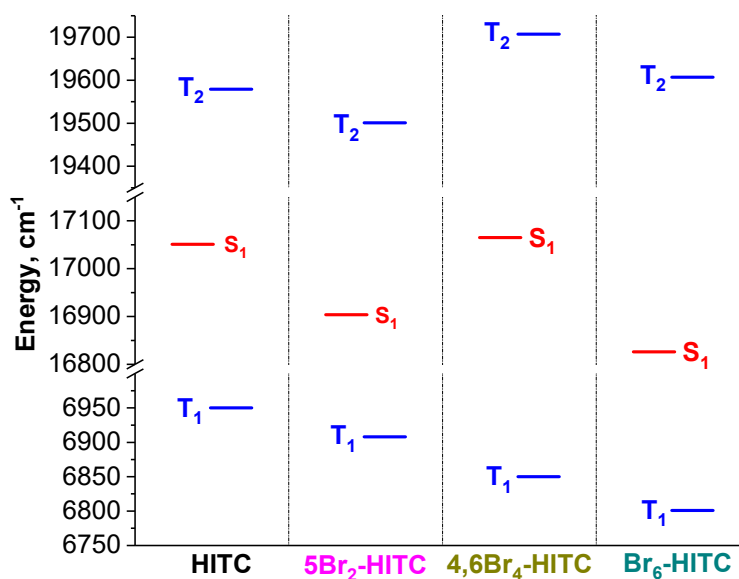

Fig. 3.3. Energy levels of the dyes **5Br$_2$-HITC**, **4,6Br$_4$-HITC**, and **Br$_6$-HITC** calculated with *TD LC-ωB97XD/6-31G**, PCM (Ethanol)*.

3.7 Conclusions to chapter 3

The incorporation of halogen atoms, such as chlorine, bromine, and iodine in the terminal indolenine moieties of heptamethine dyes does not have a significant effect on absorption and fluorescence maxima, although the introduction of iodine substituents leads to a slightly greater red shift in the spectra, as compared to brominated or unsubstituted dyes. At the same time, a fluorescence quantum yield (Φ_{Fl}) and lifetime are strongly affected by the type of halogen atom, their quantity, and position. Thus, halogenation of the dyes leads to the significant Φ_{Fl} enhancement (up to 1.35 times). In general, bromine and even chlorine atoms have a higher positive impact on Φ_{Fl} of the dyes than iodine atoms. The incorporation of halogen atoms in position 5 of terminal indolenine moieties causes a decrease of Φ_{Fl}, while, in contrast, halogen atoms in positions 4 and/or 6 facilitate strong increase of Φ_{Fl}. The combination of these positions (4,5,6) shows only a moderate Φ_{Fl} increase seemingly at the expense of halogens in position 5. At the same time, the level of Φ_{Fl} increasing is almost independent of the type of incorporated halogen (more light-weighted, chlorine, or heavier, bromine or iodine, atoms).

The halogen atom-promoted singlet oxygen quantum yield Φ_{Δ} depends not only on a number but also on the position of the halogen substituents in the heptamethine cyanine dyes. Thus, **4,6I$_4$-HITC** dye containing 4 iodine atoms in positions 4,6 of indolenine moieties have 1.5 lower Φ_{Δ} as compared to **5I$_2$-HITC** with 2 iodine atoms. Importantly, while iodine atoms strongly (up to 8.4 times) increase the Φ_{Δ} of the heptamethine cyanine dyes, bromine atoms insignificantly affect it. The incorporation of chlorine atoms reduces Φ_{Δ} even below this value for **HITC**.

We hypothesize that the incorporation of heavy atoms leads to the restriction of rotation of indolium moieties around the polymethine chain, thus increasing $\Phi_{Fl,}$ fluorescence lifetime, and even Φ_{Δ} for **I$_6$-HITC** and **4,6I$_4$-HITC** compared to **HITC**.

We show a way to adjust the key properties (Φ_{Fl} and Φ_{Δ}) for heptamethine cyanine dyes changing the amount and positions of halogen atoms.

CHAPTER 4

PHOTODYNAMIC THERAPY AND THERANOSTICS APPLICATIONS

This chapter focuses on the application of halogenated heptamethinecyanine dyes for photodynamic therapy and theranostics. One of the main characteristics of dye-sensitizers for photodynamic therapy (PDT) applications is the high singlet oxygen generation efficiency because singlet oxygen and reactive oxygen species (ROS) are responsible for the phototoxicity of the dye. Since iodine-containing heptamethinecyanine dyes indicate the highest singlet oxygen generation among other halogenated dyes (see Section 3.3), for testing in PDT we used only iodinated dyes. So, the first part of the chapter describes the investigation of the photocytotoxicity of promising iodinated heptamethine cyanine dyes in the examples of gram-positive (*S. aureus*) and gram-negative (*E. coli* and *P. aeruginosa*) photoeradication; and the second part is devoted to the development of the antibody-photosensitizer conjugate, which is exploited for theranostics (photoimmunotherapy) of human breast cancer.

4.1 Iodinated heptamethine cyanine photosensitizers for antimicrobial photodynamic therapy applications

The introduction of heavy atoms such as iodine into organic dye molecules is known to improve the efficacy of photodynamic therapy (PDT) in general and antimicrobial photodynamic therapy (APDT) in particular. As we discussed in chapter 1, such a phenomenon is attributed to the increasing probability of intersystem crossing resulting in the elevated rates of reactive species generation. To study the photodynamic effect of dyes on the eradication of bacteria, we chose iodinated heptamethine cyanine sensitizers (PS) with varying amount (up to six) and positions of iodine atoms.
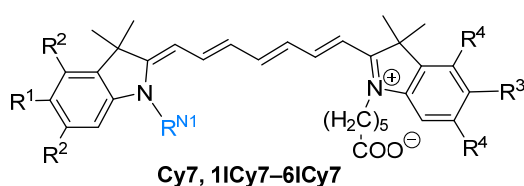
Cy7: $R^1, R^2, R^3, R^4 = H; R^{N1} = Me$
1ICy7: $R^1 = I; R^2, R^3, R^4 = H; R^{N1} = Me$
2ICy7: $R^1, R^3 = I; R^2, R^4 = H; R^{N1} = Me$
3ICy7: $R^1, R^2 = I; R^3, R^4 = H; R^{N1} = Me$
4ICy7: $R^1, R^2, R^3 = I; R^4 = H; R^{N1} = Me$
6ICy7: $R^1, R^2, R^3, R^4 = I; R^{N1} = Me$
2ICy7+: $R^1, R^3 = I; R^2, R^4 = H;$
$R^{N1} = (CH_2)_3N^+(CH_3)_3 \ CF_3COO^-$

Cy7, 1ICy7–6ICy7

We investigated their spectral properties, efficacy to generate reactive oxygen species, cell uptake, and photocytotoxicity on gram-positive *Staphylococcus aureus* (*S. aureus*) and gram-negative *Escherichia coli* (*E. coli*) and *Pseudomonas aeruginosa* (*P. aeruginosa*) bacterial pathogens [129].

4.1.1 Spectral properties and quantum yields of singlet oxygen formation

The absorption and emission spectra and the extinction coefficients (ε) of the studied heptamethine cyanines were measured at the dye concentration $c_{Dye} \sim 1$ µM in DMSO (Fig. 4.1), aqueous saline (Fig. 4.2) and MeOH (Fig. 4.3) and the corresponding characteristics are given in Table 4.1.
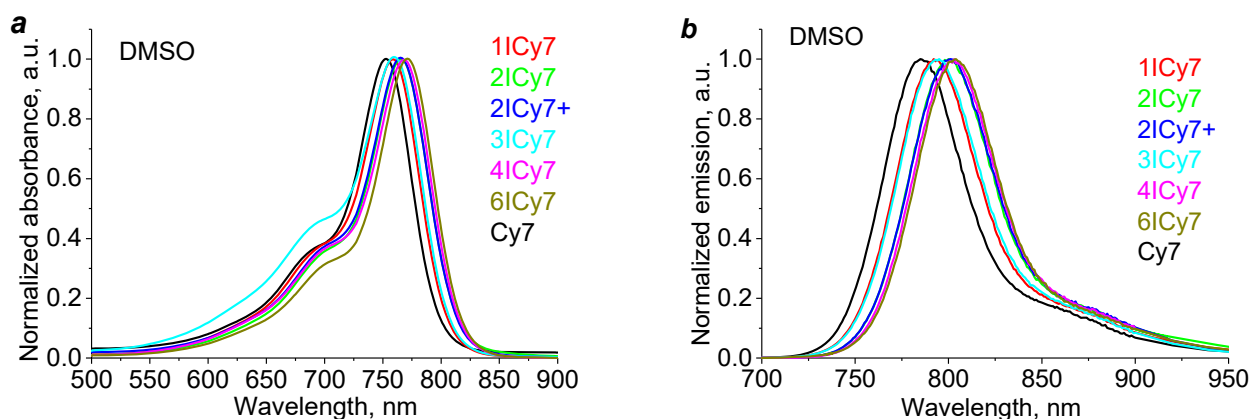
Fig. 4.1. Absorption *a*) and emission *b*) spectra of the dyes in DMSO ($c_{Dye} \sim 1$ µM). $\lambda^* = 680$ nm.
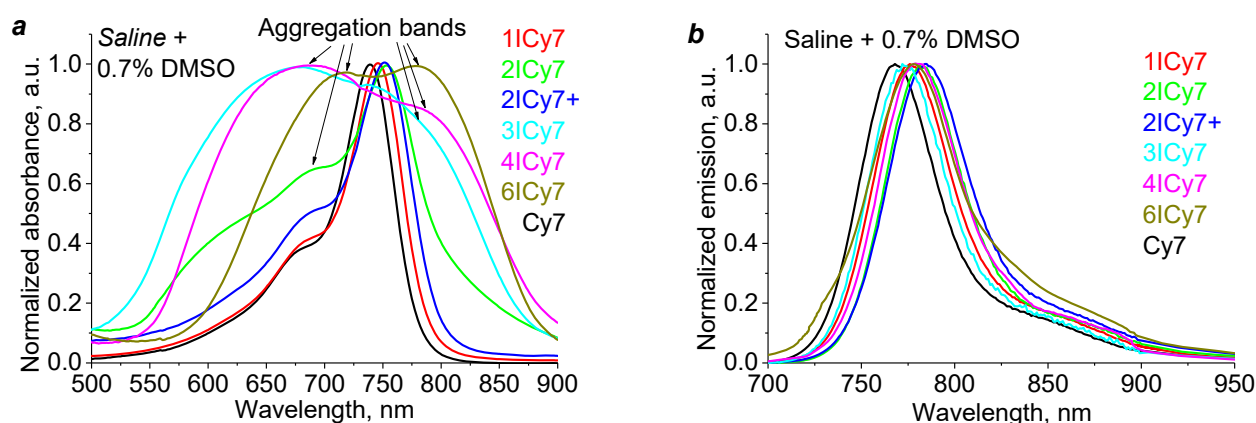
Fig. 4.2. Absorption *a*) and emission *b*) spectra of the dyes in 0.9% aqueous saline containing 0.7% DMSO ($c_{Dye} \sim 1$ µM). $\lambda^* = 680$ nm.
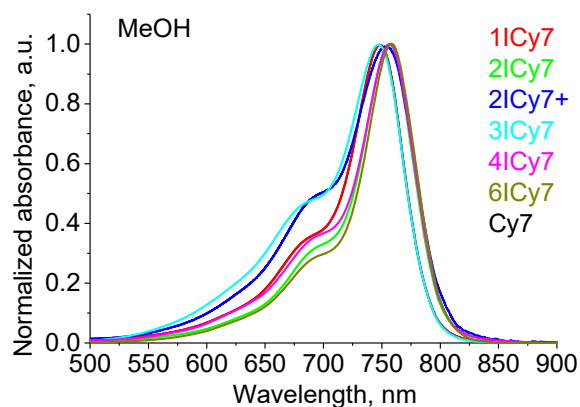
Fig. 4.3. Absorption spectra of the dyes in MeOH ($c_{Dye} \sim$ 5–7 μM).

Table 4.1. Spectral characteristics of cyanine dyes measured at $c_{Dye} \sim$ 1 μM.

Dye	Structure	DMSO				0.7% DMSO in saline			MeOH
		λ_{max}Ab, nm	ε, $M^{-1}cm^{-1}$	λ_{max}Fl, nm	Φ_{Fl}, %	λ_{max}Ab, nm	λ_{max}Fl, nm	Φ_{Fl}, %	Φ_{Δ}, %
Cy7		753	143,300	786	55	739	768	13	1.1
1ICy7		759	168,000	792	53	746	776	12	1.9
2ICy7		766	173,000	801	55	754	783	4	2.3
2ICy7+		766	176,000	801	48	752	785	10	2.3
3ICy7		760	148,000	794	49	677*, 744	774	0.8	2.4
4ICy7		768	144,000	803	48	688*	779	0.1	3.7
6ICy7		771	166,000	804	52	718*, 777*	779	0.02	7.8

* Aggregation band

These dyes absorb in the NIR, a biologically transparent spectral region with high extinction coefficients ($\varepsilon \sim$144,000–176,000 $M^{-1}cm^{-1}$), which is beneficial for applications in the body. The difference in the extinction coefficients between the dyes does not exceed ~20%. There is a tendency that the iodination of the parent dye **Cy7** results in a moderate red-shift in the absorption (up to 18 nm for hexa-iodinated **6ICy7** in DMSO) and a slight increase in the extinction coefficients.

The fluorescence quantum yield (Φ_{Fl}) of the dyes measured in DMSO (~48−55%) is substantially reduced in aqueous saline (0.02−13%), which can be attributed to the dye aggregation [136,137,138]. The aggregation bands are well recognized in the absorption spectra (Fig. 4.2). In the saline solutions, a drastic (up to ~650-fold) decrease of the quantum yield with increasing the number of iodine atoms is observed. In general, such an effect is known to be connected with the increasing probability of intersystem crossing caused by heavy atoms, which results in the growing population of the triplet state and the fluorescence quenching. However, for the investigated cyanine dyes, the decrease of the quantum yield is observed only in aqueous solutions but not in DMSO. That is, the decrease is associated with the dye aggregation rather than with the heavy atom effect.

All the dyes except **2ICy7+** contain a delocalized positive charge and a localized negative charge on the deprotonated carboxylic group. Therefore, due to the slightly polar structure, these dyes are only a little soluble in saline. The introduction of iodine atoms in organic compounds is known to reduce their solubility in aqueous media. Thus, the solubility of dimethylaniline in water at 25 °C is 1 g/L [139] while for 4-iodo-dimethylaniline it is only 0.03464 g/L [140]. The solubility of benzoic acid in water is 3.44 g/L [141] while for 4-iodobenzoic acid it is 0.04 g/L [142] and only 0.036 mg/L for 2,3,5-triiodobenzoic acid [143]. Hereby, the solubility of the investigated dyes decreases with the increasing the number of iodine atoms and the aggregation accordingly increases (Fig. 4.2). At the same time, due to the presence of an additional positive charge, dye **2ICy7+** is less aggregative compared to **2ICy7** containing the same number of iodines.

The quantum yields of the singlet oxygen formation (Φ_Δ) were measured in methanol solutions by the decrease of the **DPBF** dye, as described in [28], under the light exposure (747 nm, 1 W LED). As anticipated, the Φ_Δ were found to increase with increasing the number of iodine atoms (Table 4.1). Dyes **2ICy7** and **2ICy7+** both containing two iodines exhibited about the same Φ_Δ. In the dark, no pronounced generation of singlet oxygen was detected: the decrease in the **DPBF** absorbance did not exceed 2% during 15 h. According to the absorption spectra (Fig. 4.3), almost no

aggregation was noted in methanol at the investigated dye concentrations ($c \sim 5{-}10 \times 10^{-6}$ M).

4.1.2 Toxicity and photocytotoxicity of the dyes

All experiments with bacteria were carried out in aqueous saline solution. Commercial 0.9% saline solution, used in this work, is known to be acidic (pH ~ 5.5), which is mostly due to the presence of CO_2 [144]. On the other side, the carboxypentyl group existing in all the investigated dye molecules is more acidic (e.g. the pK_a for pentanoic and hexanoic acids are 4.84 [145] and 4.88 [146], respectively). It means that the carboxylic group is basically deprotonated and the dyes **Cy7**, **1ICy7**, **2ICy7**, **3ICy7**, **4ICy7**, and **6ICy7** exist in saline solution in the non-charged zwitterion form. In contrast, **2ICy7+** has a charge of +1 that is localized on the quaternized triethylammonium group.

To investigate the effect of the dyes on bacteria, stock solutions of the dyes were prepared in DMSO and added to the bacterial suspension in saline in such a way that the concentration of DMSO in the sample was 0.7%. Then the bacterial suspensions were incubated with each dye in the dark for 30 min (pre-irradiation incubation), exposed to light and grown in the dark for 24 h at 37 °C followed by the calculation of the number of bacterial colonies. The dye concentrations and the exposure time were varied for each dye. To verify the dark toxicity of the dyes, the same experiments were carried out in parallel without light exposure.

As the control, the bacterial suspensions containing no dye were utilized. These controls were kept (i) in the dark without DMSO, (ii) in the dark in the presence of DMSO, (iii) exposed to light without DMSO, and (iv) exposed to light in the presence of DMSO. The amount of DMSO in these control samples was the same as for the dye-stained bacteria. The number of bacterial colonies in each experiment was utilized to calculate the survival percentage as compared to the control. Importantly, no detectable bacteria inhibition was registered for all the above controls (i–iv) and the survival for these samples was taken as 100%.

Then, we found that the investigated dyes have no detectable dark toxicity to gram-positive (*S. aureus*) and gram-negative (*E. coli* and *P. aeruginosa*) bacteria at least up to the 1 µM and 50 µM dye concentrations, respectively. The dark toxicities at higher dye concentrations were not studied. In the next step, the experiments were performed with light irradiation at different exposure times using a 730-nm 30 W LED (power density 55 mW/cm^2).

4.1.2.1 Photodynamic eradication of *S. aureus*

In our study, the effect on photocytotoxicity of the three following parameters was investigated: the number of iodine atoms in the dye molecules, the concentration of the dyes, and the light doses. The methodological approach was as follows: The effect of the number of iodine atoms in the dyes was first investigated on gram-positive bacteria *S. aureus*: (i) at the "medium" (100 J/cm^2) and (ii) "low" (3 J/cm^2) light dose *vs.* the dye concentrations, and (iii) at the constant dye concentrations *vs.* the light dose. The "high" light dose (400 J/cm^2) was not applied in the initial research stage because it caused the complete killing of *S. aureus* by all the investigated dyes and, therefore, it was not possible to compare the efficacies of these dyes.

Following this approach, the impact of the number of iodine atoms and the dye concentration (c_{Dye} = 0.01–1 µM) on the *S. aureus* survival was first investigated at the constant light dose of 100 J/cm^2. The most pronounced and nearly equal photocytotoxicity was observed for **2ICy7**, **3ICy7**, and **4ICy7** which contained 2–4 iodine atoms, while **Cy7**, **1ICy7**, **2ICy7+**, and, surprisingly, **6ICy7** were less effective (Fig. 4.4). These results allow us to draw several conclusions.
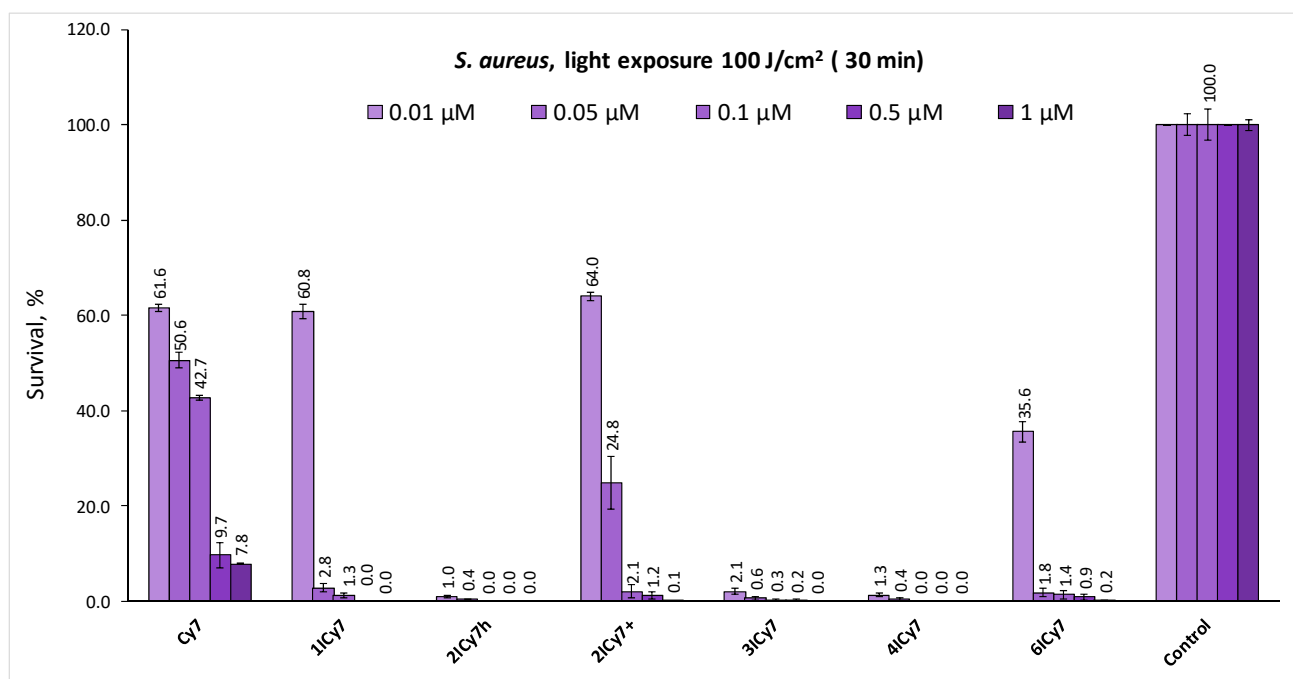
Fig. 4.4. Survival of *S. aureus* in 0.7% DMSO in saline, when exposed to 100 J/cm² light dose (56 mW/cm², 30 min) *vs.* the dye concentrations.

First, the introduction of iodine atoms in the **Cy7** molecule, which is the parent structure for all the iodinated dyes, elevates photocytotoxicity, which is an anticipated result: one iodine atom in **1ICy7** causes a distinct increase of the photocytotoxicity but this increase is less pronounced as for the 2–4 iodinated dyes (Fig. 4.4). Thus, the dyes with 2–4 iodines were the most photocytotoxic affording almost total bacteria killing (survival 0–2.1%) at 0.01–1 µM, while **1ICy7** at 0.01 µM is much less photocytotoxic exhibiting the percentage of survival of 60.8%. Obviously, this result is connected with increasing the number of heavy atoms.

The second conclusion is that increasing the number of iodines from 2 to 4 has almost no effect on the photokilling while the hexa-iodinated dye **6ICy7** surprisingly exhibits a reduced photocytotoxicity (the percentage of survival is 35.6% at 0.01 µM) compared to the 2−4 iodinated dyes (survival 0–2.1%).

Third, the non-delocalized positive charge produced by the triethylammonium group (**2ICy7+** *vs.* **2ICy7**) noticeably decreases the photocytotoxicity (Fig. 4.4).

We assume that the above phenomena, i.e. "saturation" and reduction of the bacteria photo-eradication with increasing the number of iodine atoms from 2 to 6, can

be attributed to the increasing dye aggregation in aqueous media (Fig. 4.2) resulting in the decreasing dye uptake (the aggregation reduces both the photocytotoxicity [136, 147] and the above-mentioned fluorescence quantum yields [136−138]). This conclusion contradicts, however, recently reported findings that iodination of small organic molecules such as 4-amino naphthalimides causes *vice versa* the increase of the dye uptake by several mammalian cells [148].

To check our assumption that increasing the number of iodine atoms (as well as the positive charge) in the series of the investigated cyanines reduces the dye uptake by *S. aureus* and thus decreases the photokilling effect, we measured the dye uptake and correlated it with the photocytotoxicity percentage. For this purpose, *S. aureus* suspensions in saline (10^3–10^4 cells/mL) were incubated with the dyes (1 µM) for 30 min and the fluorescence intensities of these suspensions were measured. Then, the bacteria were separated from the solvent by centrifugation (10 min, 4,000 rpm), resuspended in saline and the fluorescence intensities were again measured. In these experiments, the effect of light scattering on the relative fluorescence intensities was minimized because the samples contained the same number of cells before and after staining. The dye uptakes quantified as the ratios between the fluorescence intensities for the resuspended bacteria and for the initial suspensions were as follows: **Cy7** (0.85), **1ICy7** (0.28), **2ICy7** (0.98), **2ICy7+** (0.21), **3ICy7** (0.99), **4ICy7** (0.97), and **6ICy7** (0.73). These data indicate that **2ICy7**, **3ICy7**, and **4ICy7** exhibited the most pronounced uptake while uptake for **6ICy7** and especially for **2ICy7+** was noticeably reduced. The uptake of **Cy7** is lower compared to **2ICy7** but much higher than for **1ICy7**. The obtained uptake values are in good agreement with the photocytotoxicities (Fig. 4.5).

Thus, for the iodinated dyes, there is a clear correlation between the uptake and the photocytotoxicity ($r = 0.98$). At the same time, the non-iodinated dye **Cy7** exhibits a substantially reduced antimicrobial photocytotoxicity (elevated survival) compared to the value anticipated from the correlation curve (Fig. 4.5). More likely, this is due to the fact that the correlation curve takes into account also the contribution of the heavy atom effect.
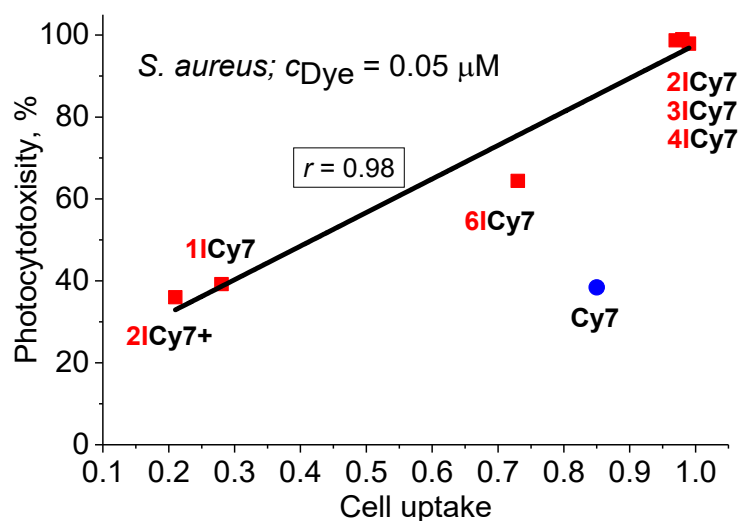
Fig. 4.5. Dye photocytotoxicity on *S. aureus vs.* the dye uptake. The uptake was estimated as the ratio between the fluorescence intensities of the stained bacteria after and before washing.

Furthermore, we studied the effect of the light dose on the dyes' photocytotoxicity towards *S. aureus* at a constant dye concentration of 0.05 μM (Fig. 4.6).
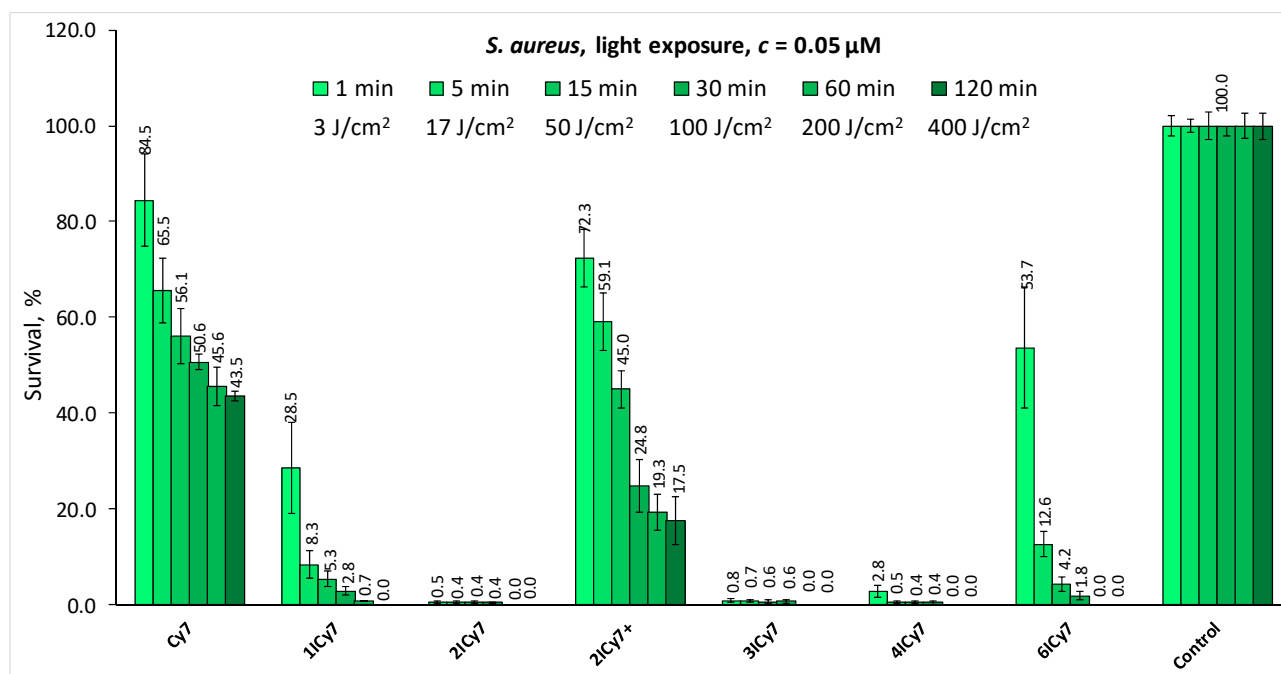
Fig. 4.6. Survival of *S. aureus* at 0.05 μM dye concentrations in 0.7% DMSO in saline, when exposed to 3 J/cm^2 (1 min), 17 J/cm^2 (5 min), 50 J/cm^2 (15 min), 100 J/cm^2 (30 min), 200 J/cm^2 (60 min), and 400 J/cm^2 (120 min) light doses.

The photocytotoxicity increases with increasing the light dose from 3 J/cm^2 (1 min) to 400 J/cm^2 (120 min). However, the dyes with two (**2ICy7**) and three (**3ICy7**) iodines almost totally eradicate bacteria even at 3 J/cm^2 and **4ICy7** at 17 J/cm^2. The data presented in Fig. 4.6 confirm also that the dyes with 2–4 iodines bearing a delocalized positive charge cause the more pronounced bacteria eradication while **1ICy7**, **6ICy7**, **2ICy7+**, and especially **Cy7** are less photocytotoxic. It can be seen from Fig. 4.6 that dyes **2ICy7** and **3ICy7** entirely eradicate *S. aureus* even at a low dye concentration (0.05 µM) and at a very low light dose of 3 J/cm^2. Therefore, we investigated the impact of the dye concentrations on the photocytotoxicity at this low light dose (Fig. 4.7).
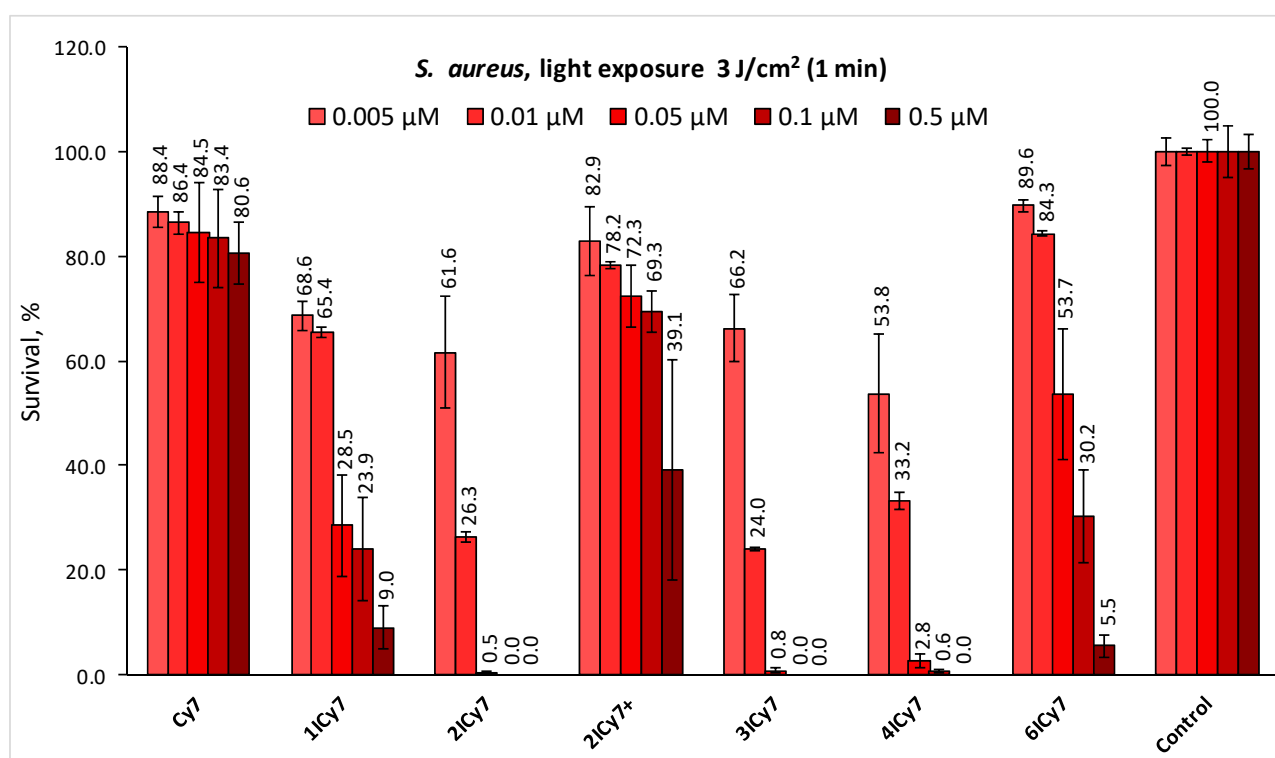
Fig. 4.7. Survival of *S. aureus* in 0.7% DMSO in saline, when exposed to 3 J/cm^2 light dose (56 mW/cm^2, 1 min) *vs.* the dye concentrations.

Thus, 0.05 µM is, actually, the minimal concentration at which **2ICy7** and **3ICy7** almost completely eradicate *S. aureus* while the dyes with fewer or more iodine atoms are less photocytotoxic. Thus, the non-charged (zwitterionic) dyes with two and three iodine atoms (**2ICy7** and **3ICy7**) were found to be the most effective against *S. aureus*.

They are more effective against this pathogen compared to other dyes at low concentrations and low light doses.

4.1.2.2 Photodynamic eradication of *E. coli* and *P. aeruginosa*

In the next step, we studied the photocytotoxicity of the dyes towards gram-negative pathogens *E. coli* and *P. aeruginosa*. The obtained data show that these bacteria are much more resistant to photodynamic treatment compared to the gram-positive *S. aureus*. Thus, all the investigated dyes do not cause a sufficient photocytotoxic effect on *E. coli* even at 50 µM and a light dose of 100 J/cm^2 (Fig. 4.8).

Fig. 4.8. Survival of *E. coli* in 0.7% DMSO in saline, when exposed to 100 J/cm^2 light dose (56 mW/cm^2, 30 min) *vs.* the dye concentrations.

There is a trend, however, that the mono-iodinated **1ICy7** is more active compared to other dyes at 100 J/cm^2 and this tendency is even more pronounced at 200−400 J/cm^2 (Fig. 4.9).

Surprisingly, the dyes containing four and six iodines are less photocytotoxic than **Cy7**. The increase of the positive charge (**2ICy7+** *vs.* **2ICy7**) has almost no effect on the dye photocytotoxicity at 100 J/cm^2 (Fig. 4.8) but noticeably improves the toxic effect at higher light dose of 200−400 J/cm^2 (Fig. 4.9). Therefore, the mono-iodinated

1ICy7 and positively charged **2ICy7+** are considered more effective against *E. coli* compared to other cyanines.

Fig. 4.9. Survival of *E. coli* at 50 µM dye concentrations in 0.7% DMSO in saline, when exposed to 100 J/cm^2 (30 min), 200 J/cm^2 (60 min), and 400 J/cm^2 (120 min) light doses.

Similar to *S. aureus*, the decrease in the photocytotoxicity towards gram-negative bacteria with increasing the number of iodine atoms between 2 and 6 is supposedly connected with the increasing dye aggregation (Fig. 4.2) and decreasing dye uptake. The aggregation effect is, however, even more pronounced for gram-negative bacteria because the dyes are used at much higher concentrations. To diminish the aggregation, we increased the content of DMSO in saline 10 times, from 0.7% (as in all the above experiments) to 7%. The obtained data in Fig. 4.10 show that the efficacy of **Cy7**, **1ICy7**, and **2ICy7** to eradicate *E. coli* was noticeably improved.

Thus, the survival percentage for these three dyes at 50 µM and 400 J/cm^2 decreased from 27.6%, 15.4%, and 50.0%, respectively, to zero. Nevertheless, the addition of even 7% DMSO to the saline solutions was insufficient to overcome the aggregation and improve the photocytotoxicity of **3ICy7**, **4ICy7**, and **6ICy7**.
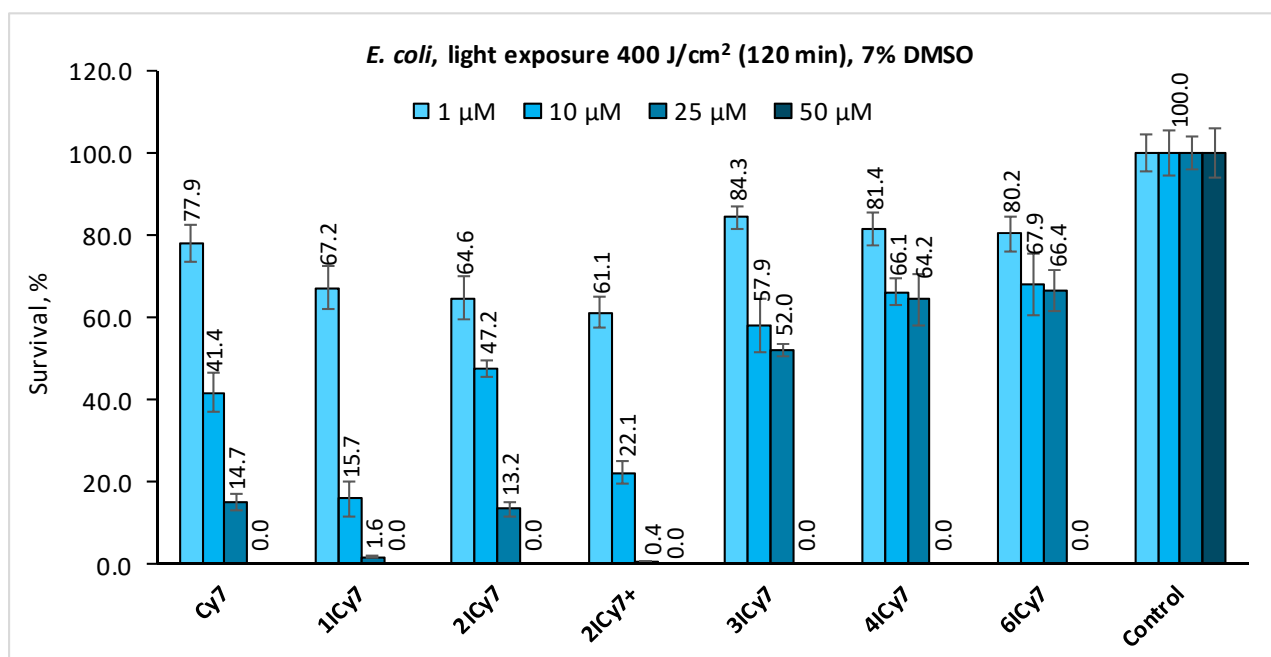
Fig. 4.10. Survival of *E. coli* in 7% DMSO in saline, when exposed to 400 J/cm^2 light dose (56 mW/cm^2, 120 min) *vs.* the dye concentrations.

P. aeruginosa was found to be even more resistant towards the investigated dyes (Figs. 4.11 and 4.12) than *E. coli*.
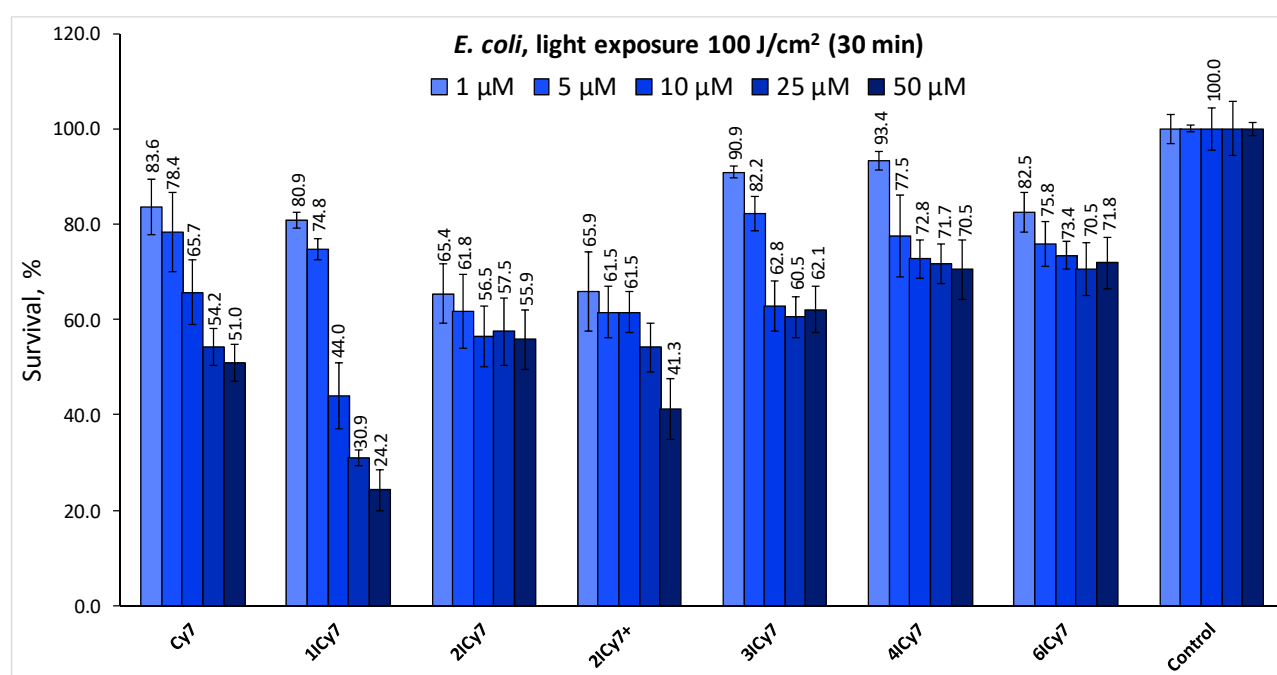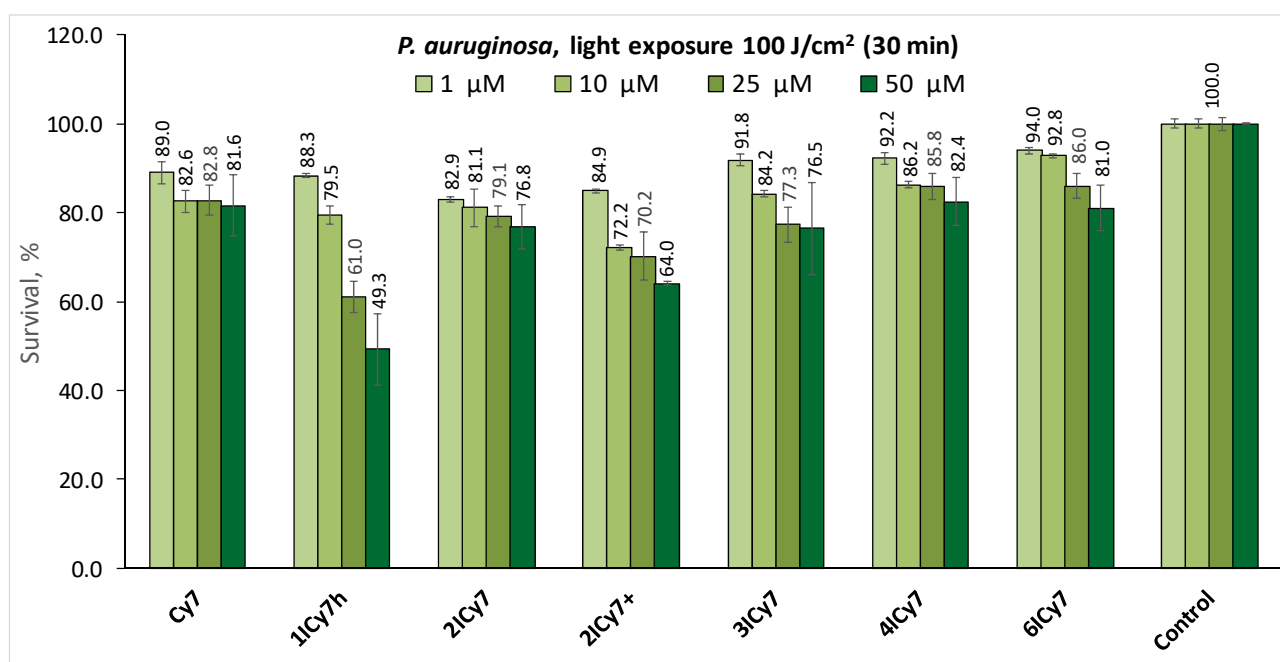

Fig. 4.11. Survival of *P. aeruginosa* in 0.7% DMSO in saline, when exposed to 100 J/cm^2 light dose (56 mW/cm^2, 30 min) *vs.* the dye concentrations.
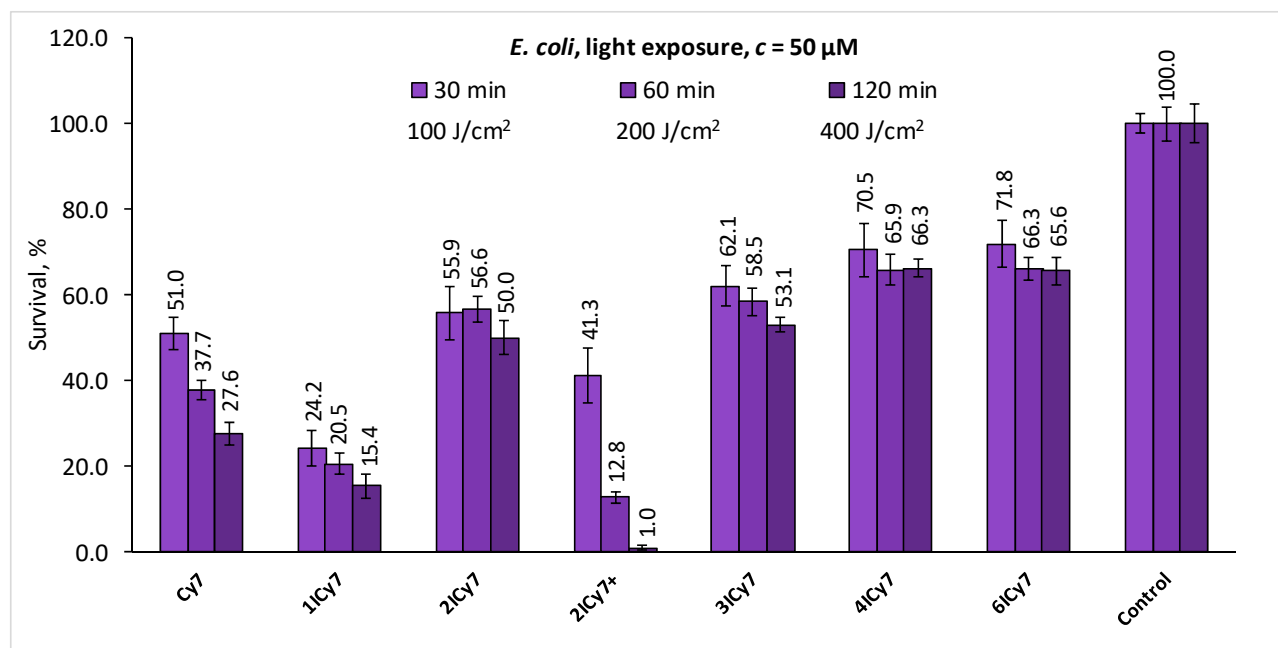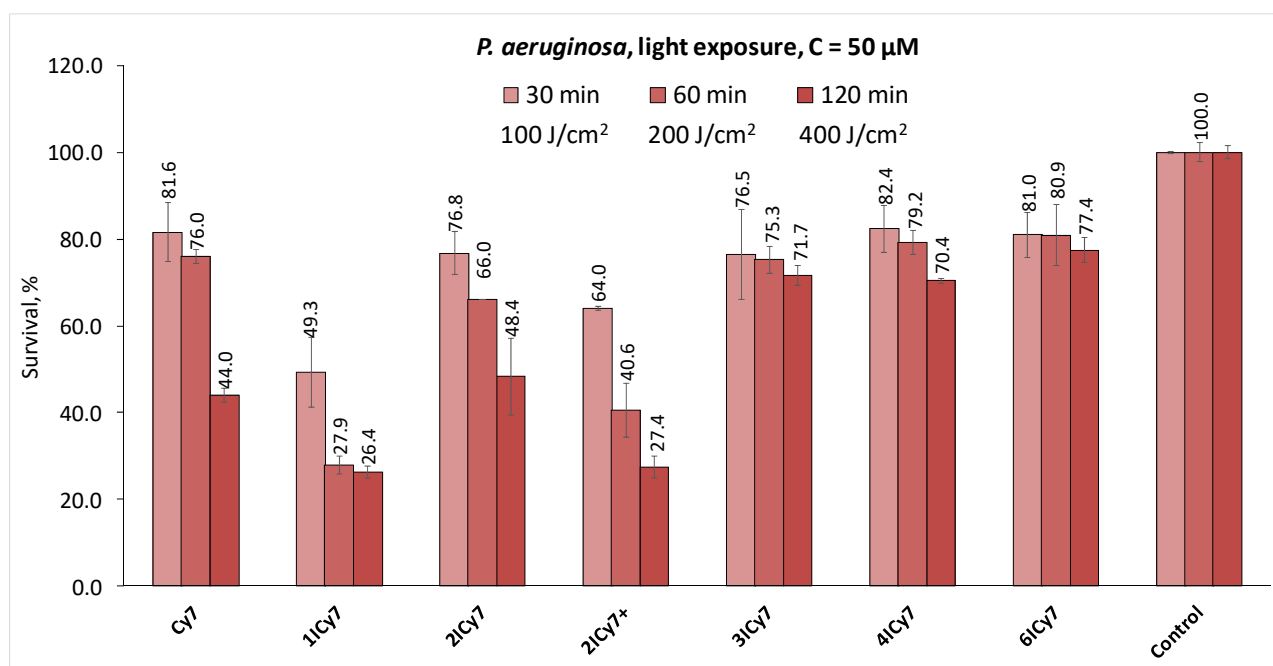
Fig. 4.12. Survival of *P. aeruginosa* at 50 µM dye concentrations in 0.7% DMSO in saline, when exposed to 100 J/cm^2 (30 min), 200 J/cm^2 (60 min), and 400 J/cm^2 (120 min) light doses.

Having the same tendency as for *E. coli*, the most photocytotoxic dyes for *P. aeruginosa* are mono-iodinated **1ICy7** and positively charged **2ICy7+**, which is different from *S. aureus*, where the most photocytotoxic are the diiodinated (**2ICy7**) and triiodinated (**3ICy7**) cyanines.

Thus, a studied series of novel, NIR, iodinated heptamethine cyanine dyes containing carboxylic function revealed the unexpected effect of the increasing number of iodine atoms (up to six) on the photodynamic eradication of gram-positive (*S. aureus*) and gram-negative (*E. coli* and *P. aeruginosa*) microbial pathogens. The efficacy of *S. aureus* photo-eradication by non-charged, zwitterionic cyanines increases with increasing the number of iodine atoms up to two, remains almost unchanged for the two-, three- and four-iodinated dyes, and reduces in the case of the hexa-iodinated cyanine. However, the mono-iodinated dye exhibits the most pronounced photocytotoxic effect on *E. coli* and *P. aeruginosa*. An additional positive charge provided by a triethylammonium group decreases the photokilling of *S. aureus* but improves the inactivation of *E. coli* and *P. aeruginosa*.

4.2 Antibody-guided, iodinated heptamethine cyanine photosensitizer for photoimmunotherapy (PIT)

Photoimmunotherapy (PIT) is a cancer treatment modality that synergistically combines immunotherapy and photodynamic (PDT) treatment. Besides being the main active agent in immunotherapy modulating the immune response on cancer cells, antibodies can be used as a carrier for target delivery. Among other carriers, antibodies have certain advantages over other carriers due to their high specificity, biodegradability, long blood circulatory half-life, and therapeutic effect. One of the well-known antibodies for immunotherapy of breast cancer is the FDA-approved humanized monoclonal antibody trastuzumab (Herceptin™) [149]. Trastuzumab targeting a human epidermal growth factor receptor 2 (HER2+) was launched in the late 1990s. It was the first immunotherapeutic agent to improve survival in women with metastatic HER2+ breast cancer, which tends to be aggressive driving the tumor's progression [149,150]. Trastuzumab also was used for the production of antibody-drug conjugates [150]. So, we used trastuzumab (**Ab**) to develop an antibody-guided photosensitizer for photoimmunotherapy with highly water-soluble diiodinated heptamethine cyanine dye, **2ICy7** (Scheme 4.1). We conjugate **2ICy7S** with **Ab**(trastuzumab), and investigate the obtained PIT conjugate in the mouse xenograft model to suppress tumor growth *versus* the parent, non-iodinated **Cy7−Ab** conjugate [151].

4.2.1 Bioconjugation

The carboxylic group of **2ICy7S** was activated with *N*-hydroxysuccinimidyl (NHS) group using *N,N,N',N'*-tetramethyl-O-(N-succinimidyl) uronium tetrafluoroborate (TSTU) in the presence of DIPEA in DMF. Then, the NHS-activated dye **2ICy7S** was bound to trastuzumab (**Ab**) in PBS by the straightforward, well-established, and commonly used procedure [152] to yield the **2ICy7S−Ab** conjugate which was then separated from the unbound dye on a Sephadex G50 column (Scheme 4.1).
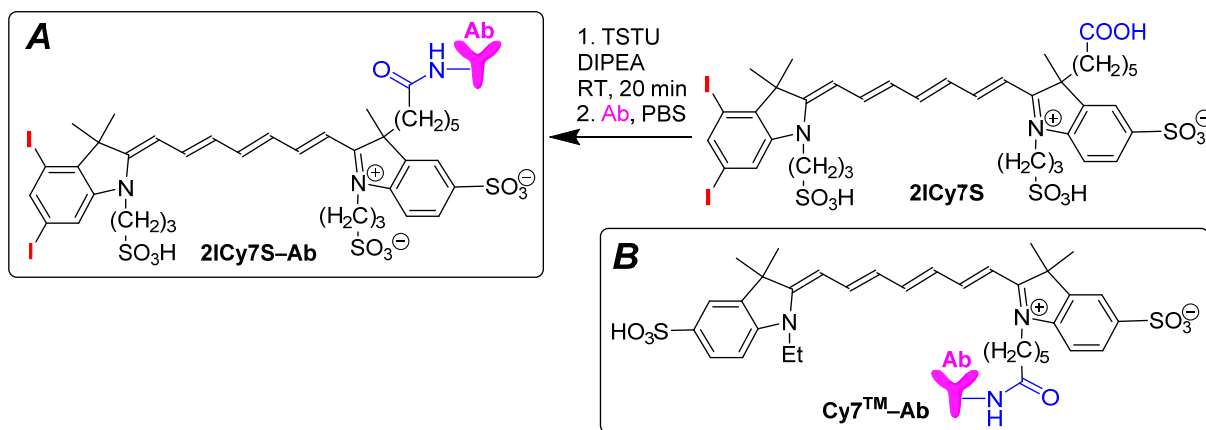
Scheme 4.1. Synthesis of **2ICy7S−Ab** conjugate (*A*) and the structure of the **Cy7^{TM}−Ab** conjugate (*B*).

For comparison, starting from the commercially available dye **Cy7^{TM}**, the **Cy7^{TM}−Ab** conjugate containing no iodine atoms was synthesized. Noteworthy, the attempts to link non-activated dyes (containing carboxylic acid group) with antibodies by using the above-mentioned conjugation procedure give the negligible level of binding, the obtained products contain only about 0.01 mol of dye per 1 mol of antibody (Fig. 4.13).
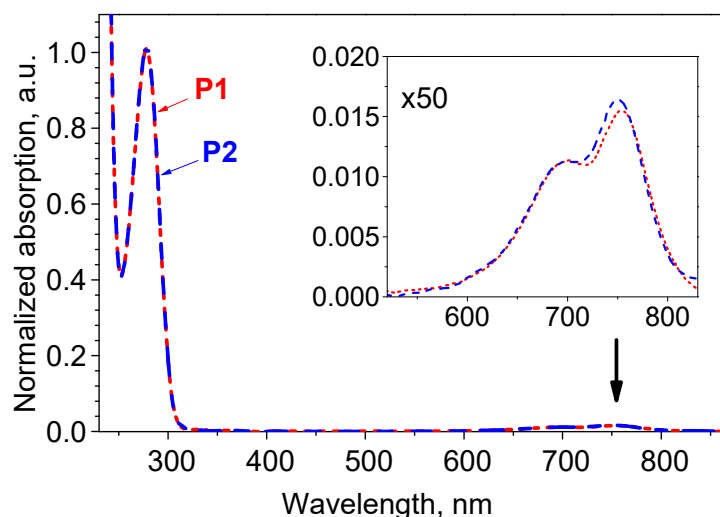
Fig. 4.13. Absorption spectra of the products isolated after purification on Sephadex G50 column when interacting of non-activated carboxylic acids of **2ICy7S** with **Ab** (**P1**) and **Cy7^{TM}** with **Ab** (**P2**) in 0.1 M PBS pH 7.4 at 25 °C.

4.2.2 Spectral properties of 2ICy7S and Cy7^{TM} dyes and their conjugates

The absorption and fluorescence maxima (λ_{max}Abs and λ_{max}Fl), extinction coefficients (ε), and the fluorescence quantum yield (Φ_{Fl}), for **Cy7^{TM}** and **2ICy7S** dyes and, additionally, Dye-to-Antibody ratio (DAR) and brightnesses for the **2ICy7S−Ab** and **Cy7^{TM}−Ab** conjugates measured in 0.1 M PBS pH 7.4 are given in Table 4.2, while the absorption and emission spectra, dye-to-antibody ratios are shown in (Fig. 4.14). The singlet oxygen quantum yields (Φ_Δ) were measured in methanol and PBS and also presented in Table 4.2.

Table 4.2. Spectral characteristics of the dyes and conjugates (λ_{max}Abs, λ_{max}Fl, Φ_{Fl}, Φ_Δ, ε). DAR and brightnesses ($B = \varepsilon \times \Phi_{Fl} \times$ DAR) were calculated only for the conjugates.

Dye	λ_{max}Abs, nm	λ_{max}Fl, nm	ε, M^{-1}cm^{-1}	Φ_{Fl}, %	Φ_Δ^1, % Methanol	Φ_Δ^2, % PBS
Cy7^{TM}	747	774	200,000	13 [153]	0.78±0.02	1.9±0.2
2ICy7S	749	779	262,000	14±1	1.10±0.03	5.8±0.3
Conjugate	λ_{max}Abs, nm	λ_{max}Fl, nm	B, M^{-1}cm^{-1}	Φ_{Fl}, %	DAR	Φ_Δ, %(PBS)
Cy7−Ab	752	777	21,400	6.3±0.5	1.7	1.1±0.1
2ICy7S−Ab	754	779	16,500	3.5±0.4	1.8	3.5±0.3

[1] **HITC** was used as the reference, $\Phi_\Delta = 0.89\%$ in methanol [28].

[2] **ICG** was used as the reference, $\Phi_\Delta = 0.2\%$ in PBS pH 7.4 [35].
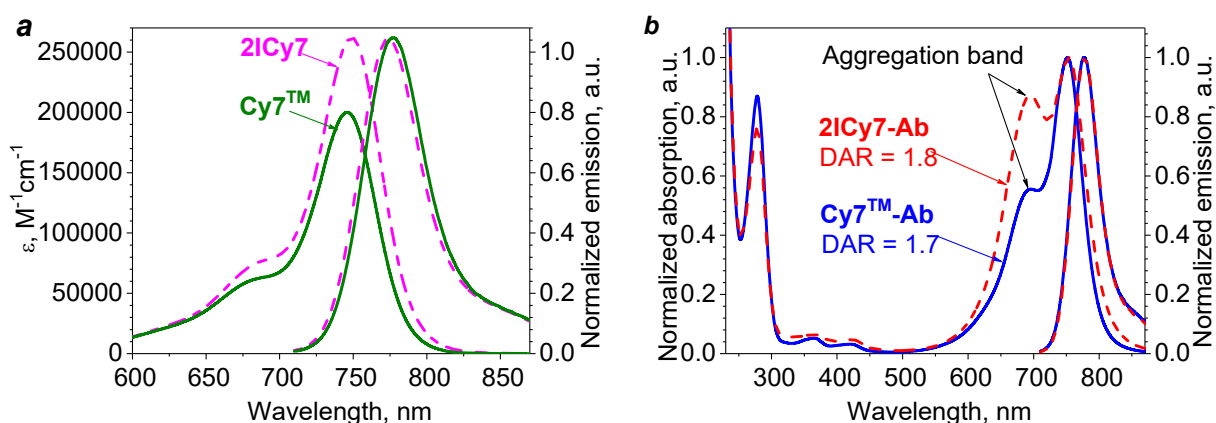
Fig. 4.14. Absorption and emission spectra of the dyes **2ICy7S** (dashed line) and **Cy7^{TM}** (solid line) *a*), as well as conjugates **2ICy7S−Ab** (dashed line) and **Cy7^{TM}−Ab** (solid line) *b*) in 0.1 M PBS pH 7.4. The dyes do not aggregate while **Cy7^{TM}−Ab** and especially **2ICy7S−Ab** exhibit aggregation bands at around 695 nm.

The modification of **Cy7$^{\text{TM}}$** with iodine atoms and additional sulfo groups yielding the **2ICy7S** dye leads to the negligible spectral red-shift of about 2−5 nm and a 1.3-fold increase in the extinction coefficient (ε) while the fluorescence quantum yield (Φ_{Fl}) remains almost the same. Both dyes exhibit no signs of aggregation in the phosphate buffer. In the absorption spectra, there is only a low-intensity shoulder at about 685 nm originating from the vibronic transition (Fig. 4.14a) [154].

Binding **Cy7$^{\text{TM}}$** and **2ICy7S** to the antibody has a minor effect on the absorption and emission maxima while the fluorescence quantum yields noticeably decrease in about 2 and 4 times, respectively (Table 4.2). This is more likely due to the dye aggregation on the antibody, which can be seen as an additional band at around 695 nm (Fig. 4.14b). Although the iodinated dye **2ICy7S** contains three sulfonic groups (one aromatic and two aliphatic), it is more aggregative on the antibody compared to **Cy7$^{\text{TM}}$** containing two aromatic sulfonic groups. As a result, the fluorescence quantum yield of **2ICy7S−Ab** is about twice as reduced compared to **Cy7$^{\text{TM}}$−Ab**. Both conjugates had very similar dye-to-antibody (DAR) ratios of 1.8 and 1.7, respectively, and the calculated brightness for **2ICy7S−Ab** is 1.3-fold smaller. Nonetheless, the brightnesses of these two conjugates are close.

4.2.3 Singlet oxygen generation

The quantum yields of the singlet oxygen generation (Φ_Δ) for **Cy7$^{\text{TM}}$** and **2ICy7S** were measured in methanol using known singlet oxygen scavenger 1,3-diphenylisobenzofuran (**DPBF**) [28]. Upon NIR light irradiation (30 W LED, 730 nm) of a mixture containing the dye and **DPBF**, the absorbance of **DPBF** reduced due to the reaction of **DPBF** with singlet oxygen formed caused by the dye sensitization of oxygen dissolved in the solvent. The corresponding plot (the example is presented in Fig. 4.15) representing the change in absorbance of **DPBF** at 410 nm *vs.* time was drawn and fitted by a first-order reaction rate function. Other plots can be found in [151].

The reaction rate (r), which is the key parameter for Φ_Δ calculation, was calculated as $r = 1 / t_1$, where t_1 was taken from the fitting

equation: $y = y_0 + A_1 \cdot \exp(-(x-x_0)/t_1$ (Table 4.3). Then, Φ_Δ was calculated relative to the reference dye (**HITC**) (see Section 5.4.3) [28].
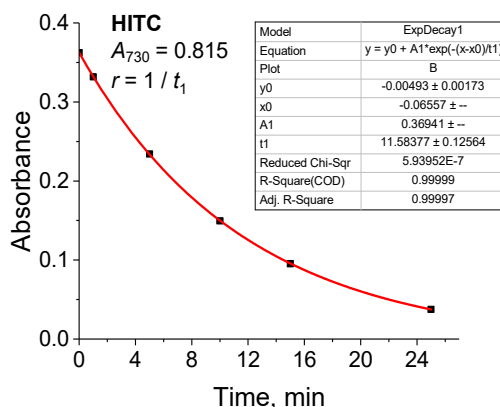
Fig. 4.15. The changes in absorbance of **DPBF** at 410 nm *vs.* time of irradiation of the mixture of **HITC** and **DPBF** in methanol with 730 nm LED, as well as fitting first-order decay function.

Table 4.3. The absorbances at 730 nm and reaction rate values of oxygen sensitization by the **Cy7^{TM}** and **2ICy7S** dyes and their conjugates were measured with **DPBF** in methanol and **SOSG** in 0.1 M PBS pH 7.4.

	DPBF methanol				SOSG 0.1 M PBS pH 7.4			
	A_{730}	r, min^{-1}	c_{Dye}, µM	Φ_Δ, %	A_{730}	r, min^{-1}	c_{Dye}, µM	Φ_Δ, %
HITC	0.815	0.0863	4.0	0.89	−	−	−	−
ICG	−	−	−	−	0.184	64.2	1.26	
					0.317	84.3	2.17	0.2
					0.629	142.3	4.30	
Cy7^{TM}	0.802	0.0739	6.0	0.78	0.183	611.6	1.26	1.91
					0.315	797.4	2.17	1.90
					0.624	1326.6	4.30	1.88
2ICy7S	0.810	0.1074	5.0	1.10	0.336	2544.4	1.7	5.8
Cy7^{TM}−Ab	−	−	−	−	0.263	428.4	1.9	1.1
2ICy7S−Ab	−	−	−	−	0.341	1575.3	1.9	3.5

As shown in Table 4.2, The Φ_Δ for **2ICy7S** in methanol was only 1.41 times higher than for **Cy7^{TM}**. Essentially, we anticipated a much higher increase of Φ_Δ upon iodination, so we assumed that the conjugation of the dyes with antibodies may affect

the singlet oxygen generation value. However, conjugates should be measured in aqueous solutions to maintain the native conformation of antibodies. Moreover, applications of conjugates for *in vivo* targeted delivery of dye-sensitizer involve the use of aqueous buffers, so the values of Φ_Δ for aqueous solutions are more practically significant. Unfortunately, **DPBF** is insoluble in water and should be used for determination of singlet oxygen only in methanol or some other organic solvents [155].

Thus, we utilized another singlet oxygen scavenger, singlet oxygen sensor green (**SOSG**), which is water-soluble and designed for the determination of singlet oxygen in aqueous solutions [156]. So, the quantum yields of the singlet oxygen generation (Φ_Δ) were measured using **SOSG** in 0.1 M PBS pH 7.4 for **Cy7^{TM}**, **2ICy7S**, **Cy7^{TM}−Ab**, and **2ICy7S−Ab**. Upon NIR light irradiation (30 W LED, 5.7 mW/cm^2, 730 nm) the emission of **SOSG** gradually increased, over up to 125 min. The corresponding plots representing the emission of **SOSG** at 530 nm *vs.* time were drawn and fitted by a zero-order reaction rate function (Fig. 4.16). Then, Φ_Δ was calculated relative to the reference dye (**ICG**).

Because the **SOSG** emission rate increase upon Φ_Δ measurements was very different with respect of the investigated dye, we used various concentrations of studied dyes (**Cy7^{TM}** and **2ICy7S**) and their conjugates (**2ICy7S−Ab** and **Cy7^{TM}−Ab**) ranged between c_{Dye} = 1.2−4.3 µM. We studied dependence of the **SOSG** reaction rate (r) from the dye concentration within the c_{Dye} = 1.2−4.3 µM on the example of **Cy7^{TM}** (Fig. 4.17), which demonstrated a positive linear correlation indicating that the calculated Φ_Δ is not dependent on the c_{Dye} within this range.

Equation	y = a + b*x
Plot	B
Weight	No Weighting
Intercept	82254.84738 ± 346.76
Slope	142.33964 ± 5.15918
Residual Sum of	2.43306E6
Pearson's r	0.99608
R-Square(COD)	0.99218
Adj. R-Square	0.99088
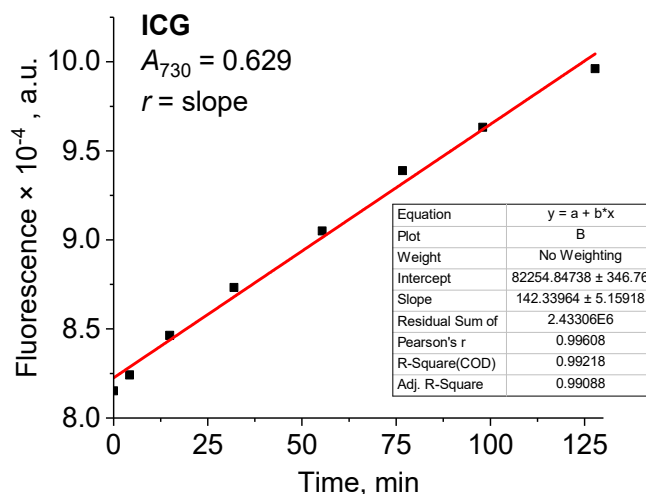
Fig. 4.16. The changes in **SOSG** fluorescence intensity over time at 530 nm due to singlet oxygen scavenging by **SOSG** upon irradiation of the mixture **ICG** and **SOSG** in 0.1 M PBS pH 7.4. A solution of **SOSG** ($c \sim 6$ µM) containing **ICG** ($c_{Dye} \sim 4.3$ µM) was light-irradiated with a 730 nm, 30 W LED, and the emission spectra were measured over time. The experimental emission values were fitted by a zero-order reaction rate function. The reaction rate (r) was calculated as $r =$ b (slope of the line), where b was taken from the fitting equation: $y = a + b \times x$.

Equation	y = a + b*x
Plot	B
Weight	No Weighting
Intercept	298.83126 ± 29.17
Slope	1636.60393 ± 69.9
Residual Sum of Squ	499.55796
Pearson's r	0.99909
R-Square(COD)	0.99818
Adj. R-Square	0.99636
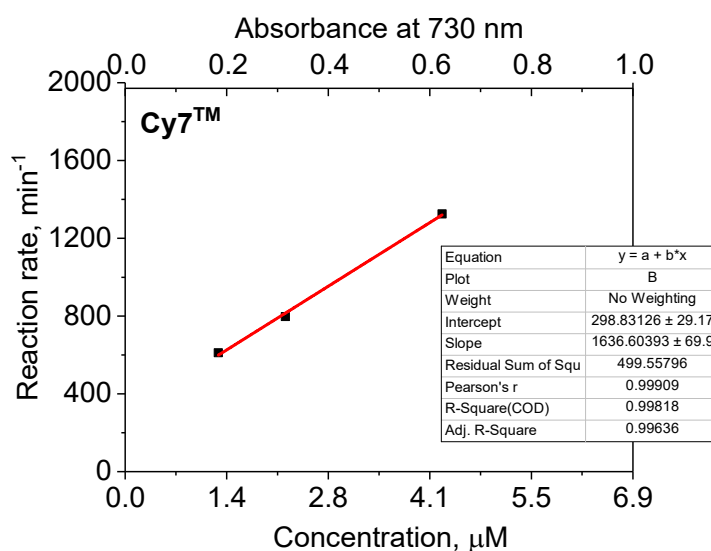
Fig. 4.17. The reaction rate of **SOSG** (6 µM) *vs.* different concentrations of **Cy7^TM**.

As shown in Table 4.2, the Φ_Δ for **2ICy7S** in PBS was 3-fold higher than for **Cy7^{TM}**. A similar effect (a 3-fold increase of Φ_Δ) was observed for **2ICy7S−Ab** compared to **Cy7^{TM}−Ab**. In addition, Φ_Δ for the **2ICy7S−Ab** and **Cy7^{TM}−Ab** conjugates were 1.7 times lower than those for the respective unconjugated dyes (**2ICy7S** and **Cy7^{TM}**), which could be attributed to the aggregation of these dyes on the antibody (Fig. 4.14).

Thus, the iodine atoms play a key role in the potency of the dyes to generate singlet oxygen and this effect is more pronounced in aqueous media compared to methanol. As will be shown below, the increase in the Φ_Δ correlates with the increase of the photodynamic effect in the tumor-bearing mice model.

4.2.4 Photoimmunotherapy

The photoimmunotherapeutic effect of the **Cy7^{TM}−Ab** and **2ICy7S−Ab** conjugates was investigated in the mouse xenograft model. Fifteen six-week-old athymic Balb/c female nude mice were subcutaneously inoculated in the dorsal right side with human breast cancer cell line BT-474 (1×10^6 cells in PBS into nu/nu mice, 100 µL per mouse) and tumors were allowed to establish over 10 days. After that, fifteen mice were randomly separated into five groups (3 mice per group). Group 1 was used as a control for tumor growth and background autofluorescence upon imaging. The rest of the mice were intravenously (IV) administered (tail vein) with **Cy7−Ab** (groups 2 and 3) and **2ICy7S−Ab** (groups 4 and 5). The administered dose of conjugate was 0.67 nmol (100 µg) (4 mg/kg) in 200 µL PBS. After 24 h post-injection, groups 3 and 5 were exposed to NIR light for 15 min (730 nm LED, 63 J/cm^2) and the tumor volumes for all the groups were monitored during 28 days (Fig. 4.18).
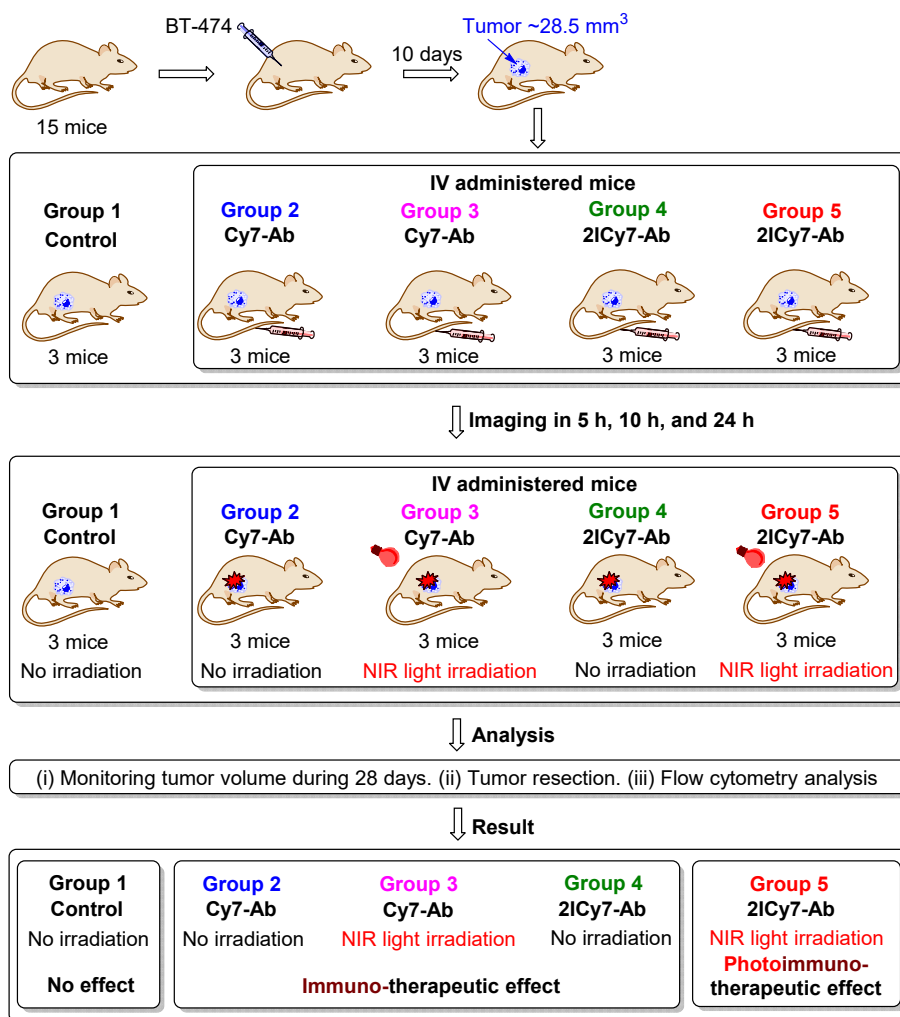
Fig. 4.18. Methodology of mice experiment to evaluate the photoimmunotherapeutic effect of dye conjugates on tumor growth.

To verify the impacts of NIR light on IV administrated free **Ab**, **2ICy7S**, and **Cy7^{TM}** on tumor growth, we performed an additional *in vivo* experiment (groups 6−10). After injection of BT-474 cells and tumor establishing over 10 days, fifteen mice were randomly separated into five groups (3 mice per group). Group 6 was used as the control for tumor growth and background autofluorescence upon imaging. After 10 days, group 7 was exposed to NIR light for 15 min (730 nm LED, 63 J/cm^2) and other mice groups were IV administered (tail) with **Cy7^{TM}** (group 8), **2ICy7S** (group 9) and **Ab** (group 10). The administered doses were 1.14 nmol (0.774 μg) of **Cy7**, 1.20 nmol (1.27 μg) of **2ICy7S**, and 0.67 nmol (100 μg) of **Ab** in 200 μL PBS (Fig. 4.19).
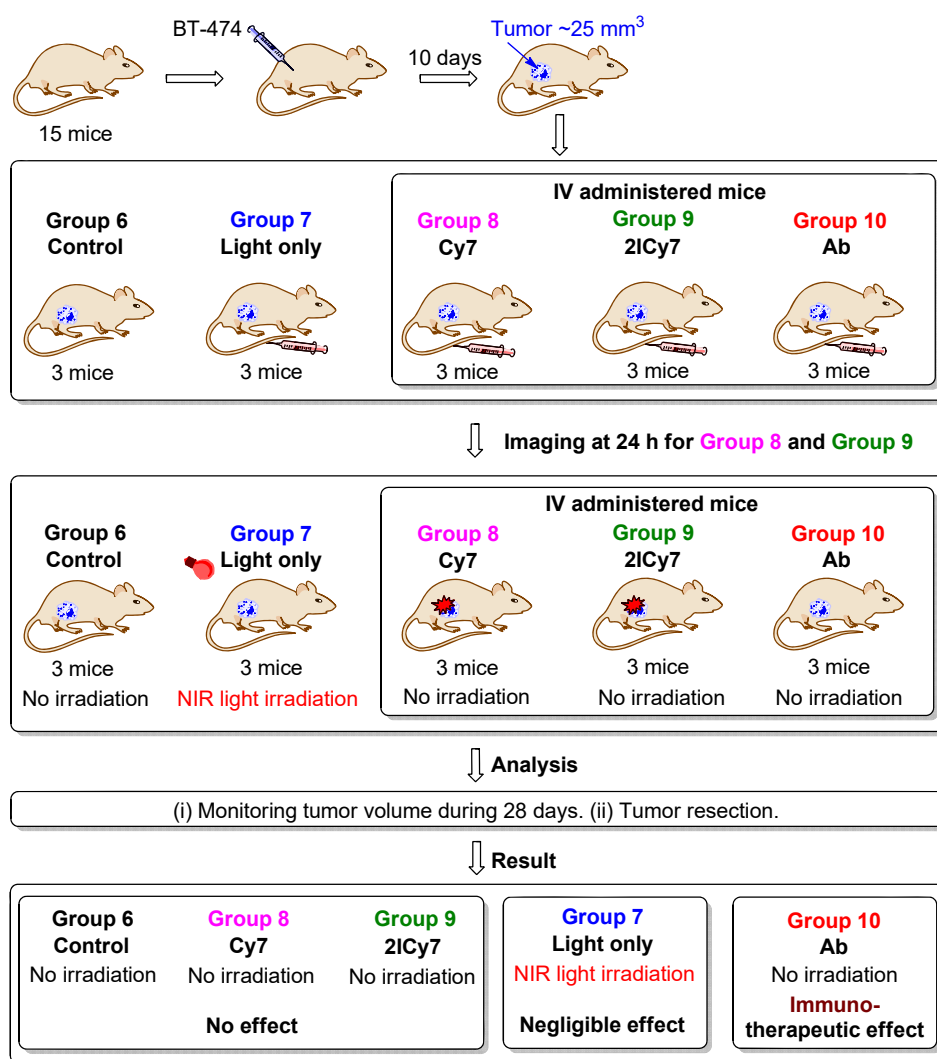
Fig. 4.19. Methodology of mice experiment to evaluate the effect of **Ab**, **2ICy7S**, and **Cy7^{TM}** on tumor growth.

4.2.4.1 Imaging

The distribution of the conjugates in mice whole body was monitored by an *in vivo* imaging system, CRi Maestro II. The images were captured in white light and NIR channel after 5 h, 10 h, and 24 h post-injection. After 5 h, an intense fluorescence signal originated from the photosensitizer was observed in the lungs while at 10 h the conjugates started to accumulate in the tumor sites (dorsal right side) followed by complete accumulation at 24 h (Fig. 4.20). At this time point (24 h), groups 3 and 5 administered with **Cy7^{TM}−Ab** and **2ICy7S−Ab**, respectively, were exposed to NIR light for 15 min (730 nm LED, 63 J/cm^2).
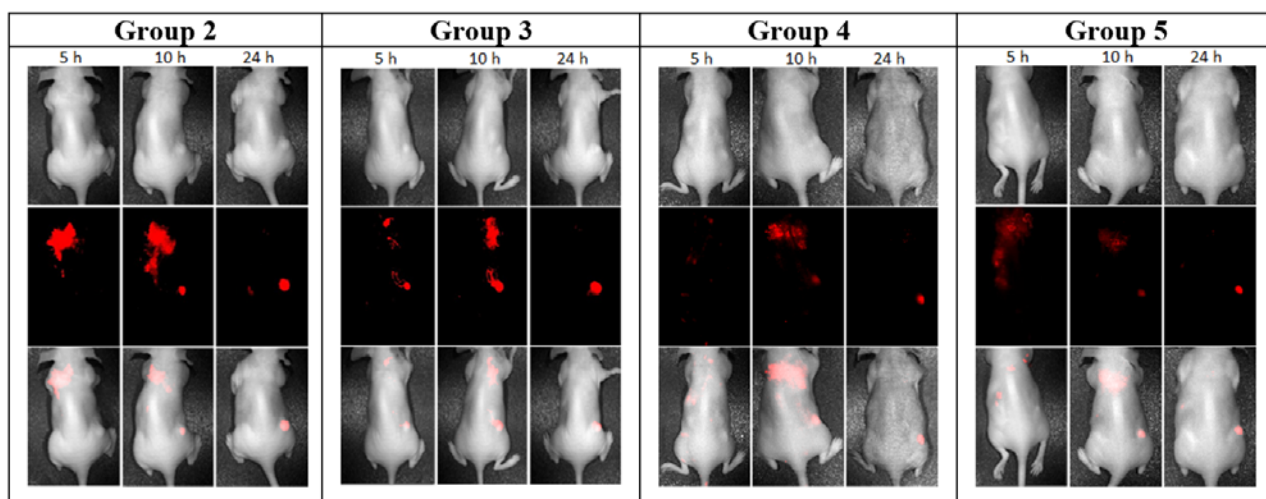
Fig. 4.20. *In vivo* whole body images of tumor-bearing mice (groups 2−5) captured at 5 h, 10 h, and 24 h after IV injection of the **Cy7^{TM}−Ab** and **2ICy7S−Ab** conjugates. 1st row − white-light, 2nd row − fluorescence channel, 3rd row − their merge.

The unconjugated dyes **Cy7^{TM}** and **2ICy7S** were almost equally distributed and remained over time in whole mouse body and organs (Fig. 4.21).
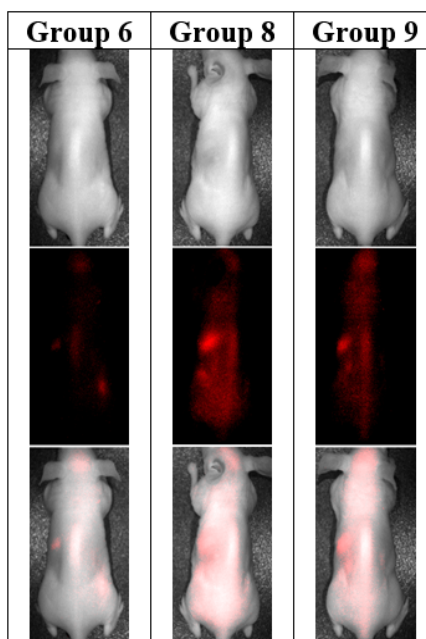
Fig. 4.21. *In vivo* whole body images of tumor-bearing mice from control group 6; and groups 9 and 10 captured at 24 h after IV injection of the **Cy7^{TM}** and **2ICy7S** dyes. 1st row − white-light channel, 2nd row − fluorescence channel, 3rd row − their merge.

Thus, to avoid healthy organs damage, these mice had not been light-irradiated (groups 8 and 9). The tumor size was monitored during 28 days by the hands-on digital caliper method [157]. On the 28th day, all the tumors were resected for further imaging and flow cytometry analysis.

4.2.4.2 Tumor development

Tumor growth curves of BT-474 tumor-bearing mice shown in Fig. 4.22 represent the impacts **Cy7^{TM}−Ab** and **2ICy7S−Ab** conjugates on tumor development.
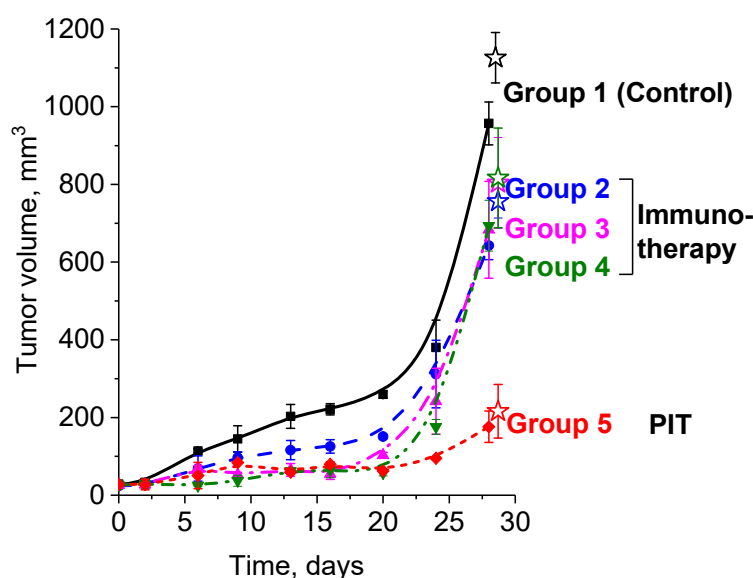
Fig. 4.22. Tumor growth curves of BT-474 tumor-bearing mice for Groups 1−5: control (group 1), monitored after a single IV administering of 100 µg (0.5 mg/mL) of **Cy7^{TM}−Ab**, when kept in the dark (group 2) or exposed to NIR light (730 nm LED, 63 J/cm^2) for 15 min (group 3), and **2ICy7S−Ab**, when kept in the dark (group 4) or exposed to the same NIR light dose (group 5). The tumor volumes were measured *in vivo* by the caliper method and calculated as $V = \text{Length} \times \text{Width}^2 / 2$. The volumes of the resected tumors are shown by stars. The tumor volume at each time point is represented by the mean ± standard error for three mice in each group.

It was found that the tumors in control group 1 started to gradually develop on the 6th day of observation. Meanwhile, the tumors of four other mice groups showed modest growth during 16 days. After that, the tumors of groups 2 and 3 began to grow while the tumors for groups 4 and 5 showed a notable increase only on the 24th day. By

the 28th day, the tumors of the control group 1 reached 957±55 mm^3, demonstrating a 34-fold volume increase compared to the initial volume (~28.5 mm^3) while the tumors of groups 2−4 exhibited almost an equal increase by the factor of about 24 (the final tumor volumes were 673±69 mm^3), which corresponded to the 1.4-fold tumor growth suppression compared to group 1. Importantly, the light-irradiated group 3 administered with the non-iodinated **Cy7^{TM}−Ab** conjugate had very similar final tumor volumes, as the groups 2 and 4 were kept in the dark (Fig. 4.22). On the other hand, the tumors in group 5 reached only 176±40 mm^3 (~6-fold increase), which corresponded to the ~5.4-fold tumor growth suppression compared to control and ~4-fold suppression compared to non-irradiated groups 2 and 4. The noticeably increased tumor suppression (5.4× *vs.* 1.4×) we explain by combined immuno- and photodynamic effects.

The tumors resected on the 28th day were captured in white light (Fig. 4.23) and their volumes were calculated from the caliper measurements.
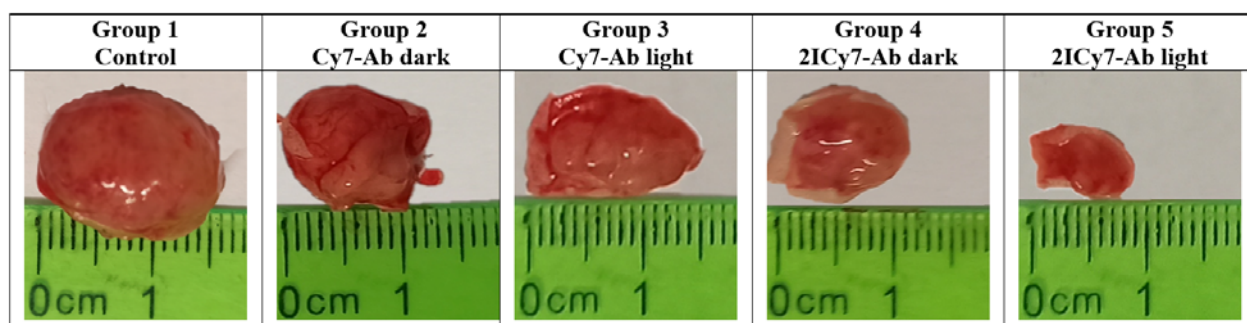
Fig. 4.23. Representative photographs of the tumors resected on the 28th day after IV injection of the conjugates.

The volumes of the tumors were similar to those determined *in vivo* by the same caliper method (Fig. 4.22). Thus, the tumors of groups 2−4 were 756±43 mm^3, 804±117 mm^3, and 816±128 mm^3, respectively, which was about 1.4-fold lower compared to group 1 (1,126±65 mm^3), while for group 5 tumors were 5.2 times lower, 216±69 mm^3.

Tumor growth curves of BT-474 tumor-bearing mice shown in Fig. 4.24 represent the impacts of NIR light (group 7), **Cy7^{TM}** (group 8), **2ICy7S** (group 9) and **Ab** (group 10) on the tumor development.
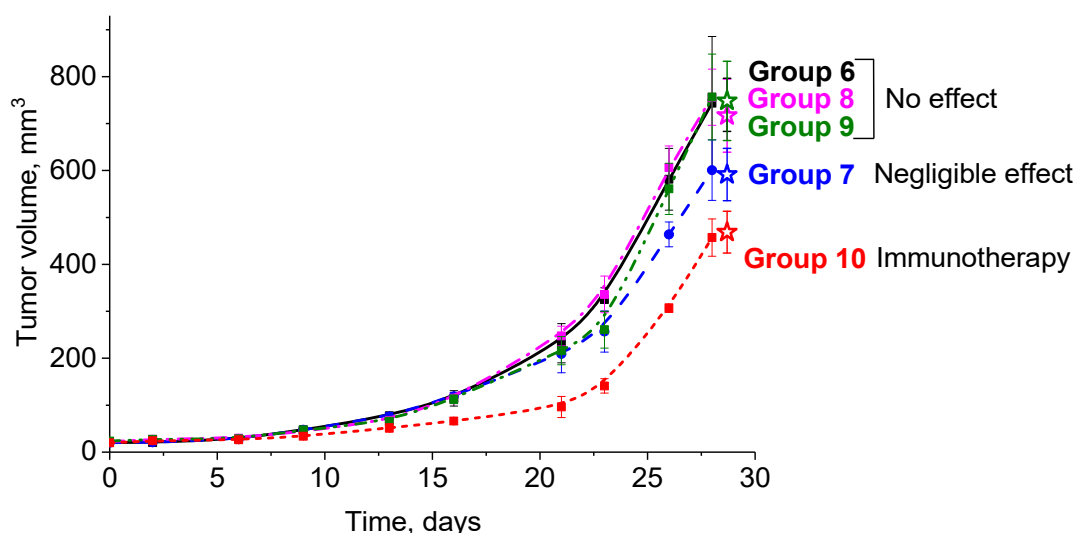
Fig. 4.24. Tumor growth curves of BT474 tumor-bearing mice for Groups 6−10: (i) control (group 6), (ii) mice monitored after NIR light exposure (730 nm LED, 63 J/cm^2) for 15 min (group 7) or (iii) mice IV administered (tail) with **Cy7^{TM}** (group 8), **2ICy7S** (group 9) and **Ab** (group 10). The administered doses were 1.14 nmol (0.774 μg) of **Cy7^{TM}**, 1.20 nmol (1.27 μg) of **2ICy7S**, and 0.67 nmol (100 μg) of **Ab** in 200 μL PBS. The tumor volumes were measured *in vivo* by the caliper method and calculated as $V = \text{Length} \times \text{Width}^2 / 2$. The volumes of the resected tumors are shown by stars. The tumor volume at each time point is represented by the mean ± standard error for three mice in each group.

The results depicted in Fig. 4.24 evidenced that the light exposure of non-administered mice (group 7) had negligible effect on the tumor growth and IV administering of free **Cy7^{TM}** (group 8) and **2ICy7S** (group 9) had no effect on the tumor growth. To estimate the contribution of the "pure" immunotherapeutic effect in mice treatment, the mice of group 10 were IV injected with the same amount of **Ab** not conjugated to dye (group 10). The tumor suppression was found to be only ~1.5-fold more pronounced compared to the control (group 6). The effectiveness of immunotherapy for the **Ab**-administered mice (group 10) was found to be almost the same as for groups 2, 3, and 4. Therefore, we can conclude that the 1.4-fold tumor growth suppression was associated only with the immunotherapeutic effect, and the **Cy7^{TM}** dye exhibited no detectable photocytotoxicity.

Thus, the major contribution in PIT treatment of xenograft mice model comes from the PDT effect of dye (**2ICy7S**) in the conjugate, while the immunotherapeutic effect is less significant.

4.2.4.3 Flow cytometry

The tumors resected on the 28th day were dissociated into the single cell suspensions, as described in the procedure [158], and the isolated cells were stained with Annexin V-FITC and propidium iodide (PI) to identify the dead apoptotic and necrotic cells, respectively. Cells that remained unstained were considered alive. As anticipated, for the control group 1 only survived cancer cells (99.2±0.1%) were detected. Flow cytometry analysis of the stained cancer cells in all other groups (groups 2−5) indicated almost no *early* apoptosis (no more than 1.2%), and, in fact, only an insignificant (up to ~3%) *late* apoptosis for groups 3 and 5 (Fig. 4.25).
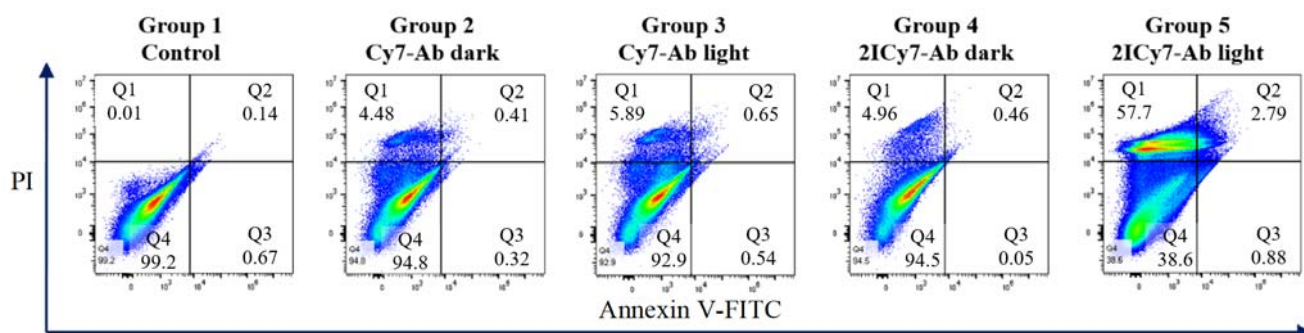
Fig. 4.25. Flow cytometry analysis of cancer cells taken from the BT-474 tumors resected on the 28th day without treatment (control group 1), after the IV administering with **Cy7−Ab** and kept in the dark (group 2) or exposed to NIR light for 15 min (730 nm LED, 63 J/cm^2) (group 3), and IV administered with **Cy7^{TM}−Ab** when kept in the dark (group 4) or exposed to the same NIR light dose (group 5). Q1 (top left section) − necrosis, Q2 (top right section) − late apoptosis, Q3 (bottom right section) − early apoptosis, Q4 (bottom left section) − live cells.

Groups 2 and 4, which were subjected to immunotherapeutic treatment without light exposure, and the light-irradiated group 3 were characterized by insignificant *necrotic* processes of 5.2±1%, 4.9±0.7%, and 5.9±1.2%, respectively. However, the percentage of the necrotic cells for the light-irradiated (PIT-treated) group 5 was much

more pronounced, 58.1±0.2%. Thus, necrosis is the main mechanism of cancer cell death upon PIT treatment.

Hence, the combination of the immuno- and photodynamic therapies has resulted in the noticeably enhanced cancer cell death.

4.3 Conclusions to chapter 4

Investigation of the spectral properties and ability for photodynamic eradication of *S. aureus*, *E. coli*, and *P. aeruginosa* pathogens of the developed new NIR heptamethine cyanine dyes containing up to six iodine atoms and an aliphatic carboxylic group demonstrate that the increasing the number of iodine atoms has an unexpected and ambiguous photocytotoxic effect on these bacteria, which is connected with two opposite factors: (i) increasing the intersystem crossing and the rates of reactive species generation and (ii) dye aggregation causing the reduced dye uptake that, supposedly, is followed by decreased rates of reactive species generation. As a result, the increase of the number of iodine atoms up to two in the series of zwitterionic cyanines increases the efficacy of *S. aureus* eradication; then the efficacy remains almost unchanged for the two-, three- and four-iodinated dyes and diminishes in the case of the hexa-iodinated cyanine. At the same time, the mono-iodinated heptamethine cyanine causes the most pronounced photocytotoxic effect on *E. coli* and *P. aeruginosa*. An additional positive charge contributed by a triethylammonium group decreases the efficacy of the dye towards *S. aureus* but improves the eradication of *E. coli* and *P. aeruginosa*. We believe that the developed dyes will be effective for the treatment of other bacteria, viruses, and cancer cells. The presence of carboxylic function potentially enables further binding of these dyes to various carriers.

The photoimmunotherapeutic agent, **2ICy7S−Ab**, based on the water soluble diiodinated heptamethine cyanine NIR dye **2ICy7S** conjugated with the trastuzumab antibody facilitates significant breast cancer tumor growth suppression in the mouse xenograft model. While the antibody-stimulated immunotherapeutic effect of **2ICy7S−Ab** can be estimated as 1.4-fold tumor growth suppression, the combined photoimmunotherapeutic action results in 5.4-fold suppression caused by necrosis. The

iodinated **2ICy7S−Ab** conjugate demonstrates a 3-fold increased quantum yield of singlet oxygen generation in aqueous media compared to its non-iodinated analog, **Cy7^{TM}−Ab**. Thus, the iodine atoms in **2ICy7S** play a key role in the augmented photocytotoxicity of the **2ICy7S−Ab** conjugate. The non-iodinated **Cy7^{TM}−Ab** does not show statistically significant photocytotoxicity on cancer cells and acts solely as an immunotherapeutic agent.

Importantly, **2ICy7S−Ab** provides a bright fluorescent signal enabling real-time monitoring of the conjugate distribution in the body and accumulation in the tumor, which is important for recognizing the optimal time for light irradiation and thus improving the precision and safety of treatment. We anticipate that the conjugation of **2ICy7S** or other cyanine-based photosensitizers of a similar structure with a wide range of antibodies can gradually expand the scope of efficient tools for photoimmunotherapeutic treatment aimed at different types of cancer.

CHAPTER 5
EXPERIMENTAL PART

5.1 Materials and methods

Starting materials were purchased from *Acros*, *Aldrich*, *Alfa Aesar Israel*. Silica gel 60 for column chromatography, and other materials were from *Merck* and used as is. Solvents were purchased from Bio-Lab Israel and used as is. 4-Iodoaniline was purchased from *Aldrich*. 3,5-Dibromoaniline, 3,5-dichlorophenylhydrazine hydrochloride, 3- and 4-bromophenylhydrazines hydrochlorides, 2,3,3-Trimethyl-3*H*-indole were purchased from *TCI*. **HITC** as the reference dye was purchased from *Sigma-Aldrich* and additionally purified by column chromatography (Silica gel 60, 5−10% methanol-chloroform). **Cy7^{TM} NHS Ester (Cy7^{TM}-NHS)** was purchased from Cytiva Amersham™, and trastuzumab from F. Hoffmann-La Roche Ltd (Basel, Switzerland). All other chemicals were supplied by Sigma-Aldrich. Chemical reactions were monitored by TLC (Silica gel 60 F-254, Merck) and LC/MS.

LC/MS analysis was performed using an Agilent Technologies 1260 Infinity (LC) 6120 quadrupole (MS), column Agilent Zorbax SB-C18, 1.8 mm, 2.1 × 50 mm, column temperature 50 °C, eluent water−acetonitrile (ACN) + 0.1% formic acid.

HRMS spectra were obtained using a Xevo G2-XS QTOF device. Data was acquired using resolution mode under positive electrospray ionization. Acquisition range was 50-1200 *m/z*. Capillary voltage was 2.0 kV. Cone voltage was 40 V. Scan times were 0.5 s. The samples were injected direct to MS. In all cases, MeOH was used as eluent.

^{1}H-NMR and **^{13}C-NMR** spectra were recorded on a Bruker Avance III HD (^{1}H at 400 MHz and ^{13}C at 100 MHz) spectrometer and a BBO probe equipped with a Z-gradient coil. ^{1}H-NMR spectra of quaternized indolenines **2.2** and **2.4** were measured in DMSO-d_6 at 300 K. ^{13}C-NMR spectra of quaternized indolenines **2.2**, **2.4, 2.1a-d** and **2.3a-c** were measured at 300 K in DMSO-d_6 and TFA-*d*, respectively. ^{1}H-NMR and ^{13}C-NMR spectra of **xHal$_n$-HITC** heptamethine cyanine dyes were measured

in DMSO-d_6 at 300 K; for **2ICy7S** were measured in DMSO-d_6 at 275 K; for **Cy7**, **1ICy7−6ICy7** were measured in a CDCl$_3$ (80%) − CD$_3$OD (20%) mixture at 275K.

5.2 Synthesis procedures

5.2.1 Synthesis of phenylhydrazines

General procedure for synthesis of phenylhydrazines 2.3b−f:

A solution of aniline **1b−1i** (1 equiv.) in 25 mL of conc. H$_2$SO$_4$ was cooled to about −10 °C and the solution of NaNO$_2$ (1-1.3 equiv.) in 5 mL of conc. H$_2$SO$_4$ was added dropwise with continuous stirring. The suspension was stirred for 40 min at −10 °C. Then, the cooled solution of SnCl$_2$·2H$_2$O (3.2 equiv.) in conc. HCl was added dropwise at −10 °C to the obtained suspension of diazocompound (**2.2b−i**). The reaction mixture was kept at 0 °C for 1 h and at 5−10 °C overnight. The obtained precipitate was filtered off, washed with 1 M aqueous solution of HCl and water to give target compound **2.3b−i**. These phenylhydrazines were used for further synthesis of indoles without additional purification.

(4-Iodophenyl)hydrazine hydrochloride (2.3b) was obtained according to the general procedure starting from 4-iodoaniline (10 g, 45.6 mmol) suspended in 10 mL of conc. HCl and 8 mL of water (instead of conc. H$_2$SO$_4$), 14 mL of 20% aqueous solution of NaNO$_2$ (3.18 g, 46 mmol) and SnCl$_2$·2H$_2$O (33 g, 146 mmol): beige powder, yield: 90%, **^{1}H-NMR** (400 MHz, DMSO-d_6), δ, ppm: 10.32 (2H, bs, NH$_2$), 7.58 (2H, d, J = 8.1 Hz, CH), 6.81 (2H, d, J = 8.2 Hz, CH). Exchangeable NH proton was not recorded in ^{1}H-NMR spectrum. **ESI-MS** *m/z* found: [M−Cl]$^+$ 234.9; C$_6$H$_8$IN$_2$$^+$ requires 235.0.

(3,5-Dibromophenyl)hydrazine hydrochloride (2.3c) was obtained according to the general procedure starting from 3,5-dibromoaniline (4.1 g, 16.3 mmol), NaNO$_2$ (1.13 g, 16.3 mmol) and SnCl$_2$·2H$_2$O (11.8 g, 52.3 mmol): beige powder, yield: 97%, **^{1}H-NMR** (400 MHz, DMSO-d_6), δ, ppm: 10.13 (2H, bs, NH$_2$), 7.33 (1H, s, CH), 7.11 (2H, s, CH). Exchangeable NH proton was not recorded in ^{1}H-NMR spectrum. **ESI-MS** *m/z* found: [M−Cl]$^+$ 266.9; C$_6$H$_7$Br$_2$N$_2$$^+$ requires 266.9.

(3,5-Diiodophenyl)hydrazine hydrochloride (2.3d) was obtained according to the general procedure starting from 3,5-diiodoaniline (5 g, 14.5 mmol), NaNO$_2$ (1.3 g, 18.8 mmol) and SnCl$_2$·2H$_2$O (10.5 g, 46.4 mmol): beige powder, yield: 87%, **^{1}H-NMR** (400 MHz, DMSO-d_6), δ, ppm: 10.33 (2H, bs, NH$_2$), 8.62 (1H, bs, NH), 7.59 (1H, s, CH), 7.34 (2H, s, CH). **ESI-MS** m/z found: [M−Cl]$^+$ 360.8; C$_6$H$_7$I$_2$N$_2$$^+$ requires 360.9.

(3,4,5-Tribromophenyl)hydrazine hydrochloride (2.3e) was obtained according to the general procedure starting from 3,4,5-tribromoaniline (7.9 g, 24 mmol), suspended in 10 mL of conc. HCl and 8 mL of water (instead of conc. H$_2$SO$_4$), 10.7 mL of 20% aqueous solution of NaNO$_2$ (2.15 g, 31 mmol) and SnCl$_2$·2H$_2$O (17.3 g, 76.6 mmol): beige powder, yield: 67%, **^{1}H-NMR** (400 MHz, DMSO-d_6), δ, ppm: 10.51 (2H, bs, NH$_2$), 8.88 (1H, bs, NH), 7.40 (2H, s, CH). **ESI-MS** m/z found: [M−Cl]$^+$ 344.7; C$_6$H$_6$Br$_3$N$_2$$^+$ requires 344.8.

(3,4,5-Triiodophenyl)hydrazine hydrochloride (2.3f) was obtained according to the general procedure starting from 3,4,5-triiodoaniline (5 g, 10.6 mmol), NaNO$_2$ (0.95 g, 13.8 mmol) and SnCl$_2$·2H$_2$O (7.7 g, 34 mmol): beige powder, yield: 95% **^{1}H-NMR** (400 MHz, DMSO-d_6), δ, ppm: 9.96 (2H, bs, NH$_2$) 7.47 (2H, s, CH). Exchangeable NH proton was not recorded in ^{1}H-NMR spectrum. **ESI-MS** m/z found: [M−Cl]$^+$ 486.7; C$_6$H$_6$I$_3$N$_2$$^+$ requires 486.8.

5.2.2 Synthesis of 3*H*-indoles

General procedure for synthesis of indoles 2.4a-i

Phenylhydrazine **3a−3i** (1 equiv.) and 3-methyl-2-butanone (1.5 equiv.) were refluxed in 15 mL of acetic acid for 5 h. The acetic acid was evaporated, the residue was washed with 20 mL of 5% aqueous solution of Na$_2$CO$_3$. Residue was dissolved in benzene and extracted with 5% aqueous solution of Na$_2$CO$_3$ and water. The organic layer was collected, concentrated and dried in a desiccator over NaOH to yield product **4a−4i**. These indoles were used for further synthesis of indolenines without additional purification.

5-Bromo-2,3,3-trimethyl-3*H*-indole (2.4a) was obtained according to the general procedure starting from (4-bromophenyl)hydrazine hydrochloride (2 g,

8.9 mmol) and 3-methyl-2-butanone (1.15 g, 13.4 mmol): brown oil, yield: 85%, **^{1}H-NMR** (400 MHz, DMSO-d_6), δ, ppm: 7.66 (1H, s, CH), 7.44 (1H, d, J = 8.2 Hz, CH), 7.36 (1H, d, J = 8.1 Hz, CH), 2.19 (3H, s, CH$_3$), 1.24 (6H, s, C(CH$_3$)$_2$). **ESI-MS** *m/z* found: [M+H]$^+$ 238.0; C$_{11}$H$_{13}$BrN$^+$ requires 238.0.

5-Iodo-2,3,3-trimethyl-3*H*-indole (2.4b) was obtained according to the general procedure starting from (4-iodophenyl)hydrazine hydrochloride (6 g, 22.2 mmol) and 3-methyl-2-butanone (2.86 g, 33.3 mmol): brown oil, yield: 57%, **^{1}H-NMR** (400 MHz, DMSO-d_6), δ, ppm: 7.80 (1H, s, CH), 7.60 (1H, d, J = 8.1 Hz, CH), 7.23 (1H, d, J = 8.0 Hz, CH), 2.18 (3H, s, CH$_3$), 1.22 (6H, s, C(CH$_3$)$_2$). **ESI-MS** *m/z* found: [M+H]$^+$ 286.0; C$_{11}$H$_{13}$IN$^+$ requires 286.0.

4,6-Dibromo-2,3,3-trimethyl-3*H*-indole (2.4c) was obtained according to the general procedure starting from (3,5-dibromophenyl)hydrazine hydrochloride (3.3 g, 11 mmol) and 3-methyl-2-butanone (1.42 g, 16.5 mmol): light brown crystals, yield: 57%, **^{1}H-NMR** (400 MHz, DMSO-d_6), δ, ppm: 7.66 (1H, s, CH), 7.58 (1H, s, CH), 2.24 (3H, s, CH$_3$), 1.36 (6H, s, C(CH$_3$)$_2$). **ESI-MS** *m/z* found: [M+H]$^+$ 317.9; C$_{11}$H$_{12}$Br$_2$N$^+$ requires 317.9.

4,6-Diiodo-2,3,3-trimethyl-3*H*-indole (2.4d) was obtained according to the general procedure starting from (3,5-diiodophenyl)hydrazine hydrochloride (3 g, 7.6 mmol) and 3-methyl-2-butanone (0.98 g, 11.4 mmol): off-white powder, yield: 43%, **^{1}H-NMR** (400 MHz, DMSO-d_6), δ, ppm: 7.92 (1H, s, CH), 7.79 (1H, s, CH), 2.22 (3H, s, CH$_3$), 1.32 (6H, s, C(CH$_3$)$_2$). **ESI-MS** *m/z* found: [M+H]$^+$ 412.0; C$_{11}$H$_{12}$I$_2$N$^+$ requires 411.9.

4,5,6-Tribromo-2,3,3-trimethyl-3*H*-indole (2.4e) was obtained according to the general procedure starting from (3,4,5-tribromophenyl)hydrazine hydrochloride (0.457 g, 5 mmol) and 3-methyl-2-butanone (0.155 g, 1.8 mmol): off-white powder, yield: 59%, **^{1}H-NMR** (400 MHz, DMSO-d_6), δ, ppm: 7.86 (1H, s, CH), 2.24 (3H, s, CH$_3$), 1.37 (6H, s, C(CH$_3$)$_2$). **ESI-MS** *m/z* found: [M+H]$^+$ 395.9; C$_{11}$H$_{11}$Br$_3$N$^+$ requires 395.8.

4,5,6-Triiodo-2,3,3-trimethyl-3*H*-indole (2.4f) was obtained according to the general procedure starting from (3,4,5-triiodophenyl)hydrazine hydrochloride (1 g,

1.9 mmol) and 3-methyl-2-butanone (0.25 g, 2.9 mmol): off-white powder, yield: 97%, ^{1}**H-NMR** (400 MHz, DMSO-d_6), δ, ppm: 8.03 (1H, s, CH), 2.19 (3H, s, CH$_3$), 1.29 (6H, s, C(CH$_3$)$_2$). **ESI-MS** *m/z* found: [M+H]$^+$ 537.8; C$_{11}$H$_{11}$I$_3$N$^+$ requires 537.8.

4-Bromo-2,3,3-trimethyl-3*H*-indole (2.4g) and 6-bromo-2,3,3-trimethyl-3*H*-indole (2.4h) were obtained according to the general procedure starting from (3-bromophenyl)hydrazine hydrochloride (1 g, 4.5 mmol) and 3-methyl-2-butanone (0.58 g, 6.7 mmol). The mixture of **2.4g** and **2.4h** was separated on RP-18 column using as eluent ACN−water (+0.05% acetic acid)−ethyl acetate from 45:50:10 to 65:25:20 v.v.%.

4-Bromo-2,3,3-trimethyl-3*H*-indole (2.4g): yellow oily liquid, yield: 18%, ^{1}**H-NMR** (400 MHz, DMSO-d_6), δ, ppm: 7.46 (1H, d, J = 7.4 Hz, CH), 7.36 (1H, d, J = 7.8 Hz, CH), 7.25 (1H, t, J = 7.6 Hz, CH), 2.25 (3H, s, CH$_3$), 1.39 (6H, s, C(CH$_3$)$_2$). **ESI-MS** *m/z* found: [M+H]$^+$ 237.9; C$_{11}$H$_{13}$BrN$^+$ requires 238.0.

6-Bromo-2,3,3-trimethyl-3*H*-indole (2.4h): light-yellow oily liquid, yield: 65%, ^{1}**H-NMR** (400 MHz, DMSO-d_6), δ, ppm: 7.61 (1H, s, CH), 7.41 (1H, d, J = 7.9 Hz, CH), 7.38 (1H, d, J = 8.2 Hz, CH), 2.25 (3H, s, CH$_3$), 1.25 (6H, s, C(CH$_3$)$_2$). **ESI-MS** *m/z* found: [M+H]$^+$ 238.0; C$_{11}$H$_{13}$BrN$^+$ requires 238.0.

4,6-chloro-2,3,3-trimethyl-3*H*-indole (2.4i) was obtained according to the general procedure starting from (3,5-dichlorophenyl)hydrazine hydrochloride (1.5 g, 7.0 mmol) and 3-methyl-2-butanone (0.9 g, 10.4 mmol): off-white powder, yield: 69%, ^{1}**H-NMR** (400 MHz, DMSO-d_6), δ, ppm: 7.50 (1H, s, CH), 7.32 (1H, s, CH), 2.23 (3H, s, CH$_3$), 1.36 (6H, s, (CH$_3$)$_2$). **ESI-MS** *m/z* found: [M+H]$^+$ 228.1; C$_{11}$H$_{12}$Cl$_2$N$^+$ requires 228.0.

5.2.3 Procedures for the synthesis of indolenines

Indole **2.4a−j** (1 equiv.) was dissolved in 2 mL of iodomethane and left at r.t. for 48 h in a sealed tube. The formed precipitate **2.5a−j** was filtered, washed with diethyl ether and dried. These indolenines were used for further synthesis of dyes without additional purification.

5-Bromo-1,2,3,3-tetramethyl-3*H*-indol-1-ium iodide (2.5a) was obtained according to the general procedure starting from 5-bromo-2,3,3-trimethyl-3*H*-indole (1.8 g, 7.6 mmol): off-white powder, yield: 42%, **¹H-NMR** (400 MHz, DMSO-d_6), δ, ppm: 8.15 (1H, s, CH), 7.87 (1H, d, J = 8.5 Hz, CH), 7.83 (1H, J = d, 8.4 Hz, CH), 3.94 (3H, s, CH$_3$), 2.75 (3H, s, CH$_3$), 1.53 (6H, s, C(CH$_3$)$_2$). **ESI-MS** *m/z* found: [M−I]$^+$ 252.1; C$_{12}$H$_{15}$BrN$^+$ requires 252.0.

5-Iodo-1,2,3,3-tetramethyl-3*H*-indol-1-ium iodide (2.5b) was obtained according to the general procedure starting from 5-iodo-2,3,3-trimethyl-3*H*-indole (2.03 g, 7.1 mmol): off-white powder, yield: 69%, **¹H-NMR** (400 MHz, DMSO-d_6), δ, ppm: 8.27 (1H, s, CH), 7.99 (1H, d, J = 8.2 Hz, CH), 7.71 (1H, d, J = 8.4 Hz, CH), 3.93 (3H, s, CH$_3$), 2.73 (3H, s, CH$_3$), 1.51 (6H, s, (CH$_3$)$_2$). **ESI-MS** *m/z* found: [M−I]$^+$ 300.0; C$_{12}$H$_{15}$IN$^+$ requires 300.0.

4,6-Dibromo-1,2,3,3-tetramethyl-3*H*-indol-1-ium iodide (2.5c) was obtained according to the general procedure starting from 4,6-dibromo-2,3,3-trimethyl-3*H*-indole (0.3 g, 0.95 mmol): off-white powder, yield: 69%, **¹H-NMR** (400 MHz, DMSO-d_6), δ, ppm: 8.34 (1H, s, CH), 8.11 (1H, s, CH), 3.94 (3H, s, CH$_3$), 2.81 (3H, s, CH$_3$), 1.63 (6H, s, C(CH$_3$)$_2$). **ESI-MS** *m/z* found: [M−I]$^+$ 332.0; C$_{12}$H$_{14}$Br$_2$N$^+$ requires 332.0.

4,6-Diiodo-1,2,3,3-tetramethyl-3*H*-indol-1-ium iodide (2.5d) was obtained according to the general procedure starting from 4,6-diiodo-2,3,3-trimethyl-3*H*-indole (0.34 g, 0.83 mmol): off-white powder, yield: 63%, **¹H-NMR** (400 MHz, DMSO-d_6), δ, ppm: 8.37 (2H, s, CH), 3.91 (3H, s, CH$_3$), 2.78 (3H, s, CH$_3$), 1.60 (6H, s, C(CH$_3$)$_2$). **ESI-MS** *m/z* found: [M−I]$^+$ 425.9; C$_{12}$H$_{14}$I$_2$N$^+$ requires 425.9.

4,5,6-Tribromo-1,2,3,3-tetramethyl-3*H*-indol-1-ium iodide (2.5e) was obtained according to the general procedure starting from 4,5,6-tribromo-2,3,3-trimethyl-3*H*-indole (1.12 g, 2.8 mmol): beige powder, yield: 60%, **¹H-NMR** (400 MHz, DMSO-d_6), δ, ppm: 8.48 (1H, s, CH), 3.92 (3H, s, CH$_3$), 2.78 (3H, s, CH$_3$), 1.61 (6H, s, C(CH$_3$)$_2$). **ESI-MS** *m/z* found: [M−I]$^+$ 409.9; C$_{12}$H$_{13}$Br$_3$N$^+$ requires 409.9.

4,5,6-Triiodo-1,2,3,3-tetramethyl-3*H*-indol-1-ium iodide (2.5f) was obtained according to the general procedure starting from 4,5,6-triiodo-2,3,3-trimethyl-3*H*-indole (1.0 g, 1.9 mmol): off-white powder, yield: 48%, **¹H-NMR** (400 MHz, DMSO-d_6),

δ, ppm: 8.52 (1H, s, CH), 3.92 (3H, s, CH$_3$), 2.76 (3H, s, CH$_3$), 1.59 (6H, s, C(CH$_3$)$_2$). **ESI-MS** *m/z* found: [M−I]$^+$ 551.8; C$_{12}$H$_{13}$I$_3$N$^+$ requires 551.8.

4-Bromo-1,2,3,3-tetramethyl-3*H*-indol-1-ium iodide (2.5g) was obtained according to the general procedure starting from 4-bromo-2,3,3-trimethyl-3*H*-indole (0.18 g, 0.76 mmol): off-white powder with reddish hue, yield: 51%, **^{1}H-NMR** (400 MHz, DMSO-*d$_6$*), δ, ppm: 7.96 (1H, d, J = 8.1 Hz, CH), 7.81 (1H, d, J = 8.2 Hz, CH), 7.60 (1H, J = d, 8.0 Hz, CH), 3.95 (3H, s, CH$_3$), 2.79 (3H, s, CH$_3$), 1.64 (6H, s, C(CH$_3$)$_2$). **ESI-MS** *m/z* found: [M−I]$^+$ 252.1; C$_{12}$H$_{15}$BrN$^+$ requires 252.0.

6-Bromo-1,2,3,3-tetramethyl-3*H*-indol-1-ium iodide (2.5h) was obtained according to the general procedure starting from 6-bromo-2,3,3-trimethyl-3*H*-indole (0.69 g, 2.9 mmol): off-white powder with reddish hue, yield: 42%, **^{1}H-NMR** (400 MHz, DMSO-*d$_6$*), δ, ppm: 8.25 (1H, s, CH), 7.80 (2H, d, J = 8.2 Hz, CH), 3.95 (3H, s, CH$_3$), 2.77 (3H, s, CH$_3$), 1.51 (6H, s, C(CH$_3$)$_2$). **ESI-MS** *m/z* found: [M−I]$^+$ 252.1; C$_{12}$H$_{15}$BrN$^+$ requires 252.0.

4,6-dichloro-1,2,3,3-tetramethyl-3*H*-indol-1-ium iodide (2.5i) was obtained according to the general procedure starting from 4,6-dichloro-2,3,3-trimethyl-3*H*-indole (0.9 g, 3.94 mmol): off-white powder, yield: 75%, **^{1}H-NMR** (400 MHz, DMSO-*d$_6$*), δ, ppm: **^{1}H-NMR** (400 MHz, DMSO-*d$_6$*), δ, ppm: 8.21 (1H, s, CH), 7.88 (1H, s, CH), 3.95 (3H, s, CH$_3$), 2.81 (3H, s, CH$_3$), 1.63 (6H, s, (CH$_3$)$_2$). **ESI-MS** *m/z* found: [M−I]$^+$ 242.0; C$_{12}$H$_{14}$Cl$_2$N$^+$ requires 242.1.

1,2,3,3-tetramethyl-3*H*-indol-1-ium iodide (2.5j) (was obtained according to the general procedure starting from 2,3,3-trimethyl-3*H*-indole (1.0 g, 6.3 mmol): off-white powder with reddish hue, yield: 74%, **^{1}H-NMR** (400 MHz, DMSO-*d$_6$*), δ, ppm: 7.91 (d, *J* = 5.2 Hz, 1H, CH), 7.83 (d, *J* = 5.4 Hz, 1H, CH), 7.62 (t, *J* = 3.6 Hz, 2H, CH), 3.98 (s, 3H, CH$_3$), 2.77 (s, 3H, CH$_3$), 1.53 (s, 6H, (CH$_3$)$_2$). **ESI-MS** *m/z* found: [M−I]$^+$ 174.1; C$_{12}$H$_{16}$N$^+$ requires 174.13.

Indolenines **2.4b, 2.4f** or **2.4j** (1 equiv.) was mixed with 6-bromohexanoic acid (1.5-2 equiv.) and heated at 90−120 °C for 15 h−3 d in a sealed tube. The reaction mixture was cooled to r.t., diluted with benzene (5 mL), the solvent was decanted, and

the residue was triturated with benzene (3×5 mL), and filtered. The obtained precipitate was washed with acetone (1 mL) and dried to yield **2.6b, 2.6f** or **2.6j**.

1-(5-Carboxypentyl)-5-iodo-2,3,3-trimethyl-3*H*-indol-1-ium bromide (2.6b) was obtained starting from 5-iodo-2,3,3-trimethyl-3*H*-indole (**2.4b**) (1.0 g, 3.5 mmol) and 6-bromohexanoic acid (1.37 g, 7.0 mmol) by heating at 90 °C for 2 days in a sealed tube. Yield: 0.81 g (48%). **^{1}H-NMR** (400 MHz, DMSO-d_6), δ, ppm: 8.31 (s, 1H), 7.99 (d, J = 8.4 Hz, 1H), 7.81 (d, J = 8.5 Hz, 1H), 4.43 (t, J = 7.7 Hz, 2H), 2.82 (s, 3H), 2.20 (t, J = 6.7 Hz, 2H), 1.82 (m, 2H), 1.53 (s, 6H), 1.42 (m, 2H), 1.34 (m, 2H). MS m/z (ESI$^+$) $C_{17}H_{23}BrINO_2$ calculated [M−Br]$^+$ 400.08, found m/z 400.12.

1-(5-Carboxypentyl)-4,5,6-triiodo-2,3,3-trimethyl-3*H*-indol-1-ium bromide (2.6f) was obtained starting from 4,5,6-triiodo-2,3,3-trimethyl-3*H*-indole (**2.4f**) (1.0 g, 1.9 mmol) and 6-bromohexanoic acid (0.73 g, 3.7 mmol) by heating at 90 °C for 3 days in a sealed tube. Yield 0.4 g (29%). **^{1}H-NMR** (400 MHz, DMSO-d_6), δ, ppm: 8.60 (s, 1H), 4.41 (t, J = 7.7 Hz, 2H), 2.83 (s, 3H), 2.20 (t, J = 6.7 Hz, 2H), 1.79 (m, 2H), 1.60 (s, 6H), 1.51 (m, 2H), 1.44 (m, 2H). MS m/z (ESI$^+$) $C_{17}H_{21}BrI_3NO_2$ calculated [M−Br]$^+$ 651.87, found m/z 651.90.

1-(5-Carboxypentyl)-2,3,3-trimethyl-3*H*-indol-1-ium bromide (2.6j) was obtained starting from 2,3,3-trimethyl-3*H*-indole (**2.4j**) (1.0 g, 6.3 mmol) and 6-bromohexanoic acid (1.84 g, 9.4 mmol) by heating at 120 °C for 15 h in a sealed tube. Yield 1.33 g, 60%. **^{1}H-NMR** (400 MHz, DMSO-d_6), δ, ppm: 7.97 (d, J = 5.1 Hz, 1H), 7.84 (d, J = 3.4 Hz, 1H), 7.62 (t, J = 4.1 Hz, 2H), 4.45 (t, J = 7.8 Hz, 2H), 2.84 (s, 3H), 2.23 (t, J = 7.2 Hz, 2H), 1.85 (m, 2H), 1.56 (m, 2H), 1.54 (s, 6H), 1.43 (m, 2H). MS m/z (ESI$^+$) $C_{17}H_{24}BrNO_2$ calculated [M−Br]$^+$ 274.18, found m/z 274.20.

5-Iodo-2,3,3-trimethyl-1-(3-(triethylammonio)propyl)-3*H*-indol-1-ium dibromide (2.7): 5-Iodo-2,3,3-trimethyl-3*H*-indole (**2.4b**) (1.0 g, 3.5 mmol) and 3-bromo-*N,N,N*-triethylpropan-1-aminium bromide (1.23 g, 3.9 mmol) were stirred in acetonitrile (14 mL) at reflux for 2 days. Reaction mixture was diluted with benzene (50 mL). In 1 h the solvent was decanted and the viscous solid was triturated with diethyl ether, filtered, washed with ether, and dried to yield **7** (0.6 g, 29%). **^{1}H-NMR** (400 MHz, DMSO-d_6), δ, ppm: 8.33 (s, 1H), 8.04 (d, J = 7.8 Hz, 1H), 7.95 (d,

$J = 7.6$ Hz, 1H), 4.56 (t, $J = 7.7$ Hz, 2H), 3.25 (m, 8H), 2.91 (s, 3H), 2.18 (m, 2H), 1.56 (s, 6H), 1.18 (t, $J = 7.3$ Hz, 9H). MS m/z (ESI⁺) $C_{20}H_{33}Br_2IN_2$ calculated [M−2Br]⁺ 428.17, found m/z 428.20.

3-(4,6-Diiodo-2,3,3-trimethyl-3H-indol-1-ium-1-yl)propane-1-sulfonate (2.8). 4,6-diiodo-2,3,3-trimethyl-3H-indole **2.4d** (1 g, 2.43 mmol) was refluxed with 1,3-propane sultone (0.44 g, 3.64 mmol) in toluene (4 mL) for 15 h and cooled to r.t. The obtained brown residue was filtered, washed with acetone, dissolved in methanol, and precipitated with diethyl ether. The product was collected and vacuum-dried to yield the quaternized indolenine **2.8** (0.53 g, 41%). **¹H-NMR** (400 MHz, DMSO-d_6), δ, ppm: 8.52 (s, 1H, CH), 8.37 (s, 1H, CH), 4.59 (t, J = 6.9 Hz, 2H, N*CH₂*), 2.85 (s, 3H, CH₃), 2.62 (t, J = 6.7 Hz, 2H, *CH₂*SO₃H), 2.06 (t, J = 6.9 Hz, 2H, *CH₂*SO₃H), 1.61 (s, 6H, (CH₃)₂). **¹³C-NMR** (100 MHz, TFA-d), δ, ppm: 201.46, 151.98, 144.66, 143.69, 126.56, 95.44, 91.70, 60.04, 50.37, 49.05, 24.82, 20.10, 15.53. **HRMS**: m/z (ESI⁺) $C_{14}H_{17}I_2NO_3S$ calculated [M+H]⁺ 533.9092, found m/z: 533.9122.

3-(3-(5-Carboxypentyl)-2,3-dimethyl-5-sulfo-3H-indol-1-ium-1-yl)propane-1-sulfonate (2.9). A solution of potassium hydroxide (0.33 g, 5.91 mmol) in methanol (5 mL) was added to a solution of 6-(2,3-dimethyl-5-sulfo-3H-indol-3-yl)hexanoic acid (**2.4k**) (1 g, 2.95 mmol) obtained according to [159] in 5 mL methanol, the mixture was stirred at r.t. for 30 min, methanol was evaporated and the product vacuum-dried. The residue (1.22 g, 2.95 mmol) was heated with 1,3-propanesultone (0.72 g, 5.9 mmol) in sulfolane (5 mL) at 130 °C for 5 h. After cooling to r.t., the solid product was dissolved in methanol, precipitated with diethyl ether, filtered and dried. Crude product was dissolved in 1 M HCl, refluxed for 3 h, cooled, alkalized with sodium hydroxide, and column-purified (LiChroprep RP-18, water) resulting in the quaternized indolenine **2.9** as a pale-yellow solid. Yield 0.5 g (37%). **¹H-NMR** (400 MHz, DMSO-d_6), δ, ppm: 8.00 (d, J = 8.4 Hz, 1H, CH), 7.97 (s, 1H, CH), 7.83 (d, J = 9.6 Hz, 1H, CH), 4.68 (t, J = 7.0 Hz, 2H, N*CH₂*), 2.86 (s, 3H, CH₃), 2.63 (t, J = 6.6 Hz, 2H, *CH₂*SO₃H), 2.34−1.97 (m, 6H, CH₂), 1.54 (s, 3H, CH₃) 1.42−1.27 (m, 2H, CH₂), 1.20−1.05 (m, 2H, CH₂), 0.78−0.45 (m, 2H, CH₂). **¹³C-NMR** (100 MHz, DMSO-d_6), δ, ppm: 174.41, 158.61, 146.49, 138.65, 133.93, 125.46, 119.47, 103.67, 74.65, 48.71, 47.38, 42.43,

40.66, 33.75, 29.40, 28.75, 24.30, 23.86, 21.95. **HRMS**: *m/z* (ESI$^+$) $C_{19}H_{27}NO_8S_2$ calculated $[M+H]^+$ 462.1251, found *m/z:* 462.1259.

5.2.4 General procedure for the synthesis of symmetrical xHal$_n$-HITC cyanine dyes

Indolenine **2.5a−i** (1 equiv.) and N-[5-(phenylamino)-2,4-pentadienylidene]aniline hydrochloride (0.45−0.5 equiv.) were dissolved in 4 mL of acetic anhydride and heated at 90−100 °C during 10 min. Then, the reaction mixture was cooled to 50 °C, following by the addition of pyridine (3 mL) and heating at 90-100 °C during 5 min, resulting in the formation of the product. Then, the reaction mass was cooled to r.t. during 5−10 min. The desired dye was precipitated with ether, filtered off and washed with ether. The crude product was column purified on Silica gel 60 using 1−20% methanol-chloroform as eluent. Fraction with the dye was collected, evaporated, washed with ether and vacuum-dried.

5-Bromo-2-((1,3,5,7)-7-(5-bromo-1,3,3-trimethylindolin-2-ylidene)hepta-1,3,5-trien-1-yl)-1,3,3-trimethyl-3*H*-indol-1-ium iodide (5Br$_2$-HITC) was obtained according to the general procedure starting from 5-bromo-1,2,3,3-tetramethyl-3*H*-indol-1-ium iodide (100 mg, 0.26 mmol) and N-[5-(phenylamino)-2,4-pentadienylidene]aniline hydrochloride (33.7 mg, 0.118 mmol): dark blue metallic powder, yield: 58%, **^{1}H-NMR** (400 MHz, DMSO-d_6), δ, ppm: 7.86 (2H, t, J = 13.1 Hz, CH), 7.84 (2H, s, CH, arom.), 7.78 (1H, t, J = 12.8 Hz, CH), 7.58 (2H, d, J = 8.1 Hz, CH, arom.), 7.32 (2H, d, J = 8.5 Hz, CH, arom.), 6.54 (2H, t, J = 12.6 Hz, CH), 6.31 (2H, d, J = 13.7 Hz, CH), 3.56 (6H, s, N-CH$_3$), 1.63 (12H, s, (CH$_3$)$_2$). **^{13}C-NMR** (100 MHz, DMSO-d_6), δ, ppm: 171.35, 156.23, 150.93, 143.17, 142.27, 131.07, 125.79, 125.50, 116.73, 112.70, 104.28, 48.71, 31.24, 26.79. **HRMS:** *m/z* (ESI$^+$) $C_{29}H_{31}Br_2N_2{}^+$ calculated $[M]^+$ 567.0836, found *m/z*: 567.0858.

5-Iodo-2-((1,3,5,7)-7-(5-iodo-1,3,3-trimethylindolin-2-ylidene)hepta-1,3,5-trien-1-yl)-1,3,3-trimethyl-3*H*-indol-1-ium iodide (5I$_2$-HITC) was obtained according to the general procedure starting from 5-iodo-1,2,3,3-tetramethyl-3*H*-indol-1-ium iodide (150 mg, 0.35 mmol) and N-[5-(phenylamino)-2,4-pentadienylidene]aniline hydrochloride (50.0 mg, 0.175 mmol): dark blue metallic powder, yield: 50%, **^{1}H-NMR**

(400 MHz, DMSO-d_6), δ, ppm: 7.96 (2H, s, CH, arom.), 7.86 (2H, t, J = 13.2 Hz, CH), 7.76 (1H, t, J = 12.6 Hz, CH), 7.73 (2H, d, J = 8.2 Hz, CH, arom.), 7.19 (2H, d, J = 8.3 Hz, CH, arom.), 6.54 (2H, t, J = 12.6 Hz, CH), 6.30 (2H, d, J = 13.7 Hz, CH), 3.54 (6H, s, N-CH$_3$), 1.62 (12H, s, (CH$_3$)$_2$). **^{13}C-NMR** (100 MHz, DMSO-d_6), δ, ppm: 171.05, 156.28, 150.93, 143.33, 142.80, 136.90, 130.99, 125.79, 113.12, 104.22, 88.72, 48.60, 31.18, 26.83. **HRMS:** *m/z* (ESI$^+$) C$_{29}$H$_{31}$I$_2$N$_2$$^+$ calculated [M]$^+$ 661.0577, found *m/z*: 661.0566.

4,6-Dibromo-2-((1,3,5,7)-7-(4,6-dibromo-1,3,3-trimethylindolin-2-ylidene) hepta-1,3,5-trien-1-yl)-1,3,3-trimethyl-3*H*-indol-1-ium iodide (4,6Br$_4$-HITC) was obtained according to the general procedure starting from 4,6-dibromo-1,2,3,3-tetramethyl-3*H*-indol-1-ium iodide (100 mg, 0.218 mmol) and N-[5-(phenylamino)-2,4-pentadienylidene]aniline hydrochloride (27.9 mg, 0.098 mmol): dark green metallic powder, yield: 48%, **^{1}H-NMR** (400 MHz, DMSO-d_6), δ, ppm: 7.93 (2H, t, J = 13.1 Hz, CH), 7.81 (1H, t, J = 12.9 Hz, CH), 7.72 (2H, s, CH, arom.), 7.60 (2H, s, CH, arom.), 6.62 (2H, t, J = 12.7 Hz, CH), 6.36 (2H, d, J = 13.8 Hz, CH), 3.56 (6H, s, N-CH$_3$), 1.75 (12H, s, (CH$_3$)$_2$). **^{13}C-NMR** (100 MHz, DMSO-d_6), δ, ppm: 171.72, 156.94, 151.66, 146.42, 136.12, 129.88, 126.84, 122.16, 117.57, 113.89, 104.46, 50.27, 31.63, 23.28. **HRMS:** *m/z* (ESI$^+$) C$_{29}$H$_{29}$Br$_4$N$_2$$^+$ calculated [M]$^+$ 724.9026, found *m/z*: 724.9028.

4,6-Diiodo-2-((1,3,5,7)-7-(4,6-diiodo-1,3,3-trimethylindolin-2-ylidene)hepta-1,3,5-trien-1-yl)-1,3,3-trimethyl-3*H*-indol-1-ium iodide (4,6I$_4$-HITC) was obtained according to the general procedure starting from 4,6-diiodo-1,2,3,3-tetramethyl-3*H*-indol-1-ium iodide (110 mg, 0.20 mmol) and N-[5-(phenylamino)-2,4-pentadienylidene]aniline hydrochloride (28.3 mg, 0.1 mmol): dark blue metallic powder, yield: 55%, **^{1}H-NMR** (400 MHz, DMSO-d_6), δ, ppm: 7.94 (2H, s, CH, arom.), 7.91 (2H, t, J = 13.3 Hz, CH), 7.80 (2H, s, CH, arom.), 7.76 (1H, t, J = 13.5 Hz, CH), 6.59 (2H, t, J = 12.6 Hz, CH), 6.33 (2H, d, J = 13.8 Hz, CH), 3.53 (6H, s, N-CH$_3$), 1.72 (12H, s, (CH$_3$)$_2$). **^{13}C-NMR** (100 MHz, DMSO-d_6), δ, ppm: 171.34, 156.51, 150.92, 143.17, 142.28, 131.07, 125.50, 116.73, 112.70, 104.28, 91.60, 48.71, 31.24, 26.79. **HRMS**: *m/z* (ESI$^+$) C$_{29}$H$_{29}$I$_4$N$_2$$^+$ calculated [M]$^+$ 912.8510, found *m/z*: 912.8514.

4,5,6-Tribromo-2-((1,3,5,7)-7-(4,5,6-tribromo-1,3,3-trimethylindolin-2-ylidene)hepta-1,3,5-trien-1-yl)-1,3,3-trimethyl-3*H*-indol-1-ium iodide (Br$_6$-HITC) was obtained according to the general procedure starting from 4,5,6-tribromo-1,2,3,3-tetramethyl-3*H*-indol-1-ium iodide (49 mg, 0.09 mmol) and N-[5-(phenylamino)-2,4-pentadienylidene]aniline hydrochloride (13.0 mg, 0.045 mmol): dark green metallic powder, yield: 82%, ^{1}**H-NMR** (400 MHz, DMSO-d_6), δ, ppm: 7.95 (2H, t, J = 13.1 Hz, CH), 7.93 (2H, s, CH, arom.), 7.81 (1H, t, J = 12.8 Hz, CH), 6.63 (2H, t, J = 12.7 Hz, CH), 6.35 (2H, d, J = 13.8 Hz, CH), 3.56 (6H, s, N-CH$_3$), 1.77 (12H, s, C(CH$_3$)$_2$). ^{13}**C-NMR** (100 MHz, DMSO-d_6), δ, ppm: 171.50, 157.12, 151.73, 144.83, 138.58, 127.11, 125.17, 122.57, 120.57, 115.46, 104.49, 51.26, 31.68, 23.09. **HRMS**: *m/z* (ESI$^+$) C$_{29}$H$_{27}$Br$_6$N$_2$$^+$ calculated [M]$^+$ 882.7216, found *m/z*: 882.7212.

4,5,6-Triiodo-2-((1,3,5,7)-7-(4,5,6-triiodo-1,3,3-trimethylindolin-2-ylidene)hepta-1,3,5-trien-1-yl)-1,3,3-trimethyl-3*H*-indol-1-ium iodide (I$_6$-HITC) was obtained according to the general procedure starting from 4,5,6-triiodo-1,2,3,3-tetramethyl-3*H*-indol-1-ium iodide (150 mg, 0.22 mmol) and N-[5-(phenylamino)-2,4-pentadienylidene]aniline hydrochloride (31.5 mg, 0.11 mmol): dark green metallic powder, yield: 32%, ^{1}**H-NMR** (400 MHz, DMSO-d_6), δ, ppm: 8.01 (2H, s, CH, arom.), 7.90 (2H, t, J = 13.7 Hz, CH), 7.76 (1H, t, J = 12.5 Hz, CH), 6.58 (2H, t, J = 12.7 Hz, CH), 6.31 (2H, d, J = 13.8 Hz, CH), 3.53 (6H, s, N-CH$_3$), 1.72 (12H, s, C(CH$_3$)$_2$). ^{13}**C-NMR** (100 MHz, DMSO-d_6), δ, ppm: 171.52, 156.57, 151.39, 145.18, 142.44, 126.61, 121.35, 120.38, 108.30, 104.33, 104.03, 51.86, 31.38, 23.18. **HRMS**: *m/z* (ESI$^+$) C$_{29}$H$_{27}$Br$_6$N$_2$$^+$ calculated [M]$^+$ 1164.6443, found *m/z*: 1164.6423.

4-Bromo-2-((1,3,5,7)-7-(4-bromo-1,3,3-trimethylindolin-2-ylidene)hepta-1,3,5-trien-1-yl)-1,3,3-trimethyl-3*H*-indol-1-ium iodide (4Br$_2$-HITC) was obtained according to the general procedure starting from 4-bromo-1,2,3,3-tetramethyl-3*H*-indol-1-ium iodide (100 mg, 0.263 mmol) and N-[5-(phenylamino)-2,4-pentadienylidene]aniline hydrochloride (36.0 mg, 0.126 mmol): dark blue metallic powder, yield: 33%, ^{1}**H-NMR** (400 MHz, DMSO-d_6), δ, ppm: 7.92 (2H, t, J = 13.0 Hz, CH), 7.78 (1H, t, J = 12.8 Hz, CH), 7.43 (2H, dd, J = 6.7 Hz, J = 2.3 Hz, CH, arom.), 7.40-7.33 (4H, m, CH, arom.), 6.58 (2H, t, J = 12.6 Hz, CH), 6.34 (2H, d, J = 13.8 Hz,

CH), 3.58 (6H, s, N-CH$_3$), 1.77 (12H, s, C(CH$_3$)$_2$). **^{13}C-NMR** (100 MHz, DMSO-d_6), δ, ppm: 171.37, 156.28, 151.14, 145.26, 136.63, 130.43, 128.63, 126.07, 116.92, 110.74, 103.85, 50.42, 31.43, 23.39. **HRMS**: *m/z* (ESI$^+$) C$_{29}$H$_{31}$Br$_2$N$_2^+$ calculated [M]$^+$ 567.0836, found *m/z*: 567.0845.

6-Bromo-2-((1,3,5,7)-7-(6-bromo-1,3,3-trimethylindolin-2-ylidene)hepta-1,3,5-trien-1-yl)-1,3,3-trimethyl-3*H*-indol-1-ium iodide (6Br$_2$-HITC) was obtained according to the general procedure starting from 6-bromo-1,2,3,3-tetramethyl-3*H*-indol-1-ium iodide (100 mg, 0.263 mmol) and N-[5-(phenylamino)-2,4-pentadienylidene]aniline hydrochloride (36.0 mg, 0.126 mmol): dark blue metallic powder, yield: 64%, **^{1}H-NMR** (400 MHz, DMSO-d_6), δ, ppm: 7.88 (2H, t, J = 13.1 Hz, CH), 7.79 (1H, t, J = 12.8 Hz, CH), 7.64 (2H, s, CH, arom.), 7.52 (2H, d, J = 7.9 Hz, CH, arom.), 7.38 (2H, d, J = 8.0 Hz, CH, arom.), 6.56 (2H, t, J = 12.4 Hz, CH), 6.34 (2H, d, J = 13.7 Hz, CH), 3.56 (6H, s, N-CH$_3$), 1.61 (12H, s, C(CH$_3$)$_2$). **^{13}C-NMR** (100 MHz, DMSO-d_6), δ, ppm: 171.97, 156.52, 151.20, 144.51, 140.12, 126.84, 125.98, 123.96, 121.03, 113.95, 104.49, 48.36, 31.28, 26.78. **HRMS**: *m/z* (ESI$^+$) C$_{29}$H$_{31}$Br$_2$N$_2^+$ calculated [M]$^+$ 567.0836, found *m/z*: 567.0840.

4,6-Dichloro-2-((1,3,5,7)-7-(4,6-dichloro-1,3,3-trimethylindolin-2-ylidene)hepta-1,3,5-trien-1-yl)-1,3,3-trimethyl-3*H*-indol-1-ium iodide (4,6Cl$_4$-HITC) was obtained according to the general procedure starting from 4,6-dichloro-1,2,3,3-tetramethyl-3*H*-indol-1-ium iodide (150 mg, 0.405 mmol) and N-[5-(phenylamino)-2,4-pentadienylidene]aniline hydrochloride (55.4 mg, 0.195 mmol): dark blue metallic powder, yield: 48%, **^{1}H-NMR** (400 MHz, DMSO-d_6), δ, ppm: 7.94 (2H, t, *J* = 13.1 Hz, CH), 7.83 (1H, t, *J* = 12.8 Hz, CH), 7.59 (2H, d, *J* = 1.7 Hz, CH, arom.), 7.36 (2H, d, *J* = 1.7 Hz, CH, arom.), 6.62 (2H, t, *J* = 12.6 Hz, CH), 6.37 (2H, d, *J* = 13.8 Hz, CH), 3.57 (6H,s, N-CH$_3$), 1.75 (12H s, C(CH$_3$)$_2$). **^{13}C-NMR** (100 MHz, DMSO-d_6), δ, ppm: 171.74, 157.12, 151.73, 146.13, 134.25, 134.09, 129.08, 126.89, 124.26, 110.79, 104.55, 79.17, 49.71, 31.71, 23.48. **HRMS**: *m/z* (ESI$^+$) C$_{29}$H$_{29}$Cl$_4$N$_2^+$ calculated [M]$^+$ 547.1059, found *m/z*: 547.1068.

5.2.4 General procedure for the synthesis of the unsymmetrical dyes Cy7, 1ICy7−6ICy7

A solution of indolenine **2.5b, 2.5f, 2.5j** or **2.7** (0.25 mmol, 1.1 equiv.) and *N*-[5-(phenylamino)-2,4-pentadienylidene]aniline hydrochloride (0.23 mmol, 1.0 equiv.) in acetic anhydride (2 mL) was heated at 90 °C for 15 min to form the corresponding *N*-phenylacetamide intermediate product. Then, the second indolenine **2.6b, 2.6f** or **2.6j** (0.25 mmol, 1.1 equiv.) was added and dissolved in the reaction mixture at 90 °C. The reaction mixture was then cooled to 50 °C, pyridine (1 mL) was added, heated at 90 °C for 5 min, and the obtained dye was precipitated with ether, filtered, and washed with ether. The raw product was column purified on Silica gel 60 using 5−10% methanol−chloroform as eluent.

6-(3,3-Dimethyl-2-(7-(1,3,3-trimethylindolin-2-ylidene)hepta-1,3,5-trien-1-yl)-3*H*-indol-1-ium-1-yl)hexanoate (Cy7).

Dye **Cy7** was synthesized from 1,2,3,3-tetramethyl-3*H*-indol-1-ium iodide (**2.5j**) (75 mg, 0.25 mmol), *N*-[5-(phenylamino)-2,4-pentadienylidene]aniline hydrochloride (64 mg, 0.23 mmol), and 1-(5-carboxypentyl)-2,3,3-trimethyl-3*H*-indol-1-ium bromide (**2.6j**) (88.5 mg, 0.25 mmol). Yield: 119 mg (52%). **^{1}H-NMR** (400 MHz, CDCl$_3$−CD$_3$OD), δ, ppm: 7.71 (t, *J* = 13.1 Hz, 2H), 7.42 (t, *J* = 12.7 Hz, 1H), 7.40−7.34 (m, 2H), 7.32 (d, *J* = 7.5 Hz, 2H), 7.18 (t, *J* = 7.4 Hz, 2H), 7.08 (d, *J* = 8.4 Hz, 1H), 7.06 (d, *J* = 8.4 Hz, 1H), 6.47 (t, *J* = 12.5 Hz, 2H), 6.08 (d, *J* = 13.4 Hz, 1H), 6.05 (d, *J* = 13.6 Hz, 1H), 3.92 (t, *J* = 7.4 Hz, 2H), 3.53 (s, 3H), 2.27 (t, *J* = 7.2 Hz, 2H), 1.84−1.67 (m, 2H), 1.62 (s, 12H), 1.67− 1.53 (m, 2H), 1.50−1.35 (m, 2H). **^{13}C-NMR** (100 MHz, CDCl$_3$−CD$_3$OD), δ, ppm: 175.63 (COOH), 171.14 (CN Ind), 170.56 (CN Ind) 155.75 (CH), 150.53 (2CH), 141.67 (Ar), 141.00 (Ar), 139.80 (Ar), 139.63 (Ar), 127.84 (2CH Ar), 124.76 (2CH), 124.26 (2CH Ar), 121.36 (CH Ar), 121.23 (CH Ar), 109.50 (CH Ar), 109.40 (CH Ar), 102.68 (CH), 102.42 (CH), 48.47 (2<u>C</u>(CH$_3$)$_2$), 43.09 (CH$_2$), 32.98 (CH$_2$), 30.23 (CH$_3$), 26.83 (4CH$_3$), 26.19 (CH$_2$), 25.45 (CH$_2$), 23.58 (CH$_2$). **HRMS** *m/z* (ESI$^+$) C$_{34}$H$_{40}$N$_2$O$_2$ calculated [M+H]$^+$ 509.3090 (509.3163), found *m/z*: 509.3168.

6-(2-(7-(5-iodo-1,3,3-trimethylindolin-2-ylidene)hepta-1,3,5-trien-1-yl)-3,3-dimethyl-3*H***-indol-1-ium-1-yl)hexanoate (1ICy7).**

Dye **1ICy7** was synthesized from 5-iodo-1,2,3,3-tetramethyl-3*H*-indol-1-ium iodide (**2.5b**) (106.75 mg, 0.25 mmol), *N*-[5-(phenylamino)-2,4-pentadienylidene]aniline hydrochloride (64 mg, 0.23 mmol), and 1-(5-carboxypentyl)-2,3,3-trimethyl-3*H*-indol-1-ium bromide (**2.6j**) (88.5 mg, 0.25 mmol). Yield: 74 mg (45%). **^{1}H-NMR** (400 MHz, CDCl$_3$−CD$_3$OD), δ, ppm: 7.76 (t, *J* = 13.1 Hz, 1H), 7.61 (t, *J* = 13.1 Hz, 1H), 7.59 (d, *J* = 8.5 Hz, 1H), 7.54 (s, 1H), 7.40 (t, *J* = 12.7 Hz, 1H), 7.37 (t, *J* = 7.9 Hz, 1H), 7.36 (d, *J* = 7.8 Hz, 1H), 7.25 (t, *J* = 7.4 Hz, 1H), 7.15 (d, *J* = 7.9 Hz, 1H), 6.77 (d, *J* = 8.4 Hz, 1H), 6.53 (t, *J* = 13.3 Hz, 1H), 6.44 (t, *J* = 13.3 Hz, 1H), 6.20 (d, *J* = 13.5 Hz, 1H), 5.92 (d, *J* = 13.3 Hz, 1H), 3.99 (t, *J* = 7.4 Hz, 2H), 3.42 (s, 3H), 2.24 (t, *J* = 7.2 Hz, 2H), 1.77 (m, 2H), 1.64 (m, 2H), 1.63 (s, 6H), 1.58 (s, 6H), 1.44 (m, 2H). **^{13}C-NMR** (100 MHz, CDCl$_3$−CD$_3$OD), δ, ppm: 176.41 (COOH), 172.48 (CN Ind), 168.14 (CN Ind), 155.64 (CH), 152.05 (2CH), 148.66 (CH), 141.83 (Ar), 141.46 (Ar), 140.63 (Ar), 140.16 (Ar), 136.45 (CH Ar), 130.15 (CH Ar), 128.06 (CH Ar), 125.46 (CH Ar), 125.20 (CH), 122.42 (CH Ar), 110.53 (CH Ar), 110.27 (CH Ar), 104.14 (CH), 101.49 (CH), 86.19 (CI Ar), 48.73 ($\underline{C}$(CH$_3$)$_2$), 47.05 ($\underline{C}$(CH$_3$)$_2$), 43.54 (CH$_2$), 33.74 (CH$_2$), 29.95 (CH$_3$), 26.86 (2CH$_3$), 26.67 (2CH$_3$), 26.35 (CH$_2$), 25.42 (CH$_2$), 23.80 (CH$_2$). **HRMS** *m/z* (ESI$^+$) C$_{34}$H$_{39}$IN$_2$O$_2$ calculated [M+H]$^+$ 635.2056 (635.2129), found *m/z*: 635.2134.

6-(5-Iodo-2-(7-(5-iodo-1,3,3-trimethylindolin-2-ylidene)hepta-1,3,5-trien-1-yl)-3,3-dimethyl-3*H***-indol-1-ium-1-yl)hexanoate (2ICy7).**

Dye **2ICy7** was synthesized from 5-iodo-1,2,3,3-tetramethyl-3*H*-indol-1-ium iodide (**2.5b**) (106.5 mg, 0.25 mmol), *N*-[5-(phenylamino)-2,4-pentadienylidene]aniline hydrochloride (64 mg, 0.23 mmol), and 1-(5-carboxypentyl)-5-iodo-2,3,3-trimethyl-3*H*-indol-1-ium bromide (**2.6b**) (120 mg, 0.25 mmol). Yield: 65 mg (38%). **^{1}H-NMR** (400 MHz, CDCl$_3$−CD$_3$OD), δ, ppm: 7.71 (t, *J* = 13.0 Hz, 2H), 7.63 (d, *J* = 8.3 Hz, 2H), 7.60 (s, 2H), 7.45 (t, *J* = 12.7 Hz, 1H), 6.87 (d, *J* = 8.2 Hz, 1H), 6.85 (d, *J* = 8.1 Hz, 1H), 6.51 (t, *J* = 12.1 Hz, 2H), 6.08 (d, *J* = 12.7 Hz, 1H), 6.06 (d, *J* = 13.5 Hz, 1H), 3.90 (t, *J* = 7.2 Hz, 2H), 3.49 (s, 3H), 2.23 (t, *J* = 7.2 Hz, 2H), 1.72 (m, 2H), 1.64 (m, 2H),

1.60 (s, 12H), 1.42 (m, 2H). ^{13}C-NMR (100 MHz, CDCl$_3$−CD$_3$OD), δ, ppm: 176.74 (COOH), 170.26 (CN Ind), 169.74 (CN Ind), 156.26 (CH), 150.81 (CH), 150.69 (CH), 142.00 (Ar), 141.75 (Ar), 141.53 (Ar), 140.86 (Ar), 136.73 (2CH Ar), 130.45 (CH Ar), 130.31 (CH Ar), 125.65 (2CH), 111.38 (CH Ar), 111.25 (CH Ar), 103.08 (CH), 102.86 (CH), 87.63 (CI Ar), 88.52 (CI Ar), 48.2 (2$\underline{C}$(CH$_3$)$_2$), 43.18 (CH$_2$), 33.48 (CH$_2$), 30.34 (CH$_3$), 26.78 (4CH$_3$), 26.12 (CH$_2$), 25.43 (CH$_2$), 23.73 (CH$_2$). HRMS m/z (ESI$^+$) C$_{34}$H$_{38}$I$_2$N$_2$O$_2$ calculated [M+H]$^+$ 761.1023 (761.1095), found m/z: 761.1101.

6-(5-Iodo-2-(7-(5-iodo-3,3-dimethyl-1-(3-(triethylammonio)propyl)indolin-2-ylidene)hepta-1,3,5-trien-1-yl)-3,3-dimethyl-3H-indol-1-ium-1-yl)hexanoate trifluoroacetate (2ICy7+).

Dye **2ICy7+** was synthesized from 5-iodo-2,3,3-trimethyl-1-(3-(triethylammonio)propyl)-3H-indol-1-ium dibromide (**2.7**) (147 mg, 0.25 mmol), N-[5-(phenylamino)-2,4-pentadienylidene]aniline hydrochloride (65 mg, 0.23 mmol), and 1-(5-carboxypentyl)-5-iodo-2,3,3-trimethyl-3H-indol-1-ium bromide (**2.5b**) (120 mg, 0.25 mmol). The product was purified on a RP-18 column (acetonitrile−water + 0.05% TFA). Yield: 34 mg (15%). ^{1}H-NMR (400 MHz, CDCl$_3$−CD$_3$OD), δ, ppm: 7.74 (t, J = 13.0 Hz, 1H), 7.70 (d, J = 8.3 Hz, 1H), 7.68 (t, J = 13.0 Hz, 1H), 7.66 (s, 1H), 7.64 (d, J = 8.1 Hz, 1H), 7.59 (s, 1H), 7.40 (t, J = 12.8 Hz, 1H), 7.01 (d, J = 8.3 Hz, 1H), 6.91 (d, J = 8.3 Hz, 1H), 6.60 (t, J = 12.7 Hz, 1H), 6.55 (t, J = 12.8 Hz, 1H), 6.28 (d, J = 13.2 Hz, 1H), 6.15 (d, J = 13.5 Hz, 1H), 4.08 (t, J = 7.0 Hz, 2H), 3.95 (t, J = 6.8 Hz, 2H), 3.43 (t, J = 7.9, 2H), 3.26 (m, 6H) 2.30 (t, J = 7.2 Hz, 2H,), 2.04 (m, 2H), 1.77 (m, 2H), 1.66 (m, 2H), 1.64 (s, 6H), 1.61 (s, 6H), 1.45 (m, 2H), 1.27 (t, J = 7.1 Hz, 9H). HRMS m/z (ESI$^+$) C$_{44}$H$_{56}$F$_3$I$_2$N$_3$O$_4$ calculated [M−CF$_3$COO]$^+$ 888.2451, found m/z: 888.2462.

6-(3,3-Dimethyl-2-(7-(4,5,6-triiodo-1,3,3-trimethylindolin-2-ylidene)hepta-1,3,5-trien-1-yl)-3H-indol-1-ium-1-yl)hexanoate (3ICy7).

Dye **3ICy7** was synthesized from 4,5,6-triiodo-1,2,3,3-tetramethyl-3H-indol-1-ium iodide (**2.5f**) (170 mg, 0.25 mmol), N-[5-(phenylamino)-2,4-pentadienylidene]aniline hydrochloride (65 mg, 0.23 mmol), and 1-(5-carboxypentyl)-2,3,3-trimethyl-3H-indol-1-ium bromide (**2.6j**) (88.0 mg, 0.25 mmol). Yield: 75 mg

(37%). **¹H-NMR** (400 MHz, CDCl₃−CD₃OD), δ, ppm: 7.82 (t, *J* = 12.4 Hz, 1H), 7.54 (t, *J* = 13.0 Hz, 1H), 7.50 (s, 1H), 7.40 (d, *J* = 7.7 Hz, 2H), 7.40 (t, *J* = 12.6 Hz, 1H), 7.31 (t, *J* = 7.6 Hz, 1H), 7.25 (d, *J* = 7.8 Hz, 1H), 6.59 (t, *J* = 12.6 Hz, 1H), 6.43 (t, *J* = 12.5 Hz, 1H), 6.36 (d, *J* = 13.5 Hz, 1H), 5.77 (d, *J* = 13.1 Hz, 1H), 4.07 (t, *J* = 7.2 Hz, 2H), 3.31 (s, 3H), 2.22 (t, *J* = 7.2 Hz, 2H), 1.79 (m, 2H), 1.69 (s, 6H), 1.65 (s, 6H), 1.64 (m, 2H), 1.45 (m, 2H). **¹³C-NMR** (100 MHz, CDCl₃−CD₃OD), δ, ppm: 177.20 (COOH), 174.33 (CN Ind), 166.58 (CN Ind), 155.22 (CH), 153.27 (CH), 146.81 (CH), 144.47 (Ar), 141.28 (Ar), 140.59 (Ar), 140.34 (Ar), 128.28 (CH Ar), 126.34 (CH), 126.11 (CH), 125.57 (CH Ar), 121.54 (CH Ar), 118.83 (2CH Ar), 116.77 (CI Ar), 111.04 (2CI Ar), 105.96 (CH), 101.98 (CH), 50.51 (C̲(CH₃)₂), 49.30 (C̲(CH₃)₂), 44.03 (CH₂), 34.28 (CH₂), 28.73 (CH₃), 26.58 (CH₂), 26.50 (2CH₃), 25.42 (CH₂), 23.98 (CH₂), 23.29 (2CH₃). **HRMS** *m/z* (ESI⁺) C₃₄H₃₇I₃N₂O₂ calculated [M+H]⁺ 886.9989 (887.0062), found *m/z*: 887.0067.

6-(5-Iodo-3,3-dimethyl-2-(7-(4,5,6-triiodo-1,3,3-trimethylindolin-2-ylidene)-hepta-1,3,5-trien-1-yl)-3*H*-indol-1-ium-1-yl)hexanoate (4ICy7).

Dye **4ICy7** was synthesized from 4,5,6-triiodo-1,2,3,3-tetramethyl-3*H*-indol-1-ium iodide (**2.5f**) (170 mg, 0.25 mmol), *N*-[5-(phenylamino)-2,4-pentadienylidene]aniline hydrochloride (65 mg, 0.23 mmol), and 1-(5-carboxypentyl)-5-iodo-2,3,3-trimethyl-3*H*-indol-1-ium bromide (**2.6b**) (120 mg, 0.25 mmol). Yield: 116 mg (50%). **¹H-NMR** (400 MHz, CDCl₃−CD₃OD), δ, ppm: 7.78 (t, *J* = 12.8 Hz, 1H), 7.68 (d, *J* = 8.3 Hz, 1H), 7.66 (s, 1H), 7.63 (t, *J* = 13.0 Hz, 1H), 7.57 (s, 1H), 7.43 (t, *J* = 12.7 Hz, 1H), 6.96 (d, *J* = 8.4 Hz, 1H), 6.58 (t, *J* = 12.6 Hz, 1H), 6.48 (t, *J* = 12.6 Hz, 1H), 5.23 (d, *J* = 13.4 Hz, 1H), 5.88 (d, *J* = 13.3 Hz, 1H), 3.98 (t, *J* = 7.8 Hz, 2H), 3.37 (s, 3H), 2.24 (t, *J* = 7.2 Hz, 2H), 1.74 (m, 2H), 1.70 (s, 6H), 1.62 (s, 6H), 1.52 (m, 2H), 1.42 (m, 2H). **¹³C-NMR** (100 MHz, CDCl₃−CD₃OD), δ, ppm: 177.01 (COOH), 172.11 (CN Ind), 168.49 (CN Ind), 156.17 (CH), 152.62 (CH), 148.84 (CH), 144.13 (Ar), 142.34 (Ar), 141.45 (Ar), 140.42 (Ar), 137.03 (CH Ar), 130.63 (CH Ar), 126.44 (2CH), 119.32 (CH Ar), 118.06 (CI Ar), 112.19 (CH Ar), 105.56 (CI Ar), 104.78 (CH), 102.10 (CI Ar), 101.18 (CH), 89.21 (CI Ar), 50.99 (C̲(CH₃)₂), 48.72 (C̲(CH₃)₂), 43.70 (CH₂), 33.48 (CH₂), 28.42 (CH₃), 26.60 (2CH₃), 26.38 (CH₂), 25.32

(CH$_2$), 23.66 (CH$_2$), 23.16 (2CH$_3$). **HRMS** *m/z* (ESI$^+$) C$_{34}$H$_{36}$I$_4$N$_2$O$_2$ calculated [M+H]$^+$ 1012.8956 (1012.9028), found *m/z*: 1012.9034.

6-(4,5,6-Triiodo-3,3-dimethyl-2-(7-(4,5,6-triiodo-1,3,3-trimethylindolin-2-ylidene)hepta-1,3,5-trien-1-yl)-3*H*-indol-1-ium-1-yl)hexanoate (6ICy7).

Dye **6ICy7** was synthesized from 4,5,6-triiodo-1,2,3,3-tetramethyl-3*H*-indol-1-ium iodide (**2.5f**) (170 mg, 0.25 mmol), *N*-[5-(phenylamino)-2,4-pentadienylidene]aniline hydrochloride (65 mg, 0.23 mmol), and 1-(5-carboxypentyl)-4,5,6-triiodo-2,3,3-trimethyl-3*H*-indol-1-ium bromide (**2.6f**) (183 mg, 0.25 mmol). Yield: 78 mg (27%). ^{1}**H-NMR** (400 MHz, CDCl$_3$−CD$_3$OD), δ, ppm: 7.73 (t, *J* = 13.0 Hz, 2H), 7.65 (s, 1H), 7.62 (s, 1H), 7.45 (t, *J* = 12.6 Hz, 1H), 6.57 (m, 2H), 6.06 (d, *J* = 13.5 Hz, 2H), 3.86 (t, *J* = 7.6 Hz, 2H), 3.47 (s, 3H), 2.26 (t, *J* = 7.1 Hz, 2H), 1.72 (s, 12H), 1.68 (m, 2H), 1.63 (m, 2H), 1.42 (m, 2H). ^{13}**C-NMR** (100 MHz, CDCl$_3$−CD$_3$OD), δ, ppm: 177.05 (COOH), 170.80 (2CN Ind), 156.82 (CH), 151.90 (CH), 151.50 (CH), 143.68 (Ar), 142.93 (Ar), 141.94 (Ar), 141.70 (Ar), 120.03 (2CH), 119.95 (2CH Ar), 119.54 (2CI Ar), 105.95 (CI Ar), 105.75 (CI Ar), 102.86 (2CI Ar), 102.45 (CH), 102.22 (CH), 51.72 (C(CH$_3$)$_2$), 51.57 (C(CH$_3$)$_2$), 43.08 (CH$_2$), 33.57 (CH$_2$), 28.72 (CH$_3$), 25.81 (CH$_2$), 25.22 (CH$_2$), 23.68 (CH$_2$), 23.01 (4CH$_3$). **HRMS** *m/z* (ESI$^+$) C$_{34}$H$_{34}$I$_6$N$_2$O$_2$ calculated [M+H]$^+$ 1264.6888 (1264.6961), found *m/z*: 1264.6967.

5.2.5 Procedure for the synthesis of 2ICy7S dye

3-(5-carboxypentyl)-2-(7-(4,6-diiodo-3,3-dimethyl-1-(3-sulfopropyl)indolin-2-ylidene)hepta-1,3,5-trien-1-yl)-3-methyl-1-(3-sulfopropyl)-3*H*-indol-1-ium-5-sulfonate (2ICy7S). *N*-[5-(Phenylamino)-2,4-pentadienylidene]aniline hydrochloride (71 mg, 0.25 mmol) and indolenine **2.9** (115 mg, 0.25 mmol) were heated in a mixture of acetic anhydride (2 mL) and acetic acid (2 mL) at 120 °C for 45 min to form the intermediate *N*-phenylacetamide derivative. After cooling to r.t., a solution of indolenine **2.8** (138 mg, 0.26 mmol) in dry pyridine (1 mL) was added, stirred at 100 °C for 10 min, the obtained dye was precipitated with ether, filtered off, washed with ether, and column-purified on LiChroprep RP-18 using 0−30% acetonitrile−water+0.05% acetic acid as eluent. Yield: 69 mg (26%). ^{1}**H-NMR** (400 MHz, DMSO-*d$_6$*), δ, ppm:

8.02 (t, J = 13.0 Hz, 1H, CH), 7.84−7.72 (m, 5H, CH), 7.67 (d, J = 8.1 Hz, 1H, CH), 7.53 (d, J = 8.4 Hz, 1H, CH), 6.74 (d, J = 14.1 Hz, 1H, CH), 6.66−6.44 (m, 2H, CH), 6.26 (d, J = 13.6 Hz, 1H, CH), 4.35 (t, J = 6.3 Hz, 2H, N$\underline{CH_2}$), 4.05 (t, J = 7.0 Hz, 2H, N$\underline{CH_2}$), 2.66−2.54 (m, 4H $\underline{CH_2}$SO$_3$H), 2.30−2.16 (m, 2H, $\underline{CH_2}$COOH), 2.09−1.96 (m, 4H, CH$_2$), 1.95−1.86 (m, 2H, CH$_2$), 1.71 (s, 6H, s, (CH$_3$)$_2$), 1.64 (s, 3H, CH$_3$), 1.36−1.26 (m, 2H, CH$_2$), 1.17−1.05 (m, 2H, CH$_2$), 0.80−0.67 (m, 1H, CH$_2$), 0.51−0.38 (m, 1H, CH$_2$). ^{13}**C-NMR** (100 MHz, DMSO-d_6), δ, ppm: 174.64 (COOH), 173.80 (CN Ind), 168.27 (CN Ind), 156.75 (CSO$_3$ Ar), 147.02 (CH), 146.63 (Ar), 146.16 (Ar), 143.02 (Ar), 142.59 (2CH), 141.26 (Ar), 139.83 (CH Ar), 139.29 (CH Ar), 127.78 (2CH), 126.86 (CH Ar), 120.19 (CH Ar), 118.98 (CH Ar), 111.64 (CH), 102.38 (CH), 95.97 (C-I), 92.03 (C-I), 54.45 ($\underline{C}$(CH$_3$)), 50.15 ($\underline{C}$(CH$_3$)$_2$), 48.39 (CH$_2$SO$_3$), 48.28 (CH$_2$SO$_3$), 43.90 (NCH$_2$), 42.39 (NCH$_2$), 33.88 ($\underline{C}$H$_2$COOH), 28.87 (2CH$_2$), 27.14 (2CH$_2$), 24.48 (CH$_3$), 24.21 (2CH$_3$), 23.33 (2CH$_2$). **HRMS:** m/z (ESI$^+$) C$_{38}$H$_{46}$I$_2$N$_2$O$_{11}$S$_3$ calculated [M+H]$^+$ 1057.0426, found m/z: 1057.0464.

5.2.6 Synthesis of the Dye−Antibody (Dye−Ab) conjugates

Synthesis of 2ICy7S-NHS. **2ICy7S** (0.82 mg, 0.78 μmol) and *N,N,N′,N′*-tetramethyl-*O*-(*N*-succinimidyl)uronium tetrafluoroborate (TSTU) (0.35 mg, 1.2 μmol) were dissolved in DMF (100 μL), and *N,N*-diisopropylethylamine (DIPEA) (0.8 μL, 4.68 μmol) was added. The mixture was stirred at r.t. for 20 min to give **2ICy7S-NHS**. The obtained solution was used as is for conjugation with antibody.

Conjugation of 2ICy7S with monoclonal antibody to get 2ICy7S−Ab. A stock solution of trastuzumab (1.34 mg, 8.66 nmol, 62 μL) was diluted with 0.1 M PBS pH 7.4 (588 μL) to the final concentration of 2.1 mg/mL. The stock solution of **2ICy7S-NHS** (1 mg) in DMF (763 μL) was prepared; the aliquot (38.9 μg, 30.3 nmol, 29.6 μL) was added dropwise to the trastuzumab solution and stirred 1 h at 25 ℃. The obtained conjugate was separated from the unbound dye by using a gel-permeation chromatography (Sephadex G50, 0.1 M PBS pH 7.4). The first blue fraction was collected to yield **2ICy7S−Ab** conjugate (1.09 mg) with DAR ~1.8 (the amount of the conjugate and DAR were determined spectrophotometrically). The second blue fraction

consisted of the unbound dye. The obtained solution was diluted with PBS to the final concentration of 0.5 mg/mL, kept at 4 °C overnight, and used next day for IV administering.

Conjugation of Cy7^{TM} with monoclonal antibody to get Cy7^{TM}−Ab. **Cy7^{TM}−Ab** was obtained by the same procedure as for **2ICy7S−Ab** starting from the stock solution of trastuzumab (1.78 mg, 11.9 nmol, 85 µL) diluted in 0.1 M PBS pH 7.4 (765 µL) and **Cy7^{TM}-NHS** (37.8 µg, 41.6 nmol, 17.5 µL). Separation on Sephadex G50 resulted in **Cy7^{TM}−Ab** conjugate (1.7 mg, DAR ~ 1.7). Conjugate was diluted with PBS to 0.5 mg/mL concentration and used as is for IV administering.

5.3 Spectral-luminescent measurement procedures

5.3.1 Spectral measurements

The absorption spectra were recorded on a Jasco V-730 UV-Vis spectrophotometer and the fluorescence spectra were taken on an Edinburgh Instruments FS5 spectrofluorometer. The absorption and fluorescence spectra were measured at 25 °C in standard 1-cm quartz cells at ~0.5 µM dye concentrations in MeOH and 0.1 M PBS pH 7.4. The excitation wavelength (λ^*) was 700 nm.

5.3.2 Molar absorptivities

To determine extinction coefficient, the dye (~5 mg) was dissolved in the selected solvent (50 mL), the stock solution was diluted to the dye concentration $c_{Dye} \sim 0.5\text{-}5$ µM and the absorbance (A) at the absorption band maximum was measured in a 1-cm standard quartz cell. The extinction coefficients were calculated according to the Beer−Lambert law. The extinction coefficient of each dye was independently measured three times and the average value was taken. The reproducibility for determining the extinction coefficients was within ±5,000 M^{-1}cm^{-1}.

5.3.3 Fluorescence quantum yield

To determine the fluorescence quantum yield (Φ_F), the integrated relative intensities of the dye or dye-antibody conjugates were measured in the appropriate solvent *vs.* the **Cy7^{TM}** (Φ_F = 13%) [153] or **HITC** in MeOH as the reference (Φ_{Fl} = 28%) [130]; and the fluorescence quantum yields were calculated according to Equation 5.1 [160].

$$\Phi_F = \Phi_{FRef} \times (F / F_{Ref}) \times (A_{Ref} / A) \times (n_{D(media)}^2 / n_{D(mediaRef)}^2), \tag{5.1}$$

where Φ_{FRef} is the quantum yield of the reference, F_{Ref} and F are the areas (integral intensities) of the emission spectra ($F = \int I(\lambda)d\lambda$) of the reference dye and the dye under examination, A_{Ref} and A, are the absorbances at the λ^* of the reference dye and the dye under examination, $n_{D(mediaRef)}$, $n_{D(media)}$ are the refractive indices of the solvent, where the reference dye and dye under examination are dissolved respectively.

The quantum yield for each dye was independently measured three times and the average value was taken.

5.3.4 Quantum yield of singlet oxygen generation

The quantum yields of the singlet oxygen generation (Φ_Δ) were measured in methanol and PBS. Φ_Δ in *methanol* were measured according to the known procedure [28]. Solutions containing (i) the singlet oxygen scavenger, 1,3-diphenylisobenzofuran (**DPBF**, $A \sim 0.3$, $c \sim 14$ µM) and (ii) a dye under investigation or reference dye ($A \sim 1.0$, $c \sim 4-6$ µM) in methanol were prepared. 1,1′,3,3,3′,3′-Hexamethylindo-tricarbocyanine iodide (**HITC**) was used as the reference dye. The obtained solutions (3.0 mL) were light irradiated from the distance of 46 cm in a standard 1-cm quartz cells by using a 730-nm, 30 W LED equipped with a 60° lens and the absorption spectra were recorded over time. The total irradiation time was up to 30 min. During this time the absorbance of **DPBF** reduced to about 10% of its initial value. The corresponding plot representing the absorbance of **DPBF** at 410 nm *vs.* time was drawn and fitted by a first-order reaction rate function (Fig. 4.15). Then, Φ_Δ was calculated relative to the reference dye (**HITC**) ($\Phi_{\Delta Ref}$ = 0.89% in methanol [28]) according to Equation 5.2.

$$\Phi_\Delta = \Phi_{\Delta\text{Ref}} \times (r\ /\ r_{\text{Ref}}) \times (A_{\text{Ref}}\ /\ A), \tag{5.2}$$

where $\Phi_{\Delta\text{Ref}}$ is the quantum yield of the singlet oxygen generation for the reference dye, r_{Ref} and r are the rates of singlet oxygen scavenger degradation obtained from the corresponding fitting curves of the reference dye and the dye under examination, and A_{Ref} and A are the absorbances at $\lambda^* = 730$ nm of the reference dye and the dye under examination.

The quantum yields of the singlet oxygen generation (Φ_Δ) in 0.1 M PBS pH 7.4 were measured according to the known procedure [156]. The solutions of Singlet Oxygen Sensor Green (**SOSG**, $c \sim 6$ µM) [161] and a dye under investigation or reference dye ($c = 1.2-4.3$ µM) in PBS were prepared in standard 1-cm quartz cells. **ICG** was used as the reference dye. The obtained solutions (3 mL) were light irradiated from the distances of 26.5 cm by a 730-nm, 30 W LED equipped with a 60° lens and the emission spectra were recorded over time. The total irradiation time was up to 125 min. During this time the emission of **SOSG** gradually increased. The corresponding plots representing the emission of **SOSG** at 530 nm *vs.* time were drawn and fitted by a zero-order reaction rate function (Fig. 4.16) [156]. Then, the singlet oxygen quantum yield Φ_Δ was calculated relative to the reference dye (**ICG**, $\Phi_{\Delta\text{Ref}} = 0.2\%$ in PBS [35]) according to Equation 5.2 [156]. Because the emission rate increase of **SOSG** upon Φ_Δ measurements was very different in respect of the investigated dye, we used various concentrations of these dyes ranged between $c_{\text{Dye}} = 1.2-4.3$ µM. To confirm that $\Phi_{\Delta\text{Ref}}$ is not dependent of the dye concentration, we demonstrated a positive linear correlation between the **SOSG** reaction rate (r) and the dye concentration within the $c_{\text{Dye}} = 1.2-4.3$ µM (see example of **Cy7**$^{\text{TM}}$, Fig. 4.17).

Each experiment of Φ_Δ measurements in methanol and PBS was carried out in triplicate and the average Φ_Δ was calculated. The reproducibility in the determination of Φ_Δ was not more than 5%.

5.3.5 Fluorescence lifetimes

Fluorescence lifetimes (τ) were acquired with ChronosFD (ISS, Champaign, IL) a frequency domain lifetime spectrofluorometer using a 695-nm laser diode as the excitation light source, a 705-nm excitation bandpass filter and a 720-nm long-pass emission filter. The measurements were done against **Cy7^{TM}** in PBS as a reference (τ = 0.57 ns) [153] at 25 ºC. Two synthesizers (Model IFR2023) provided modulation frequencies in the range from 9 KHz to 1.2 GHz; one synthesizer drove the LEDs directly at a frequency f'. The second synthesizer drove the gain of the light detector at a frequency (f' + $\Delta f'$), where the quantity $\Delta f'$, called the cross-correlation frequency, was of the order of 1 KHz. The signals of the sum (that is $2f'$ + $\Delta f'$) and the difference (that is $\Delta f'$) of the two frequencies were recorded and the low frequency component $\Delta f'$ was taken to determine DC (direct current), AC (alternating current) and the phase components of the signal. In all lifetime measurements the dye concentrations were c ~ 0.5 μM. Instrument control, data acquisition and data analysis were performed using Vinci – Multidimensional Fluorescence Spectroscopy software (ISS, Champaign, IL). The analysis of the time-resolved fluorescence data was carried out using the traditional non-linear least squares method. This method evaluates how close a model selected by the user matches the data acquired with the instrument. The Marquardt–Levenberg algorithm was utilized for the minimization routine of the χ^2-function that compares the selected model with the experimental data. Frequency-domain data were used to determine the lifetimes using the multi-exponential model expressed by Equation 5.3 [1].

$$I(t) = \sum_{i=1}^{n} \alpha_i e^{-t/\tau_i}$$

, (5.3)

where α_i is the pre-exponential factor, τ_i the lifetime, and n = 1 or 2 for the single or double exponential fits, respectively. The fractional contribution of each component in the intensity decay $I(t)$ is given by Equation 5.4 [1].

$$f_i = \alpha_i \tau_i / \sum_j \alpha_j \tau_j \,, \tag{5.4}$$

The average lifetime (τ_{mean}) for a two-exponential decay was determined according to the Equation 5.5 [1]

$$\tau_{\text{mean}} = f_1 \tau_1 + f_2 \tau_2, \tag{5.5}$$

where f_1 and f_2 are the fractional intensities, τ_1 and τ_2 are the lifetimes.

5.3.6 Determination of Dye-to-Antibody Ratio (DAR)

DAR was measured by the spectrophotometric method and calculated according to Equation 5.6 [162].

$$DAR = \frac{A_{max}(conjugate) \times \varepsilon_{Ab}}{[A_{278} - x \times A_{max}(conjugate)] \times \varepsilon_d} \times \frac{\int_{550}^{850} A_{norm}(conjugate) d\lambda}{\int_{550}^{850} A_{norm}(free\ dye) d\lambda} \,, \tag{5.6}$$

where A_{max}(conjugate) is the absorbance of dye−Ab conjugate at the dye absorption maximum; A_{278} is the absorbance of dye−Ab conjugate at 278 nm (absorption maximum of Ab); ε_{Ab} and ε_d are the extinction coefficient of the Ab and dye, respectively; x is the correction factor (the ratio of the A_{278} to A_{max}(dye) for the dye alone). A correction factor of 0.042 was applied for **2ICy7S−Ab** and 0.031 for **Cy7$^{\text{TM}}$−Ab**. A_{norm}(conjugate) is the normalized absorbance spectra of Ab−dye conjugate and A_{norm} (free dye) is the normalized absorbance spectra of the corresponding unconjugated dye.

5.4 Biological procedures

5.4.1 Antimicrobial studies

Cultures of *S. aureus* (ATCC 25923), *E. coli* (ATCC 25922) and *P. aeruginosa* (ATCC 25668) were grown on Brain Heart agar plates (BHA, Acumedia, Lansing, MI, USA) for 24 h, transferred into Brain Heart broth (BH, Acumedia, Lansing, MI, USA), grown at 37±1°C with shaking at 170 rpm until reaching the absorbance $A = 0.10\pm0.02$ at 660 nm, which corresponded to a final concentration of 10^8 cells/mL, and diluted

with commercially available sterile 0.9% saline solution to the final concentration of 10^3-10^4 cells/mL.

All preparatory operations with photosensitizers were carried out in the dark to avoid their activation and photobleaching. The stock solutions of the dyes in DMSO (3−8 mM, spectrophotometrical control by known dilutions) were prepared and the desirable final concentrations were prepared in up to three dilutions. Then, each dye solution in DMSO (7 µL) was added to bacterial suspensions (1 mL) in 0.9% saline (Falcon® 24-well polystyrene clear flat bottom plate was used). Thus, the amount of DMSO added to the bacterial suspensions was always 0.7% (7% was used in several experiments, as noted below). The bacterial suspensions were then incubated in the dark at r.t. for 30 min and then exposed to light with shaking (or kept in the dark for the control) for certain periods of time according to the experimental conditions. The light exposure was carried out by a 730-nm, 30 W LED equipped with a 60° lens from the distance of 8 cm (light power density 56 mW/cm^2).

After the light exposure, aliquots of each sample (100 µL) were spread over BHA plates with a Drigalsky spreader, incubated at 37 ºC for 24 h, and the colony forming units (CFU) were counted using a colony counter Scan 500 (Interscience, Saint-Nom-la-Bretèche, France).

To verify the dark toxicity of the dyes, the same experiments were carried out in parallel without light exposure. As the control we utilized the samples of bacteria without dye: (i) in the dark and without DMSO, (ii) in the dark in the presence of DMSO, (iii) exposed to light without DMSO, and (iv) exposed to light in the presence of DMSO.

All the experiments with bacteria were carried out in triplicate 4-5 times in different days and the average values were taken.

5.4.2 Animal studies

5.4.2.1 Animal preparation

All animal experiments were carried out in compliance with the Israel Council on Animal Care regulations and were approved by the Animal Care Committee of Ariel University (Authorization number IL-179-06-19).

Six-week-old athymic Balb/c female nude mice (Harlan Labs, Nes Ziona, Israel) were subcutaneously inoculated on the dorsal left side with human breast cancer cell line BT-474 (1×10^6 cells in PBS into nu/nu mice, 100 µL per mouse) and tumors allowed to establish over 10 days. For that time tumor volumes reached around 28.5 mm^3.

Before imaging and/or photodynamic treatment, the mice were anesthetized by an intraperitoneal injection of a combination of ketamine and xylazine (0.5 mL of ketamine + 0.25 mL of xylazine + 4.25 mL of water). The injection dose was 0.1 mL/10 g mouse, total: 0.25 mL/mouse.

5.4.2.2 Animal imaging

Imaging was carried out using multispectral fluorescence *in vivo* imaging system CRi Maestro II. For imaging acquisition mice were anesthetized, and imaging was performed after the conjugate administering at certain time intervals from 5, 10, 24 h post-injection. The images were obtained in the white light and in the fluorescence channel: excitation wavelength 705 nm, excitation filter 740 nm, registration scan 740−950 nm. The data processing was performed by Maestro 3.0 and ImageJ software [163].

5.4.2.3 PDT experiment

After 10 days of tumor development, thirty mice were randomly separated into the ten groups (3 mice per group). Groups 1 and 6 were taken as the control for tumor growth and background autofluorescence in imaging experiments. Groups 2 and 3 were administered in the tail vein (IV) with **Cy7^{TM}−Ab** and groups 4 and 5 with **2ICy7S−Ab**

(100 µg of the conjugate in 200 µL PBS). Accumulation of the conjugates was monitored by fluorescence imaging at 5 h, 10 h and 24 h. After complete accumulation (24 h) monitored by fluorescence imaging, mice from groups 3 and 5 were anesthetized and subjected to 730 nm light irradiation (30 W LED, 70 mW/cm2, 15 min) at the irradiance of 63 J/cm^2. Group 7 was exposed to NIR light for 15 min (730 nm LED, 63 J/cm^2). Mice were IV administered (tail) with **Cy7^{TM}** (group 8), **2ICy7S** (group 9) and Ab (group 10). The administered doses were 1.14 nmol (0.774 µg) of Cy7, 1.20 nmol (1.27 µg) of 2ICy7, and 0.67 nmol (100 µg) of Ab in 200 µL PBS. The amount of the administered dye was calculated as m(dye) = n(Ab) × D/P(conjugate) × MW(dye) to receive the same amount of the dye as it was in the corresponding conjugates. The tumor sizes were measured in vivo over time by using the hands-on digital caliper method and the tumor volumes were calculated according to the Equation 5.7 [157]. Tumor volumes for all the groups were monitored during 28 days:

$$\text{Tumor volume (mm}^3) = 0.5 \times \text{Tumor Length} \times \text{Tumor Width}^2 \qquad (5.7)$$

5.4.2.4 Flow cytometry

Tumor-bearing mice were sacrificed, the tumors were resected, and single-cell suspensions ($0.5-1.0 \times 10^6$ cells) were prepared from mice tumors according to the procedure [158]. Isolated cells were washed and then fixed by using paraformaldehyde in order to prevent further degradation. Then, the cells were stained with MEBCYTO$^®$ Annexin V-FITC/PI Apoptosis Detection Kit according to the manufacturer's suggested protocol. The data were acquired by a CytoFLEX (Beckman Coulter) flow cytometer and analyzed using FlowJo software.

CONCLUSIONS

We developed novel halogenated fluorescent heptamethine cyanine dyes containing different quantities of iodine, bromine, and chlorine atoms in various positions of terminal indoleninium moieties and explored heavy atom effect on dyes spectral, photophysical and photochemical properties. In order to use the developed iodinated heptamethine cyanines as the materials for theranostics, photodynamic therapy (PDT), and photoimmunotherapy (PIT) applications, we studied their photocytotoxicity against gram-positive and gram-negative bacterial pathogens, as well as against breast cancer.

1. The initial quaternized 2,3,3-trimethylindoleninium salts for halogenated heptamethine cyanine dyes synthesis can be obtained by multistep reaction starting from the diazotization of corresponding halogenated anilines followed by reduction with tin(II) chloride, and then heterocyclization with 3-methyl-2-butanone in acetic acid, with further *N*-alkylation by iodomethane, 6-bromohexanoic acid or 3-bromo-*N,N,N*-triethylpropan-1-aminium bromide. Better yields in the reaction of diazotization can be achieved by the use of nitrosylsulfuric acid and precise temperature control.

2. An efficient synthetic pathway towards the synthesis of symmetrical and unsymmetrical heptamethine cyanine dyes containing a number of different halogen atoms in terminal heterocyclic moieties is as follows: respective quaternized indoleninium salts, containing halogen substituents, are introduced into one-pot sequential reaction with *N*-[5-(phenylamino)-2,4-pentadienylidene]aniline hydrochloride with the first and then with the second quaternized indolenine. In the first step, the formation of an intermediate phenylacetamide derivative is carried out in acetic anhydride, while in the second step, the formation of heptamethine cyanine dye is initiated by the addition of pyridine. In the case of symmetrical heptamethinecyanines, the first and the second quaternized indolenine is the same compound. The synthesis of the phenylacetamide derivative in acetic anhydride is accompanied by undesired at this step symmetrical dye byproduct formation. The formation of heptamethine cyanine dye

speeds up with the addition of pyridine and slows down with acetic acid addition to acetic anhydride.

3. Incorporation of halogen atoms, such as chlorine, bromine, and iodine in the terminal indolenine moieties of heptamethinecyanines does not have a significant effect on absorption and fluorescence maxima, although the introduction of iodine substituents leads to a slightly greater red shift in the spectra, as compared to brominated or unsubstituted dyes. At the same time, the fluorescence quantum yield (Φ_{Fl}) and lifetime are strongly affected by the type of halogen atom, their quantity, and position. Thus, halogenation of the dyes leads to significant Φ_{Fl} enhancement (up to 1.35 times). In general, bromine and even chlorine atoms incorporation leads to a higher increase in Φ_{Fl} of the dyes than iodine atoms. Halogen atoms in position 5 of terminal indolenine moieties result in a slight decrease of Φ_{Fl}, while, in contrast, halogen atoms in positions 4 or 6 facilitate strong increase of Φ_{Fl}, and the introduction of two halogen atoms in positions 4 and 6 at once enhances this effect. The combination of these positions (4,5,6) shows only a moderate Φ_{Fl} increase seemingly at the expense of halogens in position 5. At the same time, the level of Φ_{Fl} increasing is almost independent of the type of incorporated halogen (more light-weighted, chlorine, or heavier, bromine or iodine, atoms).

4. The halogen atom-promoted singlet oxygen quantum yield Φ_{Δ} depends not only on a number but also on the position of the halogen substituents in the heptamethine cyanine dyes. Thus, **4,6I$_4$-HITC** dye containing 4 iodine atoms in positions 4,6 of indolenine moieties have 1.5 lower Φ_{Δ} as compared to **5I$_2$-HITC** with 2 iodine atoms. Importantly, while iodine atoms strongly (up to 8.4 times) increase the Φ_{Δ} of the heptamethine cyanine dyes, bromine atoms insignificantly affect it. The incorporation of chlorine atoms reduces Φ_{Δ} even below this value for **HITC**.

5. The inclusion of halogen atoms in terminal heterocycles of heptamethine cyanine dye leads to a decrease of internal conversion in the excited state specifically the restriction of rotation of indolium moieties around the polymethine chain, thus increasing Φ_{Fl}, fluorescence lifetime, and, in some cases, even Φ_{Δ} for halogenated dyes compared to unsubstituted one.

6. The developed new NIR heptamethine cyanine dyes containing up to six iodine atoms and an aliphatic carboxylic group demonstrate the ability for photodynamic eradication of *S. aureus*, *E. coli*, and *P. aeruginosa* pathogens, wherein the increasing the number of iodine atoms in the dye has an unexpected and ambiguous photocytotoxic effect on these bacteria, which is connected with two opposing factors: (1) increase of the intersystem crossing and the rates of reactive species generation, and (2) dye aggregation causing the reduced dye uptake that, supposedly, is followed by the decreased rates of reactive species generation. As a result, the increase of the number of iodine atoms up to two in the series of zwitterionic cyanines increases the efficacy of *S. aureus* eradication; then the efficacy remains almost unchanged for the two-, three- and four-iodinated dyes and diminishes in the case of the hexa-iodinated cyanine. At the same time, the mono-iodinated heptamethine cyanine causes the most pronounced photocytotoxic effect on *E. coli* and *P. aeruginosa*. An additional positive charge contributed by a triethylammonium group decreases the efficacy of the dye towards *S. aureus* but improves the eradication of *E. coli* and *P. aeruginosa*.

7. Water-soluble NIR diiodinated heptamethine cyanine dye **2ICy7S** conjugated with the trastuzumab antibody (**Ab**) is considered the most promising agent for photoimmunotherapy (PIT) due to its high brightness and photocytotoxicity, while the aggregation issue caused by iodine substituents is handled by the introduction of sulfogroups. The iodine atoms in **2ICy7S** play a key role in the enhanced photocytotoxicity of the **2ICy7S–Ab** conjugate. Thus, **2ICy7S–Ab** conjugate promotes significant breast cancer tumor growth suppression in the mouse xenograft model: when irradiated with light, the combined *photoimmunotherapeutic* action results in 5.4-fold suppression caused by necrosis, while the antibody-stimulated *immunotherapeutic* effect of **2ICy7S–Ab** can be estimated as 1.4-fold tumor growth suppression, the similar result as for conjugate with non-iodinated analog **Cy7^{TM}–Ab** with and without light irradiation. The iodinated **2ICy7S–Ab** conjugate demonstrates a 3-fold increased quantum yield of singlet oxygen generation in aqueous media compared to its non-iodinated analog, **Cy7^{TM}–Ab**.

8. Antibody conjugate with iodinated dye **2ICy7S–Ab** provides a bright fluorescent signal allowing real-time monitoring of the conjugate distribution in the body and accumulation in the tumor, which is crucial for diagnostics purposes and for recognizing the optimal time for light irradiation and thus improving the precision and safety of treatment. The conjugation of **2ICy7S** with a wide range of antibodies should significantly expand the scope of efficient tools for photoimmunotherapeutic treatment and theranostics targeting various types of cancer.

Thus, variation of quantity and position of halogen atoms allows adjusting the key properties (Φ_{Fl}, Φ_{Δ}, and phototocytoxicity) of heptamethine cyanine dyes and gives an opportunity to design NIR cyanines with the desired properties in order to develop effective materials for fluorescence imaging, diagnostics, and, especially, for photodynamic therapy and theranostics.

REFERENCES

1   Lakowicz JR. Principles of fluorescence spectroscopy. Springer science & business media; 2006. https://doi.org/10.1007/978-0-387-46312-4.

2   Lavis LD, Raines RT. Bright ideas for chemical biology. ACS Chem Biol 2008;3:142−55. https://doi.org/10.1021/cb700248m.

3   Otto F. DAPI Staining of Fixed Cells for High-Resolution Flow Cytometry of Nuclear DNA. Methods Cell Biol 1990;33:105−10. https://doi.org/10.1016/S0091-679X(08)60516-6.

4   Akkol EK, Genç Y, Karpuz B, Sobarzo-Sánchez E, Capasso R. Coumarins and coumarin-related compounds in pharmacotherapy of cancer. Cancers 2020;12:1−25. https://doi.org/10.3390/cancers12071959.

5   Desiatkina O, Boubaker G, Anghel N, Amdouni Y, Hemphill A, Furrer J, et al. Synthesis, Photophysical Properties and Biological Evaluation of New Conjugates BODIPY: Dinuclear Trithiolato-Bridged Ruthenium(II)-Arene Complexes. ChemBioChem 2022;23:e202200536. https://doi.org/10.1002/cbic.202200536.

6   Keerthana S, Sam B, George L, Sudhakar YN, Varghese A. Fluorescein Based Fluorescence Sensors for the Selective Sensing of Various Analytes. J Fluoresc 2021;31:1251−76. https://doi.org/10.1007/s10895-021-02770-9.

7   Beija M, Afonso CAM, Martinho JMG. Synthesis and applications of rhodamine derivatives as fluorescent probes. Chem Soc Rev 2009;38:2410−33. https://doi.org/10.1039/b901612k.

8   Lo PC, Rodríguez-Morgade MS, Pandey RK, Ng DKP, Torres T, Dumoulin F. The unique features and promises of phthalocyanines as advanced photosensitisers for photodynamic therapy of cancer. Chem Soc Rev 2020;49:1041−56. https://doi.org/10.1039/c9cs00129h.

9   Deligeorgiev T, Vasilev A, Kaloyanova S, Vaquero JJ. Styryl dyes - synthesis and applications during the last 15 years. Color Technol 2010;126:55−80. https://doi.org/10.1111/j.1478-4408.2010.00235.x.

10 Ilina K, MacCuaig WM, Laramie M, Jeouty JN, McNally LR, Henary M. Squaraine Dyes: Molecular Design for Different Applications and Remaining Challenges. Bioconjug Chem 2020;31:194−213. https://doi.org/10.1021/acs.bioconjchem.9b00482.

11 Lange N, Szlasa W, Saczko J, Chwiłkowska A. Potential of cyanine derived dyes in photodynamic therapy. Pharmaceutics 2021;13:818. https://doi.org/10.3390/pharmaceutics13060818.

12 Shindy HA. Fundamentals in the chemistry of cyanine dyes: A review. Dyes Pigm 2017;145:505−13. https://doi.org/10.1016/j.dyepig.2017.06.029.

13 Feenstra RPG, Tseng SCG. Comparison of Fluorescein and Rose Bengal Staining. Ophthalmology 1992;99:605−17. https://doi.org/10.1016/S0161-6420(92)31947-5.

14 Zhang XF, Zhang J, Liu L. Fluorescence properties of twenty fluorescein derivatives: Lifetime, quantum yield, absorption and emission spectra. J Fluoresc 2014;24:819−26. https://doi.org/10.1007/s10895-014-1356-5.

15 Gandin E, Lion Y, Van de Vorst A. Quantum Yield of Singlet Oxygen Production By Xanthene Derivatives. Photochem Photobiol 1983;37:271−8. https://doi.org/10.1111/j.1751-1097.1983.tb04472.x.

16 Verhoeven JW. Glossary of terms used in photochemistry (IUPAC Reconunendations 1996). Pure Appl Chem 1996;68:2223−86. https://doi.org/10.1351/pac199668122223.

17 Geddes CD. Optical halide sensing using fluorescence quenching: theory, simulations and applications - a review. Meas Sci Technol 2001;12:R53−88. https://doi.org/10.1088/0957-0233/12/9/201.

18 Rey YP, Abradelo DG, Santschi N, Strassert CA, Gilmour R. Quantitative Profiling of the Heavy-Atom Effect in BODIPY Dyes: Correlating Initial Rates, Atomic Numbers, and 1O2 Quantum Yields. European J Org Chem 2017;2017:2170−8. https://doi.org/10.1002/ejoc.201601372.

19 Li Y, Li G, Zhang Q, Li Y, Jia Q, Zhang W, et al. Heavy atom effect on water-soluble porphyrin photosensitizers for photodynamic therapy. Chem Phys Lett 2021;784:139091. https://doi.org/10.1016/j.cplett.2021.139091.

20 Hayashi K, Nakamura M, Miki H, Ozaki S, Abe M, Matsumoto T, et al. Photostable iodinated silica/porphyrin hybrid nanoparticles with heavy-atom effect for wide-field photodynamic/photothermal therapy using single light source. Adv Funct Mater 2014;24:503−13. https://doi.org/10.1002/adfm.201301771.

21 Amirav A, Jortner J. Resonances in mediated intersystem crossing of jet-cooled anthracene derivatives. Chem Phys Lett 1986;132:335−40. https://doi.org/10.1016/0009-2614(86)80621-2.

22 McLoughlin CK, Kotroni E, Bregnhøj M, Rotas G, Vougioukalakis GC, Ogilby PR. Oxygen-and pH-dependent photophysics of fluorinated fluorescein derivatives: Non-symmetrical vs. symmetrical fluorination. Sensors 2020;20(18):5172. https://doi.org/10.3390/s20185172

23 Spagnuolo CC, Massad W, Miskoski S, Menendez GO, García NA, Jares-Erijman EA. Photostability and spectral properties of fluorinated fluoresceins and their biarsenical derivatives: a combined experimental and theoretical study. Photochem Photobiol 2009;85(5):1082-8. https://doi.org/10.1111/j.1751-1097.2009.00565.x

24 Szaciłowski K, Macyk W, Drzewiecka-Matuszek A, Brindell M, Stochel G. Bioinorganic photochemistry: Frontiers and mechanisms. Chem Rev 2005;105:2647−94. https://doi.org/10.1021/cr030707e.

25 Li Y, Zhou Y, Yue X, Dai Z. Cyanine Conjugate-Based Biomedical Imaging Probes. Adv Healthc Mater 2020;9:2001327. https://doi.org/10.1002/adhm.202001327.

26 Gorka AP, Nani RR, Schnermann MJ. Cyanine polyene reactivity: scope and biomedical applications. Org Biomol Chem 2015;13:7584−98. https://doi.org/10.1039/c5ob00788g.

27 Choi PJ, Park TIH, Cooper E, Dragunow M, Denny WA, Jose J. Heptamethine Cyanine Dye Mediated Drug Delivery: Hype or Hope. Bioconjug Chem 2020;31:1724−39. https://doi.org/10.1021/acs.bioconjchem.0c00302.

28 Štacková L, Muchová E, Russo M, Slavíček P, Štacko P, Klán P. Deciphering the Structure-Property Relations in Substituted Heptamethine Cyanines. J Org Chem 2020;85:9776−90. https://doi.org/10.1021/acs.joc.0c01104.

29 Flanagan, Jr. JH, Romero SE, Legendre, Jr. BL, Hammer RP, Soper SA. Heavy-atom modified near-IR fluorescent dyes for DNA sequencing applications: synthesis and photophysical characterization. Adv Fluoresc Sens Technol III 1997;2980:328−37. https://doi.org/10.1117/12.273529.

30 Atchison J, Kamila S, Nesbitt H, Logan KA, Nicholas DM, Fowley C, et al. Iodinated cyanine dyes: a new class of sensitisers for use in NIR activated photodynamic therapy (PDT). Chem Commun 2017;53:2009−12. https://doi.org/10.1039/c6cc09624g.

31 Cao J, Chi J, Xia J, Zhang Y, Han S, Sun Y. Iodinated Cyanine Dyes for Fast Near-Infrared-Guided Deep Tissue Synergistic Phototherapy. ACS Appl Mater Interfaces 2019;11:25720−9. https://doi.org/10.1021/acsami.9b07694.

32 Usama SM, Thavornpradit S, Burgess K. Optimized heptamethine cyanines for photodynamic therapy. ACS Appl Bio Mater 2018;1:1195−205. https://doi.org/10.1021/acsabm.8b00414.

33 Levitz A, Marmarchi F, Henary M. Synthesis and optical properties of near-infrared meso-phenyl-substituted symmetric heptamethine cyanine dyes. Molecules 2018;23. https://doi.org/10.3390/molecules23020226.

34 Mayerhöffer U, Fimmel B, Würthner F. Bright near-infrared fluorophores based on squaraines by unexpected halogen effects. Angew Chem - Int Ed 2012;51:164−7. https://doi.org/10.1002/anie.201107176.

35 Wang S, Shang L, Li L, Yu Y, Chi C, Wang K, Zhang J, Shi R, Shen H, Waterhouse GIN, et al. Metal-organic-framework-derived mesoporous carbon

nanospheres containing porphyrin-like metal centers for conformal phototherapy. Adv Mater 2016;28(38):8379−8387. https://doi.org/10.1002/adma.201602197.

36 James NS, Chen Y, Joshi P, Ohulchanskyy TY, Ethirajan M, Henary M, et al. Evaluation of polymethine dyes as potential probes for near infrared fluorescence imaging of tumors: Part - 1. Theranostics 2013;3:692−702. https://doi.org/10.7150/thno.5922.

37 Feng L, Chen W, Ma X, Liu SH, Yin J. Near-infrared heptamethine cyanines (Cy7): from structure, property to application. Org Biomol Chem 2020;18:9385−97. https://doi.org/10.1039/d0ob01962c.

38 Chinna Ayya Swamy P, Sivaraman G, Priyanka RN, Raja SO, Ponnuvel K, Shanmugpriya J, et al. Near infrared (NIR) absorbing dyes as promising photosensitizer for photo dynamic therapy. Coord Chem Rev 2020;411:213233. https://doi.org/10.1016/j.ccr.2020.213233.

39 Mu X, Lu Y, Wu F, Wei Y, Ma H, Zhao Y, et al. Supramolecular nanodiscs self-assembled from non-ionic heptamethine cyanine for imaging-guided cancer photothermal therapy. Adv Mater 2020;32:1906711. https://doi.org/10.1002/adma.201906711.

40 Shi C, Wu JB, Pan D. Review on near-infrared heptamethine cyanine dyes as theranostic agents for tumor imaging, targeting, and photodynamic therapy. J Biomed Opt 2016;21:050901. https://doi.org/10.1117/1.jbo.21.5.050901.

41 von der Haar M, Heuer C, Pähler M, von der Haar K, Lindner P, Scheper T, et al. Optimization of cyanine dye stability and analysis of FRET interaction on DNA microarrays. Biology 2016;5:47. https://doi.org/10.3390/biology5040047.

42 Hoelzel CA, Zhang X. Visualizing and Manipulating Biological Processes by Using HaloTag and SNAP-Tag Technologies. ChemBioChem 2020;21:1935−46. https://doi.org/10.1002/cbic.202000037.

43 Polom K, Murawa D, Rho YS, Nowaczyk P, Hünerbein M, Murawa P. Current trends and emerging future of indocyanine green usage in surgery and oncology: a literature review. Cancer 2011;117:4812−22. https://doi.org/10.1002/cncr.26087.

44 Wang H, Li X, Tse BWC, Yang H, Thorling CA, Liu Y, et al. Indocyanine green-incorporating nanoparticles for cancer theranostics. Theranostics 2018;8:1227−42. https://doi.org/10.7150/thno.22872.

45 Alander JT, Kaartinen I, Laakso A, Pätilä T, Spillmann T, Tuchin V V., et al. A Review of indocyanine green fluorescent imaging in surgery. Int J Biomed Imaging 2012;2012. https://doi.org/10.1155/2012/940585.

46 Azari F, Zhang K, Kennedy G, Bou-Samra P, Chang A, Nadeem B, Chang A, Galandarova A, Ibrahimli A, Karimov Z, Din A. Prospective validation of tumor

folate receptor expression density with the association of pafolacianine fluorescence during intraoperative molecular imaging−guided lung cancer resections. European Journal of Nuclear Medicine and Molecular Imaging. 2023 Mar 11:1-3.

47 Szabó Á, Szendi-Szatmári T, Ujlaky-Nagy L, Rádi I, Vereb G, Szöllősi J, et al. The Effect of Fluorophore Conjugation on Antibody Affinity and the Photophysical Properties of Dyes. Biophys J 2018;114:688−700. https://doi.org/10.1016/j.bpj.2017.12.011.

48 Cilliers C, Nessler I, Christodolu N, Thurber GM. Tracking Antibody Distribution with Near-Infrared Fluorescent Dyes: Impact of Dye Structure and Degree of Labeling on Plasma Clearance. Mol Pharm 2017;14:1623−33. https://doi.org/10.1021/acs.molpharmaceut.6b01091.

49 Serpe L, Ellena S, Barbero N, Foglietta F, Prandini F, Gallo MP, et al. Squaraines bearing halogenated moieties as anticancer photosensitizers: Synthesis, characterization and biological evaluation. Eur J Med Chem 2016;113:187−97. https://doi.org/10.1016/j.ejmech.2016.02.035.

50 Gunaydin G, Gedik ME, Ayan S. Photodynamic therapy—current limitations and novel approaches. Front Chem 2021;9:400. https://doi.org/10.3389/fchem.2021.691697.

51 Algorri JF, Ochoa M, Roldán-Varona P, Rodríguez-Cobo L, López-Higuera JM. Photodynamic therapy: a compendium of latest reviews. Cancers 2021;13. https://doi.org/10.3390/cancers13174447.

52 Wang K, Yu B, Pathak JL. An update in clinical utilization of photodynamic therapy for lung cancer. J Cancer 2021;12:1154−60. https://doi.org/10.7150/jca.51537.

53 Nowak KM, Schwartz MR, Breza VR, Price RJ. Sonodynamic therapy: rapid progress and new opportunities for non-invasive tumor cell killing with sound. Cancer Lett 2022;532:215592. https://doi.org/10.1016/j.canlet.2022.215592.

54 Yan P, Liu LH, Wang P. Sonodynamic therapy (SDT) for cancer treatment: advanced sensitizers by ultrasound activation to injury tumor. ACS Appl Bio Mater 2020;3:3456−75. https://doi.org/10.1021/acsabm.0c00156.

55 Songca SP, Adjei Y. Applications of antimicrobial photodynamic therapy against bacterial biofilms. Int J Mol Sci 2022;23:3209. https://doi.org/10.3390/ijms23063209.

56 Dias LD, Blanco KC, Bagnato VS. COVID-19: Beyond the virus. The use of photodynamic therapy for the treatment of infections in the respiratory tract. Photodiagnosis Photodyn Ther 2020;31:101804. https://doi.org/10.1016/j.pdpdt.2020.101804.

57 Hung JH, Lee CN, Hsu HW, Ng IS, Wu CJ, Yu CK, et al. Recent advances in photodynamic therapy against fungal keratitis. Pharmaceutics 2021;13:2011. https://doi.org/10.3390/pharmaceutics13122011.

58 Alves F, Pavarina AC, Mima EG de O, McHale AP, Callan JF. Antimicrobial sonodynamic and photodynamic therapies against *Candida albicans*. Biofouling 2018

59 Zhang Y, Koradia A, Kamato D, Popat A, Little PJ, Ta HT. Treatment of atherosclerotic plaque: perspectives on theranostics. J Pharm Pharmacol 2019;71:1029−43. https://doi.org/10.1111/jphp.13092.

60 Li L, Chen Y, Chen W, Tan Y, Chen H, Yin J. Photodynamic therapy based on organic small molecular fluorescent dyes. Chinese Chem Lett 2019;30:1689−703. https://doi.org/10.1016/j.cclet.2019.04.017.

61 Shang L, Zhou X, Zhang J, Shi Y, Zhong L. Metal nanoparticles for photodynamic therapy: a potential treatment for breast cancer. Molecules 2021;26:6532. https://doi.org/10.3390/molecules26216532.

62 Nasseri B, Alizadeh E, Bani F, Davaran S, Akbarzadeh A, Rabiee N, et al. Nanomaterials for photothermal and photodynamic cancer therapy. Appl Phys Rev 2022;9:011317. https://doi.org/10.1063/5.0047672.

63 Zhao X, Liu J, Fan J, Chao H, Peng X. Recent progress in photosensitizers for overcoming the challenges of photodynamic therapy: From molecular design to application. Chem Soc Rev 2021;50:4185−219. https://doi.org/10.1039/d0cs00173b.

64 Mundekkad D, Cho WC. Nanoparticles in Clinical Translation for Cancer Therapy. Int J Mol Sci 2022;23:1685. https://doi.org/10.3390/ijms23031685.

65 Lan M, Zhao S, Liu W, Lee CS, Zhang W, Wang P. Photosensitizers for photodynamic therapy. Adv Healthc Mater 2019;8:1900132. https://doi.org/10.1002/adhm.201900132.

66 Escudero A, Carrillo-Carrión C, Castillejos MC, Romero-Ben E, Rosales-Barrios C, Khiar N. Photodynamic therapy: photosensitizers and nanostructures. Mater Chem Front 2021;5:3788−812. https://doi.org/10.1039/d0qm00922a.

67 Correia JH, Rodrigues JA, Pimenta S, Dong T, Yang Z. Photodynamic therapy review: principles, photosensitizers, applications, and future directions. Pharmaceutics 2021;13:1332. https://doi.org/10.3390/pharmaceutics13091332.

68 Prejanò M, Alberto ME, De Simone BC, Marino T, Toscano M, Russo N. Sulphur- and Selenium-for-Oxygen Replacement as a Strategy to Obtain Dual Type I/Type II Photosensitizers for Photodynamic Therapy. Molecules 2023;28:3153. https://doi.org/10.3390/molecules28073153.

69 Kou J, Dou D, Yang L. Porphyrin photosensitizers in photodynamic therapy and its applications. Oncotarget 2017;8:81591−603. https://doi.org/10.18632/oncotarget.20189.

70 Srivatsan A, Missert JR, Upadhyay SK, Pandey RK. Porphyrin-based photosensitizers and the corresponding multifunctional nanoplatforms for cancer-imaging and phototherapy. J Porphyr Phthalocyanines 2015;19:109−34. https://doi.org/10.1142/S1088424615300037.

71 Qiu H, Kim MM, Penjweini R, Finlay JC, Busch TM, Wang T, et al. A comparison of dose metrics to predict local tumor control for Photofrin-mediated photodynamic therapy. Photochem Photobiol 2017;93:1115−22. https://doi.org/10.1111/php.12719.

72 O'Connor AE, Gallagher WM, Byrne AT. Porphyrin and nonporphyrin photosensitizers in oncology: preclinical and clinical advances in photodynamic therapy. Photochem Photobiol 2009;85:1053−74. https://doi.org/10.1111/J.1751-1097.2009.00585.X.

73 Amirshaghaghi A, Yan L, Miller J, Daniel Y, Stein JM, Busch TM, et al. Chlorin e6-coated superparamagnetic iron oxide nanoparticle (SPION) nanoclusters as a theranostic agent for dual-mode imaging and photodynamic therapy. Sci Rep 2019;9. https://doi.org/10.1038/s41598-019-39036-1.

74 Ikeda A, Satake S, Mae T, Ueda M, Sugikawa K, Shigeto H, et al. Photodynamic activities of porphyrin derivative-cyclodextrin complexes by photoirradiation. ACS Med Chem Lett 2017;8:555−9. https://doi.org/10.1021/acsmedchemlett.7b00098.

75 Zheng B De, Ye J, Zhang XQ, Zhang N, Xiao MT. Recent advances in supramolecular activatable phthalocyanine-based photosensitizers for anti-cancer therapy. Coord Chem Rev 2021;447:214155. https://doi.org/10.1016/j.ccr.2021.214155.

76 Chen D, Song M, Huang J, Chen N, Xue J, Huang M. Photocyanine: a novel and effective phthalocyanine-based photosensitizer for cancer treatment. J Innov Opt Health Sci 2020;13. https://doi.org/10.1142/S1793545820300098.

77 Li X, De Zheng B, Peng XH, Li SZ, Ying JW, Zhao Y, et al. Phthalocyanines as medicinal photosensitizers: developments in the last five years. Coord Chem Rev 2019;379:147−60. https://doi.org/10.1016/j.ccr.2017.08.003.

78 Bilici K, Cetin S, Aydındogan E, Yagci Acar H, Kolemen S. Recent advances in cyanine-based phototherapy agents. Front Chem 2021;9:444. https://doi.org/10.3389/fchem.2021.707876.

79 Lange N, Szlasa W, Saczko J, Chwiłkowska A. Potential of cyanine derived dyes in photodynamic therapy. Pharmaceutics 2021;13:818.

80 Dereje DM, Pontremoli C, Moran Plata MJ, Visentin S, Barbero N. Polymethine dyes for PDT: recent advances and perspectives to drive future applications. Photochem Photobiol Sci 2022;21:397−419. https://doi.org/10.1007/s43630-022-00175-6.

81 Indocyanine Green | AAT Bioquest 2019. https://www.aatbio.com/catalog/indocyanine-green#toc_1 (accessed March 2, 2023).

82 Guerrero Y, Singh SP, Mai T, Murali RK, Tanikella L, Zahedi A, et al. Optical characteristics and tumor imaging capabilities of near infrared dyes in free and nano-encapsulated formulations comprised of viral capsids. ACS Appl Mater Interfaces 2017;9:19601−11. https://doi.org/10.1021/acsami.7b03373.

83 Wang Z, Ivanov M, Gao Y, Bussotti L, Foggi P, Zhang H, et al. Spin−orbit charge-transfer intersystem crossing (ISC) in compact electron donor−acceptor dyads: ISC mechanism and application as novel and potent photodynamic therapy reagents. Chem Eur J 2020;26:1091−102. https://doi.org/10.1002/chem.201904306.

84 Semenova O, Kobzev D, Hovor I, Atrash M, Nakonechny F, Kulyk O, et al. Effect of solubilizing group on the antibacterial activity of heptamethine cyanine photosensitizers. Pharmaceutics 2023;15:247. https://doi.org/10.3390/pharmaceutics15010247.

85 Ebaston TM, Nakonechny F, Talalai E, Gellerman G, Patsenker L. Iodinated xanthene-cyanine NIR dyes as potential photosensitizers for antimicrobial photodynamic therapy. Dyes Pigm 2021;184:108854. https://doi.org/10.1016/j.dyepig.2020.108854.

86 Birrer MJ, Moore KN, Betella I, Bates RC. Antibody-drug conjugate-based therapeutics: state of the science. J Natl Cancer Inst 2019;111:538−49. https://doi.org/10.1093/jnci/djz035.

87 Abdollahpour-Alitappeh M, Lotfinia M, Gharibi T, Mardaneh J, Farhadihosseinabadi B, Larki P, et al. Antibody−drug conjugates (ADCs) for cancer therapy: strategies, challenges, and successes. J Cell Physiol 2019;234:5628−42. https://doi.org/10.1002/jcp.27419.

88 Manzari MT, Shamay Y, Kiguchi H, Rosen N, Scaltriti M, Heller DA. Targeted drug delivery strategies for precision medicines. Nat Rev Mater 2021;6:351−70. https://doi.org/10.1038/s41578-020-00269-6.

89 Dunuweera SP, Rajapakse RMSI, Rajapakshe RBSD, Wijekoon SHDP, Nirodha Thilakarathna MGGS, Rajapakse RMG. Review on targeted drug delivery carriers used in nanobiomedical applications. Curr Nanosci 2018;15:382−97. https://doi.org/10.2174/1573413714666181106114247.

90 Tewabe A, Abate A, Tamrie M, Seyfu A, Siraj EA. Targeted drug delivery — from magic bullet to nanomedicine: principles, challenges, and future perspectives. J Multidiscip Healthc 2021;14:1711−24. https://doi.org/10.2147/JMDH.S313968.

91 Goydel RS, Rader C. Antibody-based cancer therapy. Oncogene 2021;40:3655−64. https://doi.org/10.1038/s41388-021-01811-8.

92 Borrelli A, Tornesello AL, Tornesello ML, Buonaguro FM. Cell penetrating peptides as molecular carriers for anti-cancer agents. Molecules 2018;23:295. https://doi.org/10.3390/molecules23020295.

93 Saraf S, Jain A, Tiwari A, Verma A, Panda PK, Jain SK. Advances in liposomal drug delivery to cancer: an overview. J Drug Deliv Sci Technol 2020;56:101549. https://doi.org/10.1016/j.jddst.2020.101549.

94 Ambekar RS, Choudhary M, Kandasubramanian B. Recent advances in dendrimer-based nanoplatform for cancer treatment: a review. Eur Polym J 2020;126:109546. https://doi.org/10.1016/j.eurpolymj.2020.109546.

95 Sun Z, Song C, Wang C, Hu Y, Wu J. Hydrogel-based controlled drug delivery for cancer treatment: a review. Mol Pharm 2020;17:373−91. https://doi.org/10.1021/acs.molpharmaceut.9b01020.

96 Kulkarni NS, Guererro Y, Gupta N, Muth A, Gupta V. Exploring potential of quantum dots as dual modality for cancer therapy and diagnosis. J Drug Deliv Sci Technol 2019;49:352−64. https://doi.org/10.1016/j.jddst.2018.12.010.

97 Li X, Li W, Wang M, Liao Z. Magnetic nanoparticles for cancer theranostics: advances and prospects. J Control Release 2021;335:437−48. https://doi.org/10.1016/j.jconrel.2021.05.042.

98 Amaldoss MJN, Yang JL, Koshy P, Unnikrishnan A, Sorrell CC. Inorganic nanoparticle-based advanced cancer therapies: promising combination strategies. Drug Discov Today 2022;27:103386. https://doi.org/10.1016/j.drudis.2022.103386.

99 Ghosh B, Biswas S. Polymeric micelles in cancer therapy: state of the art. J Control Release 2021;332:127−47. https://doi.org/10.1016/j.jconrel.2021.02.016.

100 Zahavi D, Weiner L. Monoclonal antibodies in cancer therapy. Antibodies 2020;9:1−20. https://doi.org/10.3390/antib9030034.

101 Waldmann H. Human monoclonal antibodies: the benefits of humanization. Methods Mol Biol 2019;1904:1−10. https://doi.org/10.1007/978-1-4939-8958-4_1.

102 Eigenmann MJ, Fronton L, Grimm HP, Otteneder MB, Krippendorff BF. Quantification of IgG monoclonal antibody clearance in tissues. MAbs 2017;9:1007−15. https://doi.org/10.1080/19420862.2017.1337619.

103 Scott AM, Allison JP, Wolchok JD. Monoclonal antibodies in cancer therapy. Cancer Immun 2012;12:34. https://doi.org/10.3390/ANTIB9030034.

104 Tan S, Li D, Zhu X. Cancer immunotherapy: Pros, cons and beyond. Biomed Pharmacother 2020;124:109821. https://doi.org/10.1016/j.biopha.2020.109821.

105 Esfahani K, Roudaia L, Buhlaiga N, Del Rincon S V., Papneja N, Miller WH. A review of cancer immunotherapy: From the past, to the present, to the future. Curr Oncol 2020;27:87−97. https://doi.org/10.3747/co.27.5223.

106 Jung AC, Moinard-Butot F, Thibaudeau C, Gasser G, Gaiddon C. Antitumor immune response triggered by metal-based photosensitizers for photodynamic therapy: Where are we? Pharmaceutics 2021;13:1788. https://doi.org/10.3390/pharmaceutics13111788.

107 Hua J, Wu P, Gan L, Zhang Z, He J, Zhong L, et al. Current strategies for tumor photodynamic therapy combined with immunotherapy. Front Oncol 2021;11:4774. https://doi.org/10.3389/fonc.2021.738323.

108 Ducry L, Stump B. Antibody-drug conjugates: linking cytotoxic payloads to monoclonal antibodies. Bioconjug Chem 2010;21:5−13. https://doi.org/10.1021/bc9002019.

109 Kobayashi H, Choyke PL. Near-infrared photoimmunotherapy of cancer. Acc Chem Res 2019;52:2332−9. https://doi.org/10.1021/acs.accounts.9b00273.

110 Thankarajan E, Tuchinsky H, Aviel-Ronen S, Bazylevich A, Gellerman G, Patsenker L. Antibody guided activatable NIR photosensitizing system for fluorescently monitored photodynamic therapy with reduced side effects. J Control Release 2022;343:506−17. https://doi.org/10.1016/j.jconrel.2022.02.008.

111 Scott AM, Wolchok JD, Old LJ. Antibody therapy of cancer. Nat Rev Cancer 2012;12:278−87. https://doi.org/10.1038/nrc3236.

112 Drago JZ, Modi S, Chandarlapaty S. Unlocking the potential of antibody−drug conjugates for cancer therapy. Nat Rev Clin Oncol 2021;18:327−44. https://doi.org/10.1038/s41571-021-00470-8.

113 Berraondo P, Sanmamed MF, Ochoa MC, Etxeberria I, Aznar MA, Pérez-Gracia JL, et al. Cytokines in clinical cancer immunotherapy. Br J Cancer 2019;120:6−15. https://doi.org/10.1038/s41416-018-0328-y.

114 June CH, O'Connor RS, Kawalekar OU, Ghassemi S, Milone MC. CAR T cell immunotherapy for human cancer. Science 2018;359:1361−5. https://doi.org/10.1126/science.aar6711.

115 Waldman AD, Fritz JM, Lenardo MJ. A guide to cancer immunotherapy: from T cell basic science to clinical practice. Nat Rev Immunol 2020;20:651−68. https://doi.org/10.1038/s41577-020-0306-5.

116 Markova LI, Terpetschnig EA, Patsenker LD. Comparison of a series of hydrophilic squaraine and cyanine dyes for use as biological labels. Dyes Pigm 2013;99:561−70. https://doi.org/10.1016/j.dyepig.2013.06.022.

117 Myrzakhmetov B, Arnoux P, Mordon S, Acherar S, Tsoy I, Frochot C. Photophysical properties of protoporphyrin IX, pyropheophorbide-a and photofrin® in different conditions. Pharmaceuticals 2021;14:1−21. https://doi.org/10.3390/ph14020138.

118 Moan J. The photochemical yield of singlet oxygen from porphyrins in different states of aggregation. Photochem Photobiol 1984;39:445−9. https://doi.org/10.1111/j.1751-1097.1984.tb03873.x.

119 Markova LI, Fedyunyayeva IA, Povrozin YA, Semenova OM, Khabuseva SU, Terpetschnig EA, et al. Water soluble indodicarbocyanine dyes based on 2,3-dimethyl-3-(4- sulfobutyl)-3H-indole-5-sulfonic acid. Dyes Pigm 2013;96:535−46. https://doi.org/10.1016/j.dyepig.2012.09.007.

120 Štacková L, Russo M, Muchova L, Orel V, Vitek L, Štacko P, Klán P. Cyanine-flavonol hybrids for near-infrared light-activated delivery of carbon monoxide. Chem Eur J 2020;15;26(58):13184-90. https://doi.org/10.1002/chem.202003272

121 Kobayashi H, Furusawa A, Rosenberg A, Choyke PL. Near-infrared photoimmunotherapy of cancer: a new approach that kills cancer cells and enhances anti-cancer host immunity. Int Immunol 2021;33:7−15. https://doi.org/10.1093/intimm/dxaa037.

122 Wakiyama H, Kato T, Furusawa A, Choyke PL, Kobayashi H. Near infrared photoimmunotherapy of cancer; Possible clinical applications. Nanophotonics 2021;10:3135−51. https://doi.org/https://doi.org/10.1515/nanoph-2021-0119.

123 Kobayashi M, Harada M, Takakura H, Ando K, Goto Y, Tsuneda T, et al. Theoretical and experimental studies on the near-infrared photoreaction mechanism of a silicon phthalocyanine photoimmunotherapy dye: photoinduced hydrolysis by radical anion generation. Chempluschem 2020;85:1959−63. https://doi.org/10.1002/cplu.202000338.

124 Sato K, Ando K, Okuyama S, Moriguchi S, Ogura T, Totoki S, et al. Photoinduced ligand release from a silicon phthalocyanine dye conjugated with monoclonal antibodies: a mechanism of cancer cell cytotoxicity after near-infrared photoimmunotherapy. ACS Cent Sci 2018;4:1559−69. https://doi.org/10.1021/acscentsci.8b00565.

125 Takakura H, Matsuhiro S, Kobayashi M, Goto Y, Harada M, Taketsugu T, et al. Axial-ligand-cleavable silicon phthalocyanines triggered by near-infrared light

toward design of photosensitizers for photoimmunotherapy. J Photochem Photobiol A Chem 2022;426:113749. https://doi.org/10.1016/j.jphotochem.2021.113749.

126 Bokan M, Nakonechny F, Talalai E, **Kobzev D**, Gellerman G, Patsenker L. Photodynamic effect of novel hexa-iodinated quinono-cyanine dye on *Staphylococcus aureus*. Photodiagnosis Photodyn Ther 2020;31:101866. https://doi.org/10.1016/j.pdpdt.2020.101866.

127 Konovalova IS, Shishkina SV, **Kobzev D**, Semenova O, Tatarets A. Crystal structures and Hirshfeld analysis of 4,6- dibromoindolenine and its quaternized salt. Acta Crystallogr Sect E Crystallogr Commun 2021;77:1203−7. https://doi.org/10.1107/S2056989021011385.

128 Burgi HB, Dunitz JD. Structure correlation. Weinheim: VCH. 1994;2:741−784.

129 Semenova O, **Kobzev D**, Yazbak F, Nakonechny F, Kolosova O, Tatarets A, et al. Unexpected effect of iodine atoms in heptamethine cyanine dyes on the photodynamic eradication of Gram-positive and Gram-negative pathogens. Dyes Pigm 2021;195:109745. https://doi.org/10.1016/j.dyepig.2021.109745.

130 Altinoğlu EI, Russin TJ, Kaiser JM, Barth BM, Eklund PC, Kester M, et al. Near-infrared emitting fluorophore-doped calcium phosphate nanoparticles for in vivo imaging of human breast cancer. ACS Nano 2008;2:2075−84. https://doi.org/10.1021/nn800448r.

131 Berezin MY, Achilefu S. Fluorescence lifetime measurements and biological imaging. Chem Rev 2010;110:2641−84. https://doi.org/10.1021/cr900343z.

132 Soper SA, Mattingly QL. Steady-State and Picosecond Laser Fluorescence Studies of Nonradiative Pathways in Tricarbocyanine Dyes: Implications to the Design of Near-IR Fluorochromes with High Fluorescence Efficiencies. J Am Chem Soc 1994;116:3744−52. https://doi.org/10.1021/ja00088a010.

133 Lee H, Berezin MY, Henary M, Strekowski L, Achilefu S. Fluorescence lifetime properties of near-infrared cyanine dyes in relation to their structures. J Photochem Photobiol A Chem 2008;200:438−44. https://doi.org/10.1016/j.jphotochem.2008.09.008.

134 Hu D, Yao L, Yang B, Ma Y. Reverse intersystem crossing from upper triplet levels to excited singlet: A "hot excition" path for organic light-emitting diodes. Philos Trans R Soc A Math Phys Eng Sci 2015;373. https://doi.org/10.1098/rsta.2014.0318.

135 Gastilovich EA, Klimenko VG, Korol'Kova N V., Nurmukhametov RN. Effect of a heavy atom in the S1($\pi\pi$*) T 1($\pi\pi$*) nonradiative transition. 9,10-

Dichloroanthracene. Opt Spectrosc 2008;105:489−95. https://doi.org/10.1134/S0030400X08100020.

136 Ishchenko AA. Structure and spectral-luminescent properties of polymethine dyes. Russ Chem Rev 1991;60:865−84. https://doi.org/10.1070/rc1991v060n08abeh001116.

137 Levitus M, Ranjit S. Cyanine dyes in biophysical research: The photophysics of polymethine fluorescent dyes in biomolecular environments. Q Rev Biophys 2011;44:123−51. https://doi.org/10.1017/S0033583510000247.

138 Smith GJ. The effects of aggregation on the fluorescence and the triplet state yield of hematoporphyrin. Photochem Photobiol 1985;41:123−6. https://doi.org/10.1111/j.1751-1097.1985.tb03459.x.

139 N,N-Dimethylaniline. Sigma-Aldrich. Safety data sheet, https://www.sigmaaldrich.com/IL/en/sds/aldrich/515124; 2021, [accessed 1 August 2021].

140 Chemistry: 4-Iodo-N,N-dimethylaniline, https://handwiki.org/wiki/Chemistry:4-Iodo-N,N-dimethylaniline; 2021, [accessed 1 August 2021].

141 Jorge K. Soft drinks. Chemical composition. In: Caballero B, Finglas P, Toldrá F, editors. Encyclopedia of food sciences and nutrition, Academic Press; 2003, p. 5346−52. https://doi.org/10.1016/b0-12-227055-x/01101-9.

142 4-Iodobenzoic acid, https://www.chemicalbook.com/ChemicalProductProperty_EN_CB4374473.htm; 2021, [accessed 1 August 2021].

143 2,3,5-tri-iodobenzoic acid. PPDB: Pesticide Properties DataBase. University of Hertfordshire. http://sitem.herts.ac.uk/aeru/ppdb/en/Reports/2941.htm, [accessed 4 June 2021]. Lewis KA, Tzilivakis J, Warner DJ, Green A. An international database for pesticide risk assessments and management. Hum Ecol Risk Assess 2016;22:1050−64. https://doi.org/10.1080/10807039.2015.1133242.

144 Reddi BAJ. Why is saline so acidic (and does it really matter?). Int J Med Sci 2013;10:747−50. https://doi.org/10.7150/ijms.5868.

145 Dean JA. Handbook of Organic Chemistry. New York, NY: McGraw-Hill Book Co.; 1987, p. 8-45.

146 Riddick JA, Bunger WB, Sakano TK. Techniques of Chemistry, Vol II. Organic Solvents. Physical properties and methods of purification. 4th ed. New York, NY: John Wiley and Sons; 1985.

147 Zhao B, He YY, Chignell CF, Yin JJ, Andley U, Roberts JE. Difference in phototoxicity of cyclodextrin complexed fullerene $[(\gamma\text{-CyD})_2/\text{C}_{60}]$ and its

aggregated derivatives toward human lens epithelial cells. Chem Res Toxicol 2009;22:660−7. https://doi.org/10.1021/tx800478u.

148 Ungati H, Govindaraj V, Mugesh G. The remarkable effect of halogen substitution on the membrane transport of fluorescent molecules in living cells. Angew Chem 2018;130:9127−31. https://doi.org/10.1002/ange.201804128.

149 Krishnamurti U, Silverman JF. HER2 in breast cancer: A review and update. Adv Anat Pathol 2014;21:100−7. https://doi.org/10.1097/PAP.0000000000000015.

150 Ferraro E, Drago JZ, Modi S. Implementing antibody-drug conjugates (ADCs) in HER2-positive breast cancer: state of the art and future directions. Breast Cancer Res 2021;23:1−11. https://doi.org/10.1186/s13058-021-01459-y.

151 **Kobzev D**, Semenova O, Tatarets A, Bazylevich A, Gellerman G, Patsenker L. Antibody-guided iodinated cyanine for near-IR photoimmunotherapy. Dyes Pigm 2023;212:111101. https://doi.org/10.1016/j.dyepig.2023.111101.

152 Hermanson GT. Bioconjugate Techniques: Third Edition. 2013. https://doi.org/10.1016/C2009-0-64240-9.

153 Texier I, Goutayer M, Da Silva A, Guyon L, Djaker N, Josserand V, et al. Cyanine-loaded lipid nanoparticles for improved in vivo fluorescence imaging. J Biomed Opt 2009;14:054005. https://doi.org/10.1117/1.3213606.

154 Mustroph H, Towns A. Fine structure in electronic spectra of cyanine dyes: are sub-bands largely determined by a dominant vibration or a collection of singly excited vibrations? ChemPhysChem 2018;19:1016−23. https://doi.org/10.1002/cphc.201701300.

155 Lindig BA, Rodgers MA, Schaap AP. Determination of the lifetime of singlet oxygen in water-d2 using 9,10-anthracenedipropionic acid, a water-soluble probe. J Am Chem Soc 1980;102(17):5590-3.

156 Lin H, Shen Y, Chen D, Lin L, Wilson BC, Li B, Xie S. Feasibility study on quantitative measurements of singlet oxygen generation using Singlet Oxygen Sensor Green. J Fluoresc 2013;23(1):41−47. https://doi.org/10.1007/s10895-012-1114-5.

157 Faustino-Rocha A, Oliveira PA, Pinho-Oliveira J, Teixeira-Guedes C, Soares-Maia R, Da Costa RG, et al. Estimation of rat mammary tumor volume using caliper and ultrasonography measurements. Lab Anim 2013;42:217−24. https://doi.org/10.1038/laban.254.

158 Thermo Fisher Scientific. BestProtocols: Cell Preparation for Flow Cytometry Protocols | Thermo Fisher Scientific - DK 2019;3−5. https://www.thermofisher.com/dk/en/home/references/protocols/cell-and-tissue-analysis/protocols/cell-preparation-flow-cytometery.html#protocol-b (accessed June 10, 2022).

159 Leung WY, Cheung CY, Yue S. Modified carbocyanine dyes and their conjugates. US 6974873, 2005.

160 Parker CA. Photoluminescence of Solutions. Amsterdam, London, New York: Elsevier; 1968.

161 ThermoFisher scientific. Singlet Oxygen Sensor Green Reagent | Thermo Fisher Scientific - DK 2019:3−5. https://www.thermofisher.com/document-connect/document-connect.html?url=https://assets.thermofisher.com/TFS-Assets%2FLSG%2Fmanuals%2Fmp36002.pdf (accessed October 29, 2022).

162 Grabolle M, Brehm R, Pauli J, Dees FM, Hilger I, Resch-Genger U. Determination of the labeling density of fluorophore-biomolecule conjugates with absorption spectroscopy. Bioconjug Chem 2012;23:287−92. https://doi.org/10.1021/bc2003428.

163 Schneider CA, Rasband WS, Eliceiri KW. NIH Image to ImageJ: 25 years of image analysis. Nat Methods 2012;9:671−5. https://doi.org/10.1038/nmeth.2089.